INŻYNIERIA BIOMATERIAŁÓW

ENGINEERING OF BIOMATERIALS

CZASOPISMO POLSKIEGO STOWARZYSZENIA BIOMATERIAŁÓW

Numer 56-57
Rok IX
ISSN 1429-7248

CZERWIEC - WRZESIEŃ 2006

WYDAWCA:

Polskie Stowarzyszenie Biomateriałów w Krakowie

KOMITET REDAKCYJNY:

Redaktor naczelny
Stanisław Błażewicz
Sekretarz redakcji,
Skład komputerowy
Augustyn Powroźnik

RADA NAUKOWA:

Jan Ryszard Dąbrowski

Jan Chłopek

Tadeusz Cieślik

Monika Gierzyńska-Dolna

Andrzej Górecki

Wojciech Maria Kuś

Jan Marciniak

Stanisław Mazurkiewicz

Stanisław Mitura

Roman Pampuch

Bogna Pogorzelska-Stronczak

ADRES REDAKCJI:
Akademia Górniczo-Hutnicza
al. Mickiewicza 30/A-3
30-059 Kraków

Nakład: 200 egz.
Wydawnictwo Naukowe AKAPIT
e-mail: wn@akapit.krakow.pl

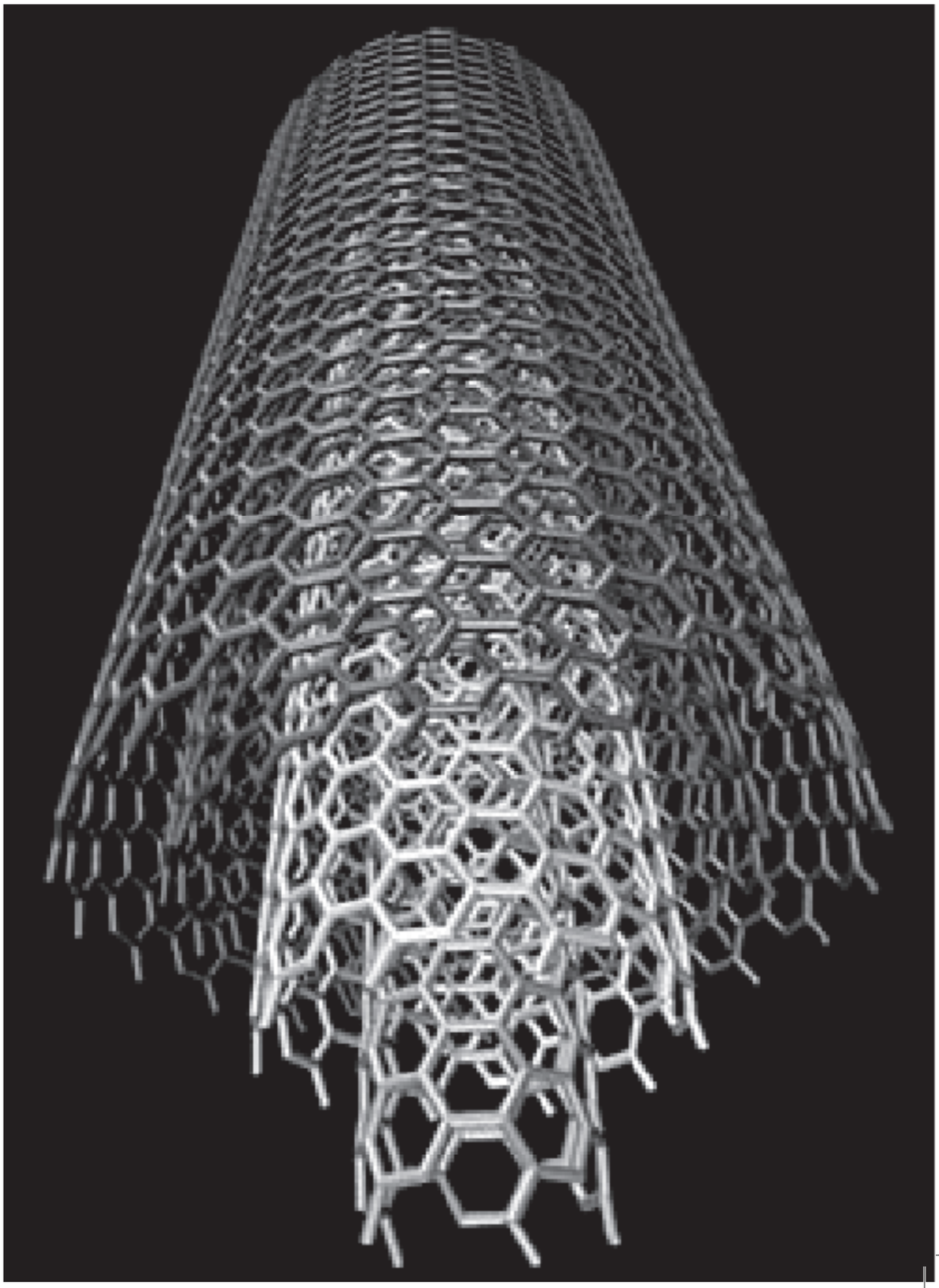

XVI Conference on

BIOMATERIALS IN MEDICINE AND VETERINARY MEDICINE

October, 12-15, 2006,
Hotel „Perla Poludnia", Rytro

http://galaxy.uci.agh.edu.pl/~apowroz/biomat/

INŻYNIERIA BIOMATERIAŁÓW

SPIS TREŚCI

Streszczane w Applied Mechanics Reviews
Abstracted in Applied Mechanics Reviews

CONTENTS

Wydanie dofinansowane przez Ministra Nauki i Szkolnictwa Wyższego
Edition financed by the Minister of Science and Higher Education

INŻYNIERIA BIOMATERIAŁÓW

THE INFLUENCE OF NANOCRYSTALLINE DIAMOND LAYERS OBTAINED BY MW/RF PECVD METHOD ON SURFACE PROPERTIES OF AISI 316 L STEEL 31
T. Blaszczyk, B. Burnat, H. Scholl, P. Niedzielski, W. Kaczorowski

CORROSIVE FEATURES OF Ti WITH NANO-CRYSTALLINE DIAMOND LAYERS OBTAINED BY MEANS RADIO FREQUENCY AND MICROWAVE / RADIO FREQUENCY PLASMA CHEMICAL VAPOR DEPOSITION METHODS 34
B. Burnat, W. Kaczorowski, G. Boguslawski, T. Blaszczyk, H. Scholl

PROPERTIES OF NiTi - SHAPE MEMORY ALLOY AFTER MODIFICATION BY RF PCVD METHOD 37
M. Czerniak-Reczulska, P. Couvrat, J. Grabaczyk, P. Niedzielski

BIOMATERIALS IN THE TREATMENT OF PERIPHERAL NERVE INJURIES – AN OVERVIEW OF METHODS AND MATERIALS 40
D. Szarek, W. Jarmundowicz, A. Frączek, S. Błażewicz

DESIGN OF RESORPTION PROPERTIES OF THE METAL BONE IMPLANTS – APPLICATION *IN VIVO* 54
F.W. Bach, R. Kucharski, D. Bormann, D. Besdo, S. Besdo, C. Hackenbroich, F. Thorey, A. Meyer-Lindenberg

MAGNESIUM COMPOUND STRUCTURES FOR THE TREATMENT OF BONE DEFECTS 58
F.W. Bach, R. Kucharski, D. Bormann

MODYFIKACJA POWIERZCHNI TYTANU POWŁOKĄ DIAMENTOPODOBNĄ

Biel Gołaska Marta*, Kalemba Izabela, Radzikowska Janina*, Warmuzek Małgorzata*, Rajchel Bogusław***, Rakowski Wiesław****

*Instytut Odlewnictwa, Kraków
**AGH, Wydział Inżynierii Mechanicznej i Robotyki, Kraków
***Instytut Fizyki Jądrowej PAN, Kraków
E-mail: martabiel@iod.krakow.pl

Streszczenie

Artykuł dotyczy uszlachetniania powierzchni tytanu powłoką diamentopodobną w celu zwiększenia jego biotolerancji w organiźmie ludzkim.
Na powierzchni próbek z tytanu wytworzono ochronną warstwę diamentopodobną, stosując metodę implantacji jonowej. Dokonano oceny jej własności mechanicznych oraz adhezji do podłoża metalowego.
Scharakteryzowano własności użytkowe implantów metalowych oraz stawiane im wymagania.
Omówiono metodę jonową IBAD formowania powłok węglowych na materiałach metalowych, jak również metodykę badań wytrzymałości, mikrotwardości, szczelności i adhezji powłok do podłoża metalowego.
Przedstawiono wyniki badań mechanicznych i adhezji do podłoża oraz zamieszczono sugestie odnośnie kierunków dalszych badań.

Słowa kluczowe: *implanty metalowe, tytan, powłoka diamentopodobna, implantacja jonów, adhezja, mikrostruktura, właściwości mechaniczne.*
[Inżynieria Biomateriałów, 56-57,(2006),1-11]

Wstęp

Próby wykorzystania obcych materiałów w organiźmie ludzkim sięgają praktycznie początków medycyny. W tym celu stosowane były różne materiały: drewno, kości zwierząt oraz metale szlachetne, takie jak złoto i srebro. W latach czterdziestych XX wieku przeprowadzono pierwsze próby zastosowania tytanu i jego stopów w chirurgii kostnej. O ich przydatności zdecydowała bardzo dobra odporność korozyjna w środowisku tkankowym. Należy podkreślić, że mają one mniejszy ciężar właściwy w porównaniu ze stopami na osnowie żelaza i kobaltu, co stanowi ważną zaletę tworzywa wykorzystywanego na endoprotezy stawowe. Stopy tytanu znalazły również zastosowanie w protetyce stomatologicznej oraz kardiologii [1, 2].
Tytan i jego stopy znajdują szerokie zastosowanie jako wszczepy czasowe w postaci prętów, gwoździ, grotów, drutów, wkrętów i płytek w rekonstrukcji złamań kości oraz jako wszczepy trwałe w postaci protez stawów lub ich części, sztucznych zastawek serca, a także w wielu wyrobach, takich jak stymulatory serca.
Niekiedy stosowane nazwy implantów nawiązują do ich konkretnego umiejscowienia. Można tu zaliczyć różne rodzaje implantów pokazane na RYS. 1-7:
- **implant ortopedyczny** - stosowany by wspomóc kość, chrząstkę, więzadła, ścięgna lub powiązane z nimi tkanki, albo zastępujący lub uzupełniający tymczasowo brak na stałe tkanki (RYS. 5,6,7),
- **implant czaszkowo-twarzowy** - stosowany w obszarze czaszkowo-twarzowym wyłączając obszar jamy ustnej, który ma na celu poprawienie lub zastąpienie określonych tka-

MODIFICATION OF THE TITANIUM SURFACE WITH A DIAMOND-LIKE CARBON COATING

Biel Gołaska Marta*, Kalemba Izabela, Radzikowska Janina*, Warmuzek Małgorzata*, Rajchel Bogusław***, Rakowski Wiesław****

*Foundry Research Institute, Cracow, Poland
**AGH-USC, Faculty of Mechanical Engineering and Robotics, Cracow, Poland
***Institute of Nuclear Physics, Polish Academy of Science Cracow, Poland
martabiel@iod.krakow.pl

Abstract

Modification of the surface of titanium alloy biomaterial with the diamond--like carbon coating (DLC) in order to increase its biocompability in the human organism, its hardness and wear resistance were analyzed.
The diamond-like carbon coatings were formed on the titanium specimens, then their adhesion to the metal substrate was evaluated. Ion Beam Assisted Deposition method was used for improving the titanium surface. The mechanical properties of the coating and substrate and adhesion to the base metal were evaluated.
Morphology of titanium and the diamond-like carbon films were examined under the Light and Scanning Microscope. The microscopic examinations revealed satisfying structural homogeneity on the coated surface.
The results of microstructural and mechanical tests as well as of those concerning the adhesion to the base are given. The utilization properties of metal implants and the requirements which are imposed onto them were characteristed.

Keywords*: metal implants, titanium, diamond-like carbon coating (DLC), ion implantation, adhesion,*
[Engineering of Biomaterials, 56-57,(2006),1-11]

Introduction

Attempts at introducing foreign materials to the human organism practically date back to the beginnings of medicine. To this end various materials, such as wood, animal bones and precious metals were used. In forties of the 20th century, first attempts at the application of titanium and its alloys in bone surgery were made. Very good corrosion resistance in the medium of the tissues decided about their utility. It should be stressed that, compared with iron- and cobalt-based alloys, they have lower mass density which is an important advantage of the material used for endoprostheses of joints. Titanium alloys also found application in dental protectics and in cardiology [1,2].
Titanium and its alloys find extensive application as temporary implants in the form of bars, nails, wires, darts, screws and plates for the reconstruction of fractured bones, and as durable implants of the joint endoprostheses or parts of those endoprostheses, artificial heart valves and numerous other products, e.g. heart pacemakers.
Sometimes the names of the implants refer to their specific location. Among various implants, the following ones can be distinguished. (FIGs.1-7)
· **orthopaedic implants** - used to support bones, gristles,

nek twardych lub miękkich, z wyjątkiem mózgu, oczu i ucha wewnętrznego (RYS. 2, 3),
- **implant dentystyczny** - to rodzaj implantu ustnego stosowany do uzupełnienia ubytku zęba (RYS. 4).

Z biomateriałów tytanowych wytwarzane są różne użytkowe postacie implantów (RYS. 1) [3].

Pozostaje jednak nierozwiązany do końca problem, a mianowicie: czy tytan jest całkowicie bezpieczny, czy też zmieni się w środowisku tkanek i z jakimi ewentualnymi konsekwencjami dla biorcy [4].

Metale i ich stopy stosowane w implantacji powinny charakteryzować się następującymi cechami [5, 6, 7]:
- dobrą odpornością na korozję,
- biotolerancją (nietoksyczność),
- odpowiednim składem chemicznym i drobnoziarnistą strukturą,
- dobrą wytrzymałością,
- określonym stanem powierzchni,
- brakiem tendencji do tworzenia zakrzepów,
- posiadaniem odpowiednich właściwości elektrycznych oraz magnetycznych,
- podatnością na obróbkę mechaniczną.

Biotolerancja (biokompatybilność, zgodność biologiczna) jest jedną z najważniejszych cech implantów. Związana jest ona z podatnością wszczepu na korozję lub biodegradacją, a co z tym się wiąże - skłonnością do inicjowania reakcji toksycznych i alergicznych, a także mechaniczną reakcją tkanek na obce ciało. Największy wpływ na stopień zgodności biologicznej implantu mają odporność na korozję, odpowiednie właściwości elektryczne oraz odporność na zużycie ścierne.

W celu zabezpieczenia implantów metalowych przez korozją, ich powierzchnię pokrywa się cienką warstwą wierzchnią. Struktura i właściwości warstwy wierzchniej w dużym stopniu decydują o zachowaniu się wyrobów w czasie ich eksploatacji.

Zatem zadaniem na najbliższą przyszłość jest stworzenie podstaw umożliwiających projektowanie procesów wytwarzania warstw powierzchniowych o określonych właściwościach, stosownie do wymagań.

Węgiel jako podstawowy składnik struktury tkanek człowieka jest idealnym materiałem stanowiącym element implantów stosowanych w medycynie. Wszystkie odmiany alotropowe węgla spełniają wymagania stawiane wszczepom.

Diament (RYS. 8a) jest jedną z alotropowych postaci węgla. Charakteryzuje się cennymi właściwościami, które czynią go przydatnym w wielu dziedzinach, a szczególnie w medycynie. Diament odznacza się bardzo dużą trwałością, odpornością na korozję, jest chemicznie nieaktywny, ma bardzo duża przewodność cieplną, jest materiałem biozgodnym. Od ponad pięćdziesięciu lat prowadzone są badania mające na celu opracowanie metod syntezy cząstek diamentowych i warstw diamentowych. W ciągu ostatnich dwudziestu lat do wytwarzania warstw diamentowych oraz diamentopodobnych zastosowano techniki jonowe. Jedną z technik jonowych zastosowano do zsyntetyzowania nanokrystalicznych warstw węglowych. Właściwości warstw węglowych zależą od sposobu ich wytwarzania. Stwarza to problemy z ujednoliceniem opisu warstw o poszczególnych cechach. Generalnie, w zależności od struktury, wytwarzany materiał węglowy można podzielić na zasadnicze grupy [8]:

Diament obejmujący warstwy diamentowe i warstwy polikrystalicznego diamentu składające się z atomów o hybrydyzacji elektronów typu σsp^3.

Diament nanokrystaliczny, tetraedryczny lub amorficzny - to nazwy używane dla podkreślenia tego, że chociaż prawie 100% atomów węgla posiada hybrydyzację elektronów typu ssp^3, to jednocześnie rozmiary krystalitów diamen-

ligaments, tendons or tissues connected with them, or to replace or make up for a permanent lack of the tissues (FIGs. 5,6,7);
· **skull-facial implants** - used in the skull-facial area excluding oral cavity, which should improve or replace some specific hard or soft tissues, except the brain, eyes and inner ear (FIGs.2,3);
- **dental implants** - used in the oral cavity to make up for the lacking teeth (FIG. 4).

Various usable forms of implants are made from titanium biomaterials (FIG.1) [3].

There is still one problem not solved to the very end, namely whether titanium is completely safe and whether it can get transformed in the human tissues and with what possible consequences for the recipient [4].

Metals and their alloys used in implantation should be characterised by the following features [5, 6, 7]:
- high corrosion resistance,
- biocompability (atoxicity),
- required chemical composition and fine-grained structure,
- suitable strength,
- required surface condition,
- no tendency to formation of thrombi,
- suitable electric and magnetic properties,
- susceptibility to mechanical working,
- reasonable manufacturing costs.

Biocompability (biological comformity) is one of the most important characteristic features of implants. It is connected with the implant susceptibility to corrosion or biodegradation, and the related predisposition to the initiation of toxic or allergic reactions and also with tissues response to the presence of a foreign body. The most important influence on the degree of biological compatibility have corrosion resistance, electric properties, and abrasion wear resistance.

To protect metal implants against corrosion, their surface is covered with a fine layer. The structure and properties of the top layer decide to a large extent on the behaviour of products during their performance.

The task for the nearest future of this field of science is creating a background against which the processes enabling manufacture of the surface layers characterised by some specific properties tailored to the individual requirements can be successfully developed.

Carbon as a main component in the structure of the human body tissues is an ideal material for implants used in medicine. All allotropic forms of carbon meet the requirements imposed onto implants.

Diamond (FIG.8a) is one of the allotropic forms of carbon. It possesses a number of valuable properties, which make it useful in many fields, especially in medicine. It is characterised by very high durability and corrosion resistance, is chemically inactive, and has very high thermal conductivity. It is, moreover, biocompatible. Investigations aiming at the elaboration of various methods of the synthesis of diamond particles and diamond layers have been carrying out for more than 50 years. In the last twenty years, ionic techniques were applied to fabricate diamond or diamond-like carbon layers. One of the ionic techniques was applied to the synthesis of nanocrystalline carbon layers.The properties of carbon layers depend on the method of their fabrication. There are problems with unification of the description of the layers with individual features. Generally, depending on the structure, the produced carbon material can be divided into the following main groups [8].

Diamond - containing diamond layers and layers of polycrystalline diamond, composed of atoms with hybrid forms of the σsp^3 type electrons.

Nanocrystalline, tetrahedral or amorphous diamond - are the terms used to stress the fact that although almost

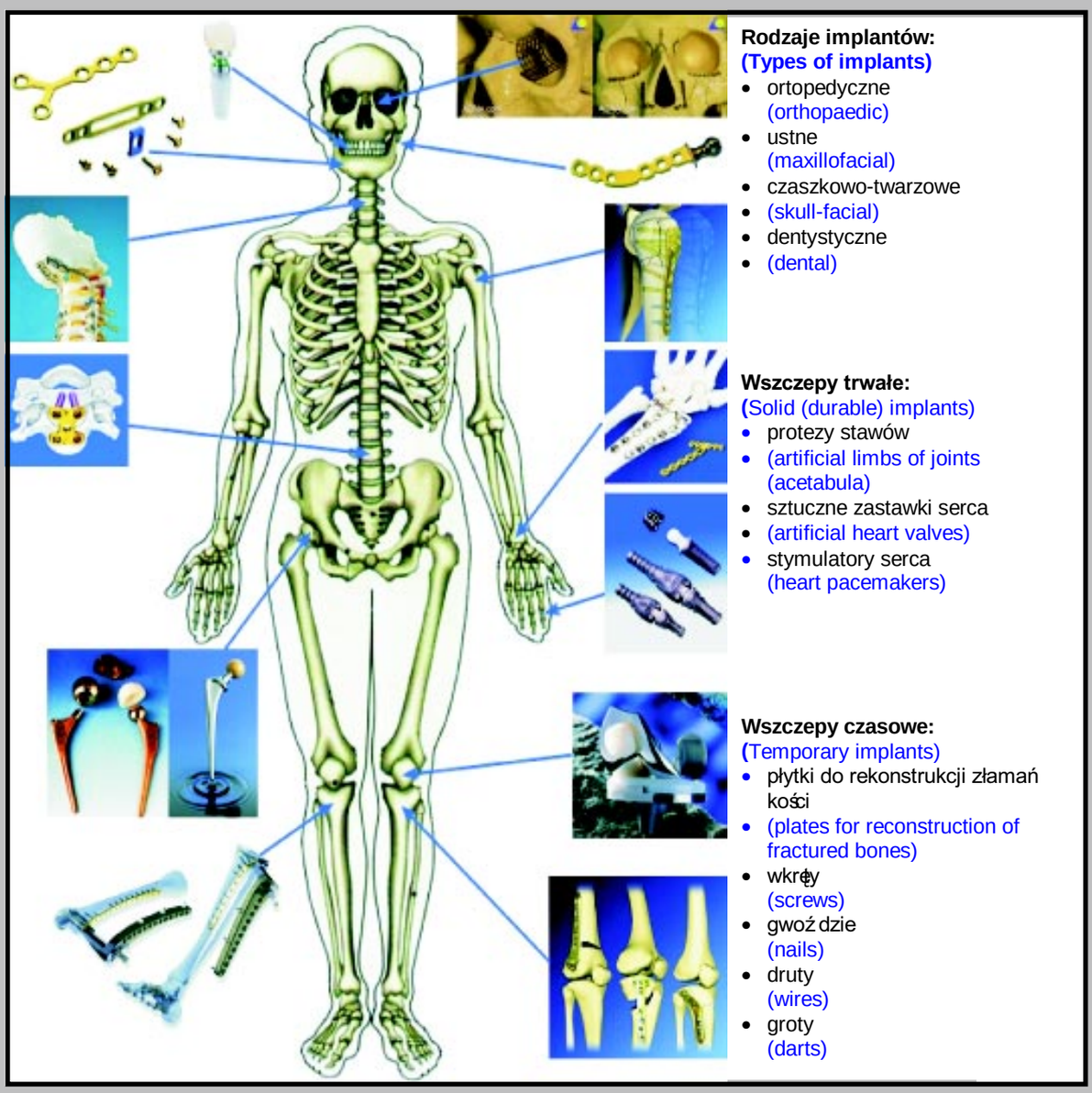

RYS. 1. Przykłady zastosowania materiałów implantacyjnych w organizmie człowieka [3].
FIG. 1. Examples of the application of implant materials in a human organism [3].

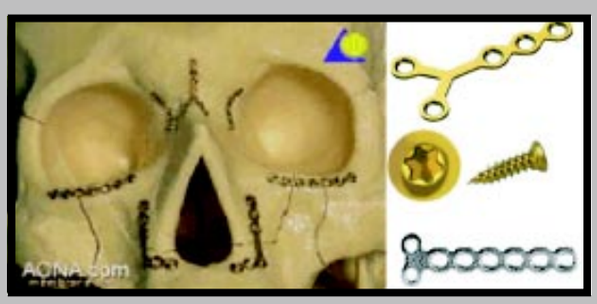

RYS. 2. Mikropłytki stosowane w chirurgii czaszki [15].
FIG. 2. Mikroplates used in skull surgery [15].

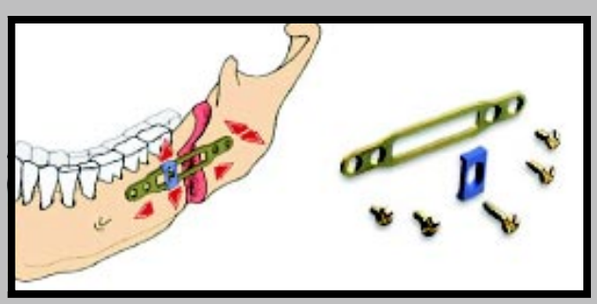

RYS. 3. Płytka stosowana w chirurgii szczękowej [15].
FIG. 3. Plate used in the jaw surgery [15].

RYS. 4. Implant dentystyczny [16].
FIG. 4. Dental implant [16].

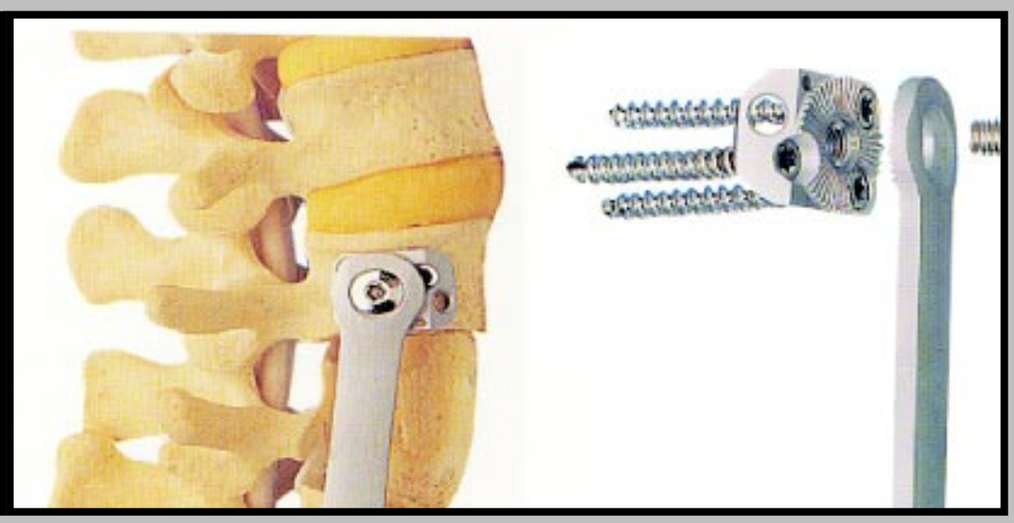

RYS. 5. Płytka łącząca elementy kręgosłupa [3].
FIG. 5. Plate binding the vertebrae [3].

RYS. 6. Endoproteza stawu biodrowego [18].
FIG. 6. Endoprosthesis of a hip joint [18].

RYS. 7. Endoproteza całkowita stawu kolanowego [18].
FIG. 7. Endoprosthesis of a knee joint [18].

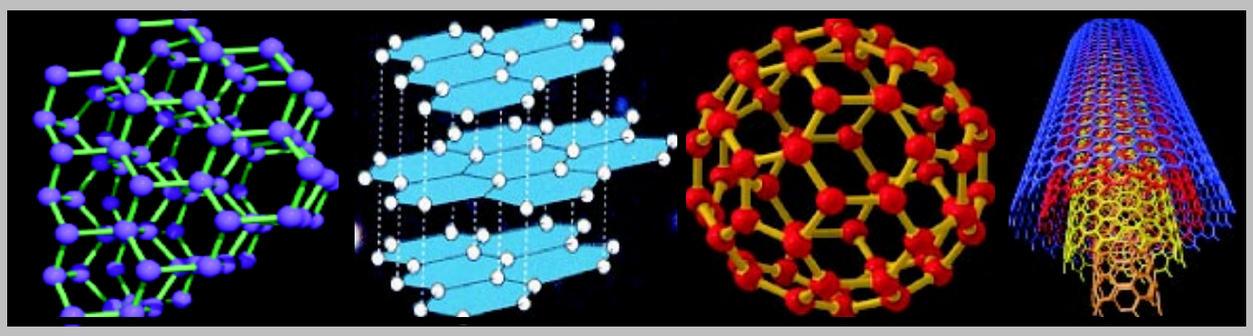

a) diament
a) diamond

b) grafit
b) graphite

c) fuleren
c) fulleren

d) nanorurki
d) nanotubes

RYS. 8. Odmiany alotropowe węgla [17].
FIG. 8. Allotropic forms of carbon [17].

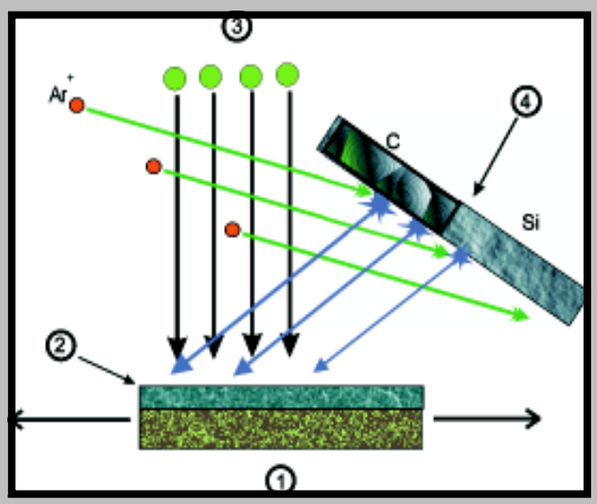

RYS. 9. Schemat przebiegu procesu implantacji jonów: 1-podłoże, 2-powłoka, 3-wiązka "implantująca", 4-"rozpylana" tarcza pomocnicza [9].
FIG. 9. A scheme representing the course of the ions implantation process; 1 - substrate; 2 - coating; 3 - "implanting" beam; "sputtering" auxiliary shield [9].

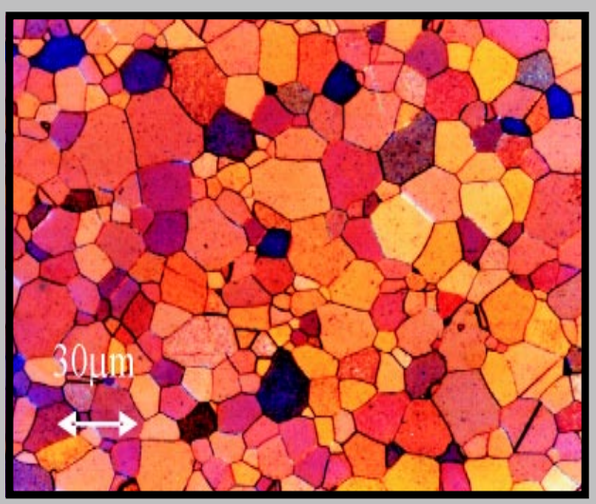

RYS. 10. Mikrostruktura tytanu, pow..260x [19]
FIG. 10. Titanium microstructure (LM), mag.260x [19].

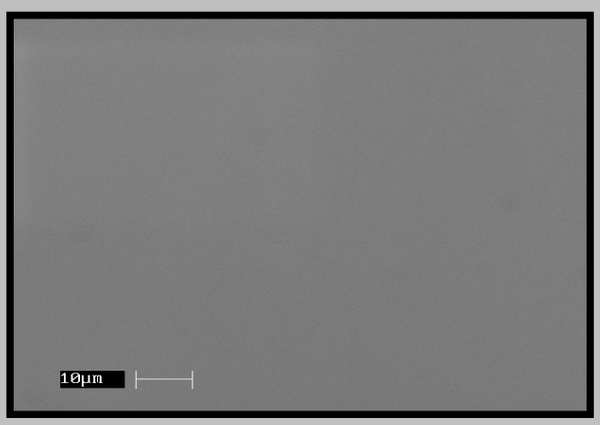

RYS. 11. Powłoka DLC (SEM)[3].
FIG. 11. Diamond-like carbon coating (SEM) [3].

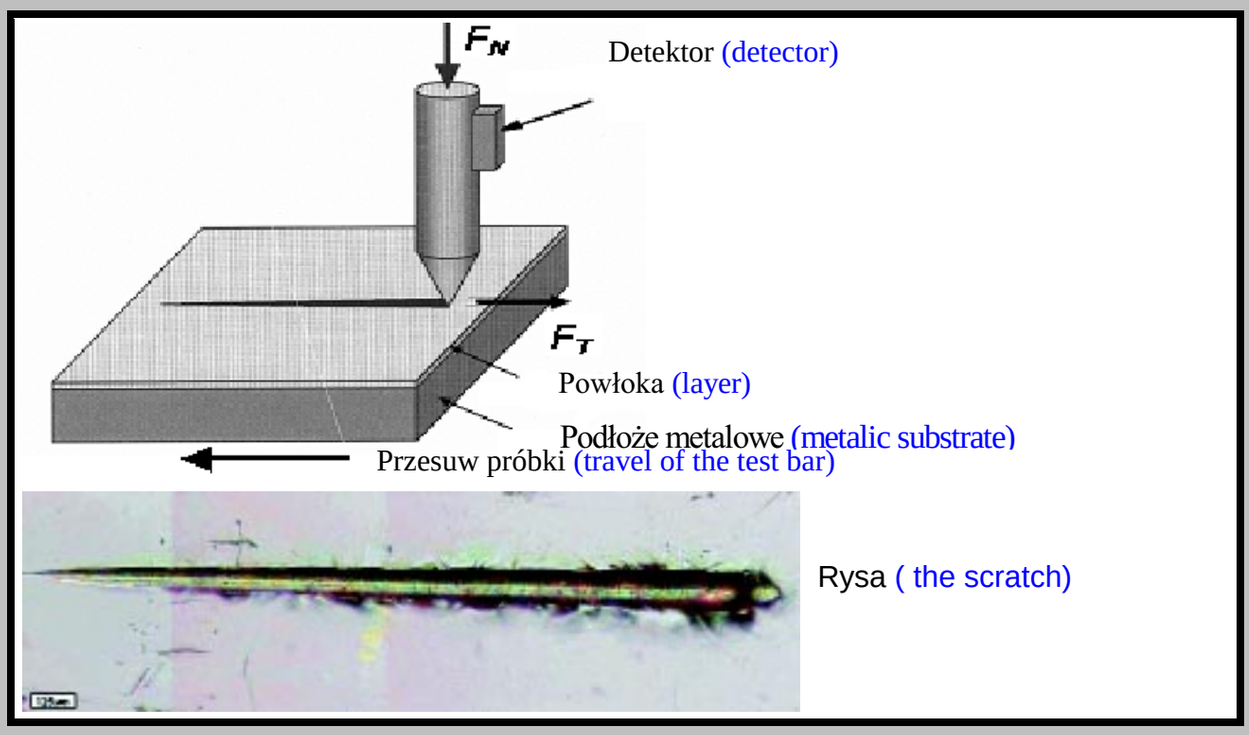

RYS.12. Schemat testu zarysowania (scratch testu) wraz z rysą wykonana w próbie [3].

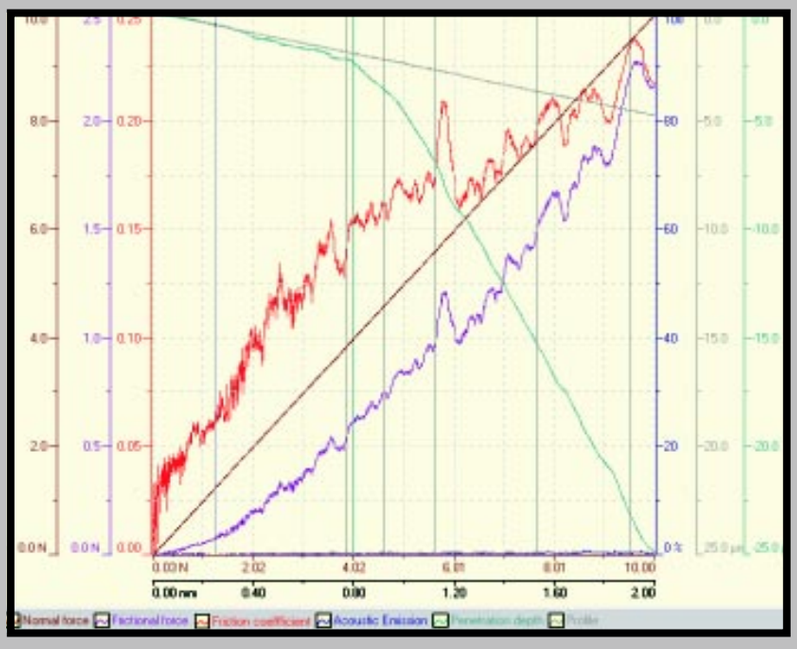

- **Obciążenie normalne** (normal loading)
- **Siła tarcia** (friction force)
- **Współczynnik tarcia** (coefficient of friction)
- **Emisja akustyczna** (acoustic emission)
- **Głębokość penetracji** (penetration depth)
- **Profil toru rysy** (profile of the scratch track)

RYS. 13. Wyniki testu zarysowania powłoki wykonane na próbce z tytanu pokrytej powłoką diamentopodobną [3].
FIG. 13. Results of the scratch test for a titanium test bar with diamond-like carbon coating [3].

towych nie przekraczają nanometrów.
Węgiel diamentopodobny (DLC) będący mieszaniną amorficznego lub superdrobnego węgla, w którym przy przewadze wiązań σsp^3, właściwych dla struktury diamentu, występują wiązania σsp^2, właściwe dla grafitu (RYS.8b)) i wiązania sp^1. Często spotykana nazwą dla DLC jest węgiel jonowy lub węgiel amorficzny zawierający wodór.
Karbiny: **α-karbin**, który zawiera wiązanie acetylenowe (-C≡C-) i dlatego może być określany mianem poliacetylenu; **ß-karbin**, który zawiera wiązanie kumulenowe (=C=C=) i dlatego może być określany mianem polikumulenu.
Fulereny (RYS.8c)oraz **nanorurki węglowe**(RYS.8d), w których typowym wiązaniem jest tutaj, podobnie jak w graficie σsp^2; wytworzone warstwy zawierają zwykle mieszaninę grafitu, fulerenów i nanorurek.
Skład diamentopodobnych powłok węglowych zwanych w skrócie DLC (diamond like coating) nie jest jednolity, mają one strukturę amorficzną z obszarami mikrokrystalicznymi. Ich właściwości również nie są określone w sposób jednoznaczny, ale mogą się znacznie różnić w zależności od metody użytej do ich otrzymywania, ponieważ w zależności od sposobu wytworzenia powłoki zawiera ona atomy węgla o rozmaitych kombinacjach wiązań.
Powłoki DLC są mieszaniną amorficznego lub superdrobnokrystalicznego węgla o hybrydyzacji orbitali elektronowych typu σsp^3, σsp^2, sp^1, a stosunek atomów sp^3 i sp^2 w warstwach uzyskanych za pomocą tej samej metody silnie zależy od przyjętych parametrów nanoszenia. Tak więc własności powłoki DLC zależą nie tylko od metody wytworzenia, ale również od parametrów nanoszenia stosowanych w danej metodzie. Właściwości te mogą zmieniać się w szerokich granicach [9].
Celem tej pracy było więc zmodyfikowanie powierzchni tytanu, zmierzające do zwiększenia jego biotolerancji w organiźmie ludzkim, poprzez wytworzenie powłoki diamentopodobnej, a następnie dokonanie oceny jej własności mechanicznych oraz adhezji do podłoża metalowego.

Materiał i metodyka

Do wytworzenia powłok diamentopodobnych przeznaczono trzy próbki wykonane z tytanu. Próbki po odpowiednim odtłuszczeniu powierzchni acetonem a następnie oczyszczeniu jej w płuczce ultradźwiękowej, zostały poddane implantacji jonowej celem pokrycia powierzchni metalowej powłoką diamentopodobną DLC.
Implantacja jonów, jest procesem wprowadzania do ciała stałego obcych dla tego ciała zjonizowanych atomów dowolnego rodzaju, dzięki dużej energii (od kilku do kilkuset keV), jakiej nabywają one w próżni, w przyspieszającym i formującym jony w wiązkę polu elektrycznym. (RYS.9.)[10]
Do wybicia z powierzchni płaskiej płyty grafitowej atomów węgla użyto wiązkę jonów Ar^+ o energii 25 keV. Wiązka ta ("rozpylająca") bombardowała powierzchnię grafitu pod kątem 67.5° względem normalnej do tej powierzchni. Formującą się powłokę bombardowano wiązką jonów C^+ o energii 25 keV. Wiązka jonów C^+ bombardowała powierzchnię formowanej warstwy prostopadle do niej (kąt 0°).
Przed rozpoczęciem procesu formowania wiązkę zogniskowano tak, że jej obraz
w płaszczyźnie pokrywanego przedmiotu był prostokątem o wysokości 100 mm i szerokości 5 mm. Z tego powodu w trakcie procesu formowania powłoki pokrywane próbki przesuwano kilkakrotnie w poprzek wiązki bombardujących jonów C^+ w celu ujednorodnienia formowanej powłoki.
Przed rozpoczęciem procesu formowania w komorze implantacyjnej zapewniono próżnię rzędu 10^{-6} mbara. W trakcie procesu formowania powłok mierzono prądy obu wią-

100% of carbon atoms possess hybrid forms of electrons of the σsp type ^{3}, the size of the diamond crystallites is within the range of nanometres.
Diamond-like carbon (DLC) - being a mixture of amorphous or superfine carbon in which, with prevalence of the σsp^3 bonds characteristic of the diamond structure, some σsp^2 bonds, characteristic of the graphite (FIG.8b), and sp1 bonds are present as well. The terms which are often used for DLC are ionic carbon or amorphous carbon containing hydrogen.
Carbines: **α-carbine**, which contains triple carbon bonds (-C≡C-) and due to this can be called polyacetylene,
ß-carbine, which contains cumulene bonds (=C=C=C) and for this reason is also known under the name of polycumulene.
Fullerens (FIG.8c) and **carbon nanotubes** (FIG.8d), in which the typical bond is similarly as in graphite, σsp^2; the formed layers usually consist of a mixture of graphite, fullerens and nanotubes.
The composition of diamond-like carbon coatings, called in short DCL, is not uniform. They have amorphous structure with microcrystalline areas. Their properties have not been as yet defined in a clear manner, either; they can differ considerably depending on the method used to produce them because, depending on the method of making a coating, it can contain the atoms of carbon in various bond combinations.
DLC coatings are a mixture of amorphous or superfine crystalline carbon with hybridation of electronic orbitals of the σsp^3, σsp^2 and sp^1 type, where the sp^3 to sp^2 atoms ratio in layers produced by the same method depends to a large extent on the adopted parameters of application. Thus, the properties of a DLC coating depend not only on the method of its fabrication, but also on the spreading parameters determined by the method of its application. These properties can vary to a large extent [9].
The aim of the investigations was modification of the titanium surface to increase its biotolerance in the human organism due to the production of a diamond-like carbon coating and making next an evaluation of its mechanical properties and adhesion to the metal substrate.

Material and methodology

To produce diamond-like carbon coatings, three test bars of titanium were designed. The test bars after a suitable degreasing of their surfaces with acetone and the subsequent cleaning in an ultrasonic washer were subjected to ionic implantation to cover the metal surface with a diamond-like carbon coating (DLC).
Implantation of ions is the process of introducing to a solid body ionised atoms of any type, foreign to this body, utilising the great energy (from several to a few hundreds of keV) that they acquire in vacuum, in the electric field accelerating these ions and forming them into a beam. [10].
The diamond-like carbon coating was formed by a double-beam IBAD method. A beam of ions Ar^+ with the energy of 25 keV was used to "knock out" carbon atoms from the surface of a flat graphite plate. This "sputtering" beam was bombing the graphite surface at an angle of 67.5° with respect to a normal to this surface. Thus formed coating was bombed with a beam of ions C^+ of the 25 keV energy. The beam of ions C^+ was bombing the surface of the layer being formed in direction perpendicular to this surface (angle 0°).
Before the beginning of the coating formation process, the beam was focused in a way such that its image in the plane of the coated object was forming a rectangle 100 mm high and 5 mm wide. For this reason, during the process of the

zek stosowanych w procesie IBAD.
W wyniku implantacji jonów, do przypowierzchniowego obszaru materiału implantowanego została wprowadzona pewna liczba atomów, tworząc przypowierzchniową warstwę implantowaną o grubości 0,01÷1μm o innych właściwościach fizykochemicznych niż materiał wyjściowy.

Badania metalograficzne

Obserwacje struktury metalograficznej tytanu przeprowadzono przy pomocy mikroskopu optycznego Neophot 32, stosując do trawienia zgładu odczynnik Wecka. W wyniku obserwacji w świetle spolaryzowanym, otrzymano strukturę tytanu, pokazaną na RYS. 10.
Obserwacje powłoki DLC dokonano na mikroskopie skaningowym Stereoscan 420, w wyniku czego uwidoczniono na RYS. 11.

Badania mikrotwardości, modułu sprężystości oraz adhezji do powierzchni tytanu

Badania własności mechanicznych powłok naniesionych na próbki z tytanu oraz adhezji powłok DLC do powierzchni próbek, przeprowadzono przy użyciu urządzenia Mikro-Combi-Tester (MCT), wykonanego przez szwajcarską firmę CSEM, wyposażonego w system zbierania i archiwizacji wyników pomiarowych. Urządzenie to spełnia wymagania norm ASTM dotyczących mikrotwardościomierzy i umożliwia:

· określenie mikrotwardości metodą Vickersa materiałów metalowych oraz powłok
· wyznaczenie modułu sprężystości materiałów miękkich, twardych, kruchych oraz plastycznych
· wykonanie testu zarysowania zwanego scratch-testem, w którym można wyznaczyć obciążenie normalne, siłę tarcia, współczynnik tarcia, wielkość sygnału emisji akustycznej, związanego z początkiem pękania powłoki, głębokość penetracji wgłębnika oraz profil toru rysy

Test zarysowania (scratch-test) polegał na zarysowaniu powierzchni badanego materiału wgłębnikiem Rockwella, który obciążony był określonym obciążeniem (RYS.12). Wartości siły obciążającej i głębokości penetracji ostrza wgłębnika były rejestrowane w sposób ciągły w czasie całego cyklu obciążania i odciążania.
Po wykonaniu testu na powierzchni próbki powstała rysa, którą obserwowano pod mikroskopem optycznym, zainstalowanym na urządzeniu. Mierzone parametry geometryczne zarysowania, analiza mikroskopowa rysy, a także sygnały emisji akustycznej, pojawiające się w przypadku pękania kruchych warstw wierzchnich próbki były źródłem informacji o charakterze zużycia i wytrzymałości badanego materiału.
Scratch-test jest skuteczną metodą określenia stopnia przywierania powłok (warstw) do podłoża, której miarą jest wyznaczana siła krytyczna L_C. Na podstawie wykreślonej krzywej obciążenia w funkcji przemieszczenia wyznaczane są takie właściwości jak: twardość, moduł Younga, głębokość penetracji, odporność na kruche pękanie. Stosując minimalne siły obciążające wgłębnik, możliwe jest wykonanie pomiaru na głębokościach poniżej 1μm, co jest szczególnie istotne podczas badania cienkich powłok, w przypadku których należy wyeliminować wpływ odkształcenia podłoża na wyznaczane właściwości.

Micro-Combi-Tester jest urządzeniem umożliwiającym wykonywanie pomiarów twardości klasycznymi i nowoczesnymi metodami, poprzez:
- dynamiczne wgłębnikowanie - mikrotwardość i moduł Younga są automatycznie obliczane z krzywej głębokości penetracji w funkcji obciążenia przy zastosowaniu ustalonego modelu obliczeniowego. Twardość jest obliczana jako stosunek maksymalnego obciążenia wgłębnika do powierzchni kontaktu wgłębnika z próbką po odciążeniu.

coating formation, the coated test bars were shifted several times crosswise the beam of the bombing C^+ ions to make the deposited coating homogeneous.
Before the beginning of the coating-deposition process, in the implantation chamber, the vacuum of 10^{-6} mbar was produced. During the coating deposition process the currents of both beams used in the IBAD process were measured.
As a result of the ion implantation, to the near-surface area of the implanted material some atoms were introduced, forming a near-surface implanted layer of the thickness of 0.01÷1μm, characterised by the physico-chemical properties different than those of the core material. The course of the ion implantation process is schematically represented in FIG. 9.

Metallographic examinations

The observations of titanium metallographic structure were carried out under a NEOPHOT 32 optical microscope, using Weck's reagent for etching of metallographic specimens. As a result of observations in polarised light, the titanium microstructure was revealed. It is shown in FIG.10.
Observation of the DLC coating was made under the scanning microscope STEREOSCAN 420, the result of which is shown in FIG. 11.

Examinations of microhardness, of the modulus of elasticity gradient and of the DLC coatings adhesion to titanium surface

Testing of the mechanical properties of coatings applied to the surface of titanium test bars and of the adhesion of DLC coatings to the test bar surface was carried out on a Micro-Combi-Tester, made by CSEM in Switzerland. The tester is equipped with a system for data collection and storing (FIG. 13). The device satisfies the requirements of ASTM standards regarding microhardness testers and enables:

· determination of the microhardness of metallic materials and coatings by Vickers method;
· determination of the modulus of elasticity gradient of the soft, hard, brittle or plastic materials,
· conducting the scratch test in which the following parameters are examined: normal loading, friction force, coefficient of friction, the level of acoustic emission signal monitoring the initiation of cracks in coating, the depth of indenter penetration, and profile of the scratch track.

The scratch test consisted in scratching the surface of the tested material with Rockwell stylus under a specific load (FIG.12). The values of the loading force and the stylus tip penetration depth were recorded in a continuous manner during the whole cycle of loading.
After the test, a scratch appeared on the surface of the test bar; it was examined next under an optical microscope installed on the device. The measured geometrical parameters of the scratch, the microscopic analysis of the scratch, and the signals of acoustic emission which appeared in the case of cracks forming in the brittle top layers of the bar were used as a source of information about the wear behaviour and strength of the tested material.
The scratch test is an effective method to determine the coefficient of the coating layers adhesion to the substrate, a measure of which is the determined critical load L_c. From the loading curve plotted in function of displacement, properties such as: hardness, Young's modulus, penetration depth, and fracture toughness are determined. Applying a minimum stylus loading force, it is possible to take measurements to the depth of less than 1μm, which is of special importance for testing of thin coatings in the case of which any possible effect of substrate deformation on the measured properties should be eliminated.

- mikrotwardość Vickersa - jest automatycznie obliczana przez software MCT, ale może być również wyznaczona pośrednio poprzez pomiar przekątnych odcisku pod mikroskopem urządzenia i przeprowadzeniu dalszych obliczeń własnych.

Pomiary mikrotwardości wykonano stosując następujące parametry[11]:
- maksymalne obciążenie wgłębnika równe 50mN,
- prędkość obciążania i odciążania równa 50 mN/min
- czas działania maksymalnego obciążenia 5s

Wyniki

Test zarysowania (scratch test)

Test zarysowania odbywał się w trzech etapach:
- w pierwszej kolejności wgłębnik Rockwella o promieniu 200 µm, obciążony siłą 0,03N "skanował" powierzchnię próbki w celu określenia jej profilu;
- następnie wykonywany był ruch roboczy - wgłębnik obciążany wzrastającą liniowo siłą aż do wartości 10N, na drodze o długości 2 mm, zarysowywał powierzchnię próbki, która przesuwała się ze stałą prędkością równą 2 mm/min;
- końcowy etap polegał na powtórnym przejściu wgłębnika obciążonego siłą 0,03N po torze rysy, w celu zarejestrowania jej profilu po odciążeniu (R_d).

Przykładowy wykres z badań w postaci zmian wartości siły normalnej, siły tarcia, współczynnika tarcia, głębokości penetracji oraz profilu powierzchni przedstawiono na RYS. 13. Wartość obciążenia krytycznego L_c określono na podstawie pomiaru emisji akustycznej pojawiającej się podczas pękania powłoki oraz optycznie, w wyniku obserwacji miejsc, w których nastąpiło jej zniszczenie (TABELA 1). Wyniki stanowiące średnie arytmetyczne z badań mikrotwardości HV, modułu Younga E oraz zagłębienia wgłębnika Hm w próbce z tytanu bez powłoki oraz w próbce pokrytej powłoką DLC znajdują się w TABELI 2.

Dyskusja

Na podstawie przeprowadzonych badań stwierdzono wyraźny wzrost twardości (HV) próbek z warstwą DLC w stosunku do materiału podłoża oraz nieznacznie większą

Pomiar Measurement	Metoda Method		Wartość średnia Mean value of critical load
	optyczna optical L_c	z emisji akustycznej from acoustic emission L_c	N
1	6,21	5,66	5,94
2	4,34	4,92	4,63
3	5,52	5,07	5,30
			5,29

TABELA 1. Obciążenie krytyczne L_c wyznaczone metodą optyczną oraz z sygnału emisji akustycznej dla trzech pomiarów, wykonanych na próbce z tytanu.
TABLE 1. Critical load L_c determined by optical method and from the signal of acoustic emission for three measurements taken on titanium test bars.

Measurement of microhardness and of the modulus of elasticity gradient

The Micro-Combi-Tester is a device which enables taking hardness measurements by means of the traditional and modern methods through:
· dynamic penetration - microhardness and Young's modulus gradient are automatically computed from the curve of the penetration depth in function of loading, applying the established model of computations. Hardness is computed as a ratio between maximum stylus loading and area of stylus contact with the test bar surface after the load has been released;
· Vickers microhardness - is automatically computed by MCT software, but it can also be determined directly by measuring the diagonals of the indentantion under the microscope of the apparatus and further computations done by the person taking the measurement.

The measurements of microhardness were taken applying the following parameters [11]:
· maximum stylus loading equal to 50nM;
· the rate of load application and release equal to 50 mM/min,
· the duration of maximum load application 5 s.

Results

Scratch test

The scratch test was conducted in three sequences:
· sequence one - the Rockwell stylus of a 200 µm radius, loaded with a force of 0.03 N, was "scanning" the test bar surface to determine its profile;
· sequence two - a working movement of the stylus which, loaded with the force increasing linearly up to a value of 10 N, was scratching the test bar surface along a distance of 2 mm, moving at a constant velocity of 2 mm/min;
· sequence three - the final stage of the test, which consisted in the second movement of the stylus, loaded with a force of 0.03 N, along the scratch track to register its profile after the load had been released (R_d).

Examples of the diagrams where the results of the tests are plotted as changes of normal force, friction force, coefficient of friction, penetration depth and surface profile are presented in FIG.13.
The value of the critical load L_c was determined by the technique of acoustic emission from the crack which appeared in coating and optically as a result of visual inspection of

	Mikrotwardość Microhardness HV	Moduł Younga Young's modulus E [GPa]	Głębokość profilu Penetration profile depth Hm [nm]
tytan	413 ±61	136 ±14	577 ±53
DLC /tytan	747 ±67	153 ±16	461 ±50

TABELA 2. Średnie wartości wyników pochodzących z pięciu pomiarów: mikrotwardości HV, modułu Younga E oraz zagłębienia wgłębnika Hm w próbce z tytanu bez powłoki oraz w próbkach pokrytych powłoką DLC.
TABLE 2. Mean values from the results obtained on five measurements of microhardness HV, Young's modulus E and stylus tip penetration depth Hm in titanium test bars with and without DLC coating.

wartość modułu Younga (E). Twardość warstwy DLC zmierzona przy głębokości penetracji wgłębnika ok. 500nm wynosi 750 HV (ok. 7,36 GPa) i jest mniejsza w porównaniu z danymi literaturowymi (10-25 GPa) [11,12,13]. Prawdopodobnie twardość warstwy, jak również moduł Younga w przypowierzchniowych warstwach są znacznie większe, lecz duża chropowatość powierzchni (wynikająca z chropowatości powierzchni podłoża) uniemożliwia pomiary przy minimalnym zagłębieniu wgłębnika. Ponadto przy głębokości penetracji 500nm i grubości warstwy mniejszej od 1 mm, wpływ na mierzone wartości mikrotwardości HV i modułu Younga E warstwy, ma lokalne uplastycznienie miękkiego podłoża. Niewielka twardość oraz moduł Younga badanej warstwy DLC może być spowodowana również tworzeniem się miękkich obszarów o strukturze charakterystycznej dla polimerów.

Procesowi niszczenia warstwy w teście zarysowania towarzyszy emisja sprężystej fali akustycznej, której źródłem są mikropęknięcia oraz deformacja materiału. Zatem na podstawie analizy sygnału emisji akustycznej można określić siłę, która w tym samym czasie powoduje zniszczenie warstwy. W wykonanych testach zarysowania warstwy DLC na podłożu tytanu, sygnał emisji akustycznej (AE) zarejestrowano po przekroczeniu obciążenia 5N, pomijając wcześniejsze przypadkowe, pojedyncze piki AE (RYS.12). Wartość obciążenia krytycznego L_c=5,3N określono na podstawie analizy sygnału AE oraz obserwacji miejsc, w których wystąpiło jej zniszczenie. W miejscach występowania zniszczenia warstwy, zauważyć można charakterystyczne wytarcia, początkowo na brzegach bruzdy, następnie w jej środkowej strefie, aż do przerwania (przetarcia) powłoki do podłoża. Generalnie stwierdzono dobrą adhezję warstwy do podłoża, a w porównaniu z wynikami literaturowymi, wyznaczona wartość obciążenia krytycznego L_c stanowi zadawalającą wartość [14].

Próbka posiada dobrą sprężystość, a pomimo dużego odkształcenia przy obciążeniu, obserwuje się znaczny powrót sprężysty próbki po odciążeniu. W początkowym zakresie (do obciążenia F_n=0,15N) po odciążeniu jest to powrót całkowity, przy sile F_n ok. 5N głębokość penetracji ostrza (Pd) wynosi ok. 8 µm, a głębokość pozostająca (R_d) po odciążeniu odpowiednio 4 µm. Współczynnik tarcia utrzymuje się na niskim poziomie ok. 0,1 do momentu przerwania warstwy i styku ostrza wgłębnika z podłożem, osiągając maksymalną wartość 0,2 w badanym zakresie.

W celu szerszej interpretacji wyników badań właściwości mikromechanicznych cennym uzupełnieniem byłoby wykonanie analizy struktury warstwy, zwłaszcza określenie charakteru i proporcji wiązań węglowych.

Wnioski

Z dotychczasowych wstępnych badań tytanu przeprowadzonych w ramach niniejszej pracy wynika, że metoda wytwarzania powłok diamentopodobnych techniką implantacji jonowej daje zadowalające wyniki własności mechanicznych i adhezji do podłoża, pod warunkiem bardzo starannego przygotowania powierzchni podłoża .

Przeprowadzone badania pozwoliły na sformułowanie ogólnych wniosków:

1. Modyfikacja warstwy wierzchniej próbek wykonanych z tytanu, ochronnymi powłokami diamentopodobnymi (DLC), przyczyniła się do utworzenia na próbkach, nowej jakości szczelnych warstw wierzchnich, mających na celu zwiększenie biotolerancji materiału, w porównaniu z tradycyjnymi implantami metalowymi.
2. Uzyskane powłoki diamentopodobne wykazały dobrą adhezję do podłoża metalowego oraz korzystne zmiany

the places where the coating failed (TABLE 1). The results, calculated as an arithmetic mean from the measurements of microhardness HV, Young's modulus gradient E, and penetration depth Hm on a titanium test bar with and without the DLC coating, are given in TABLE 2.

Discussion of results

Basing on the results of the carried out tests, a considerable increase in the hardness [HV] of the test bars with a DLC layer compared to the substrate material was stated, while the value of the Young's modulus gradient was only slightly higher. The hardness of the DLC layer measured with the stylus tip penetration depth of 500 nm amounts to 750 HV (about 7.36 GPa) and is lower when compared with the data given in literature (10-25GPa) [11, 12, 13]. Probably, both hardness and the Young's modulus gradient in subsurface layers are much higher, but very rough surface (resulting from the substrate roughness) makes the measurements with minimum stylus tip penetration impossible. Moreover, with the penetration depth of 500 nm and the layer thickness below 1 mm, the measured values of microhardness HV and Young's modulus E are affected by the soft substrate forming local plastic areas. Low values of hardness and Young's modulus in the tested DLC layer may also be due to the formation of soft areas with structure typical of polymers.

The process of the layer destruction in the scratch test is accompanied by the emission an elastic acoustic wave, the source of which are microcracks and material deformation. So, by analysing the signal of acoustic emission, one can also determine the force which causes the destruction of the layer. In the performed tests of scratches made on the DLC layer deposited on titanium substrate, the signal of acoustic emission (AE) was recorded after exceeding the loading of 5 N, omitting earlier, accidental, single peaks of the signal of this emission (FIG.12).

The value of the critical load L_c = 5.3 N was determined from analysis of the signal of acoustic emission and basing on visual inspection of the spots where failures occurred. In the places in which the layer suffered destruction, one can observe characteristic worn-out marks, appearing first on the edges of the groove, and next in its central part until complete breaking (wearing down) of the coating running to the substrate. Good adhesion of the layer to the substrate has generally been stated and, compared with the results published in literature, the determined value of the critical load Lc is quite satisfactory [14].

The test bar has good elasticity, and in spite of the considerable deformation during loading, a distinct elastic spring back of the test bar after release of loading can be observed. In the initial range of the loading values, i.e. up to F_n = 0.15 N, the spring back after load release is complete; with the force F_n reaching approx. 5 N, the stylus tip penetration depth (P_d) amounts to about 8 µm, and the depth remaining (R_d) after load release is 4 µm. The coefficient of friction remains at a low level of about 0.1 till the moment when the layer breaks completely and the stylus tip touches the substrate; then it reaches the value of 0.2, i.e. the maximum within the tested range.

To enable a more comprehensive interpretation of the results of the tests of micromechanical properties, a very valuable supplement would be an analysis of the layer structure, and specially the determination of the character and proportion of carbon bonds.

własności mikromechanicznych powierzchni, a mianowicie: nastąpił istotny wzrost mikrotwardości powłoki w stosunku do mikrotwardości podłoża oraz wzrost odporności na zużycie badanych próbek.
3. Obserwacje mikroskopowe wykazały zadowalającą jednorodność strukturalną na powierzchni oraz na grubości powłoki.
4. W przyszłości, wykonując powłoki metodą implantacji jonowej należy zwrócić uwagę na konieczność bardzo precyzyjnego przygotowania (mycia i czyszczenia) powierzchni metalu przed implantacją.
5. Technologia implantacji jonów, mająca możliwość implantowania dowolnym pierwiastkiem w niskiej temperaturze, pozwoliła na zachowanie niezmienności kształtu i wymiarów elementów obrabianych.

Podziękowania

Badania mikrostrukturalne tytanu zostały wykonane w Instytucie Odlewnictwa w Krakowie, powłoka diamentopodobna DLC na próbkach z tytanu została wytworzona w Instytucie Fizyki Jądrowej w Krakowie, a badania adhezji powłoki DLC do powierzchni tytanu wykonano na Akademii Górniczo-Hutniczej w Krakowie, w Zakładzie Konstrukcji i Eksploatacji Maszyn.

Pismiennictwo

[1] John Enderle i in.. Introduction to Biomedical Engineering. Elsevier Biomaterials Science, Rok 2005
[2] Buddy D.Ratner i in.. Elsevier Biomaterials Science. An introduction to Materials in Medicine. Rok 2003.
[3] Biel Gołaska M., Żuczek R., Warmuzek M.: Dobór materiału oraz warstwy powierzchniowej na implanty metalowe. Praca naukowo-badawcza Instytutu Odlewnictwa zl-2066/00. Kraków 2003.
[4] Shi, Biomaterials and Tissue Engineering. Rok 2004, Wydawnictwo Springer.
[5] Kuś H.: Problemy biocybernetyki i inzynierii biomedycznej. Tom IV Biomateriały. Wyd. Komunikacji i Łączności, Warszawa 1990.
[6]. Marciniak J.: Biomateriały.. Wydawnictwo Politechniki Śląskiej, Gliwice 2002.
[7] Będziński R.: Biomechanika inżynierska. Zagadnienia wybrane. Oficyna Wydawnicza Politechniki Wrocławskiej. Wrocław 1997.
[8] Mitura S., Bąkowski K., Bogusławski G. i in.: Nanokrystaliczny diament dla medycyny.. Inżynieria Materiałowa 2000, Tom. 21, Nr 3, str. 120-124.
[9] Qi Jun and al.: Mechanical and tribological properties of nonhydrogeneted DLC film synthesized by IBAD. Surface and Coatings Technology 128-129 (2000), str. 324-328.
[10] Burakowski T. Implantacja jonów do metalu, Prace Instytutu Lotnictwa, Nr 2-3, Tom 121-122, Warszawa 1990, str.5-51
[11] Rakowski W., Kot M., Zimowski S., Badania adhezji i mikrotwardości powłoki DLC na próbkach metalowych, Raport Laboratorium Tribologii i Inżynierii Powierzchni, Kraków, styczeń 2005
[12] Grabarczyk J. Louda P., Niedzielski P., Poprawa adhezji warstw diamentopodobnych do podłozy z WC-Co przy wykorzystaniu metody RF PACVD, Inzynieria Materiałowa, Nr 5/2005, str. 274-276
[13] Platon F., Fournier P., Rouxel S.: Tribological behaviour of DLC coating compared to different materails used in hip joint prostheses., Elsevier, wear 250(2001) str. 227-236
[14] Yoshinori F., Kaoru A., Haruyuki Y., Tadaaki S.: Adhesion strength of DLC films on glass with mixing layer prepared by IBAD. Surface and Coatings Technology 128-129 (2000), str. 308-312.
[15] http://www.chm.pl
[16] Implantoprotetyka, Tom I, Nr.1, Wrzesień 2000
[17] http://www.fulleren.com.pl
[18] http://www.chifa.com.pl
[19] Biel Gołaska M., Warmuzek M., Żuczek R., Improvement of the titanium surface with a diamond-like carbon coatings, European Congress on Advanced Materials and Processes, 5-8 wrzesień 2005, Praga.naptycznego.

Conclusions

From the initial studies of titanium, which have been carried out so far within the framework of this work, it follows that the method of manufacturing diamond-like carbon coatings by means of ions implantation gives satisfactory results as regards the mechanical properties and adhesion to the substrate, providing that the substrate surface has been very carefully prepared.
The investigations carried out so far allowed formulating the following conclusions:
1. The modification of a top layer on test bars made of titanium and protected with diamond-like carbon coatings (DLC) contributed to the formation on these test bars of the tight top layers of a new quality, increasing the material biotolerance in comparison with the traditional metal implants.
2. The obtained diamond-like carbon coatings showed good adhesion to the metal substrate and advantageous changes of micromechanical properties of the surface, i.e. an essential improvement of substrate microhardness and increased wear resistance of the tested bars.
3. The microscopic observations revealed a satisfactory homogeneity of structure on the coating surface and accross its thickness.
4. In the future, when making coatings by the method of ionic implantation, attention should be paid to the necessity of very careful preparation (washing and cleaning) of the metal surface before implantation.
5. The technology of the ionic implantation, which offers the possibility of implanting any element at low temperature, allows maintaining unchanged the shape and dimensions of the treated objects.

Acknowledgements

The microstructural examinations were performed at the Foundry Research Institute in Cracow, the diamond-like carbon coatings DLC were applied onto titanium test bars at the Institute of Nuclear Physics in Cracow, the adhesion of DLC coatings to titanium substrate was tested at the Department of Machine Design and Terotechnology, Faculty of Mechanical Engineering and Robotics, AGH University of Science and Technology in Cracow. The support and assistance of all these organisations is hereby gratefully acknowledged.

PULSED CATHODIC ARC PLASMA TECHNOLOGY DEPOSITION OF THROMBORESISTANT NANOSTRUCTURAL CARBON COATING ON COMPONENTS OF ARTIFICIAL HEART VALVES

E.I. Tochitsky

Plasmoteg Sciences Engineering Centre of FTI of National Academy of Sciences of Belarus
1/3 Kuprevich st., Minsk, 220141, Belarus.
E-mail: tochitski@bas-net.by

Abstract

This paper describes the results of applying of pulsed cathodic-arc plasma (PCAP) method formation in vacuum biocompatible and thromboresistant t-a carbon coatings on the components of artificial heart valves (AHV).

The special pulsed arc plasma source was used for evaporation of the graphite cathode to form pulsed accelerated carbon plasma flows and deposited them on polished samples of titanium alloys and components AHV made of the same alloys. Influence of the initial voltage of cathode arc discharge in range of 100÷450V and temperature of substrate during the deposition in the range 293÷773°K on structure, phase composition, hardness and biomedical properties coatings were investigated .

The results of investigation of biomedical properties t-a carbon films deposited by PCAP method have shown that the best biocompatibility and thromboresistivity have the nanostructural carbon coatings with cluster size 10-20nm and thickness 0,08÷0,1 microns. The artificial heart valves with deposited nanostructural t-a carbon coatings were implanted on ten animals (dogs). The obtained results have shown that the passing of blood through AHV leads to moderate activation of coagulation processes.

[Engineering of Biomaterials, 56-57,(2006),12-16]

Introduction

Nowadays biological and mechanical artificial heart valves (AHV) are successfully used to treat heart valve function disorders. Comparison of there two kinds of AHV has discovered, that biological prosthesis causes less thrombogenity but it has shorter mechanical durability and life period. It wears out rather quickly, valve insufficiency is developed, the valve doesn˘t close property. Mechanical AHV has longer mechanical durability and is resistant to wear [1]. Its life period is more that 30 years. However it injures blood elements shapes, causes blood coagulation process activation, that results in developing of thromboembolitic complications.

The problem of creating biomaterials for artificial human organs, especially artificial heart valves, arises from a number of specific requirements connected to their influence on living body. A material should not be toxic, allergic, traumatizing living tissue, it should be resistant to wear and mechanical destruction and should not cause hemoles and blood coagulation, change its structure and surface configuration, transform chemically or decompose [2, 3]. Such metals and alloys as stainless steel, Ti, Ta, Co-Cr and others have received the greatest spreading as biomaterials for medical purposes. But side by side with such merits of these materials as high strength, long life, good technology of treatment, they have great shortcomings, such as biological incompatibility, not sufficient resistance to the influence of biological environment, and excite allergy. This problem can be solved by protection of an implant surface with special coatings [4, 5].

Methods of preparation and examination DLC coatings

The special pulsed are plasma source was used for evaporation of the graphite cathode to form accelerated pulses carbon plasma flows and to deposit them on polished titanium alloys samples and AHV components. The deposition conditions were as follows: initial voltage of arc discharge 100÷350V, arc current amplitude 2000÷3500A, pulse energy 10÷150J, pulse frequency 5÷8Hz, pressure of the vacuum chamber~10^{-3}Pa, substrate temperature 293÷673°K.

Transmission electron microscope (TEM) JEM 200CX was used to investigate structure of the DLC films.

Raman and X-ray photoelectron spectroscopies were employed to characterize the chemical atomic bond and composition of the DLC coating. The photoelectron spectrometer EC-2401 with Mg-Ka radiation ($h\omega$=1253.6 eV) was used.

Nanohardness was measured by Scanning Probe Microscope and nanotribology was determined by Digital Scan-3100 (both made of Digital Instruments).

Medical tests were carried out with blood of ten dogs which had implanted AHV with DLC coating.

Results and discussion

Contact of an alien material with blood leads to formation of a blood plasma albumen layer on the material surface, the dynamic of composition and structure alteration of which to a great extend determines physicochemical and biocompatible properties of an implant surface. As it is shown by results of scientific research and practical surgery with organs implantation the best biocompatible and medico-biological properties have the surfaces with minimal value of interface free energy of implant's surface and biological habitat which are composed of interchanging hydrophile and hydrophobe domains with size less than 10-50nm (i.e. nanostructural surfaces). If such conditions are observed the surface absorbs a minimal albumen quantity easily interchangeable with blood plasma albumen what results in the rise of bio- and hemocompatibility of the implant. The DLC coatings are the more preferable [6-11]. Carbon coatings don't have general toxic, allergenic and carcinogenic influence and they aren't histotoxic. These coatings are thromboresistive, biocompatible with blood sells don't make influence on blood plasma albumen and don't change activity of plasma enzymes.

We produces biocompatible thromboresistant DLC coatings manufactured from pulsed flows of carbon plasma by the method of pulsed cathodic-arc deposition. The results of DLC coatings deposition in vacuum on the AHV components from titanium alloy VT16 are presented. The influence of the initial voltage of cathode arc discharge in the range of 100-450V and the temperature of AHV components during the deposition in the ranges of 293 -773°K on structure, phase composition, adhesion, tribology and hardness of DLC coatings were investigated. The deposited

particles in our process are usually high energetic ions (carbon is once ionized at 98%). High ionization takes place due to a very high power density presenting at the surface of the feedstock material, i.e. carbon in the case of diamond-like carbon. Deposition by high energetic ions has two advantages. The first advantage is that the ions react more likely with the substrate than with neutral atoms and molecules and the second advantage is that usually at impact of high energy ions, which embed partially into substrate surface. As a result dense, inorganic coatings with an excellent adhesion can be deposited virtually on any material. All our pulsed plasma processes were executed in a vacuum chamber with a base pressure of about 10-3Pa. The pulsed plasma discharge was formed by a short-time electrical arc erosion of cathode material by extremely hot microspots of a vacuum arc discharge. In addition the plasma can be accelerated with a Hall-type plasma accelerator and directed towards the substrate where a coating is deposited.

The generation of the pulsed plasmoids is obtained by short-term electrical erosion of cathodic material by hot cathodic microspots of pulsed vacuum arc, burning on the integral "cool" surface. The plasma flows or plasmoids, periodically generated by the Hall's arc accelerator, were accelerated and directed onto the substrate, fixed in the substrate holder. As a result of condensation of the plasmoid material thin films and coatings are formed on the substrate surfaces.

A new Hall's pulsed accelerator of electroerosive plasma for technological purpose has been designed and developed to realise the pulsed method [12]. The plasma source gives a possibility to obtain the thin films and coatings on the base of metals, their allows and combinations of nitrides, carbides etc, and also of diamond-like carbon.

The scheme of without contact ignition plasma source is presented in the FIG.1. The plasma source has ignition system which to use a localised electrical contact between cathode 1 and the thin film conductor 2, deposited on the surface of an insulator 6. In our plasma source the above localised contact moves from pulse to pulse by the cathode 1. A such technical design provide a high discharge ignition probability and practically avoid the erosion of an insulator, providing a long life of the ignition system.

The plasma source consists from three main units: a cathode unit, an anode unit and a discharge ignition unit. The cathode unit has the main plasmaforming expendable electrode - the cylindrical cathode 1 which is fixed on the end of cooling cathode holder 3. There is a bellows which allow to move the cathode in the plasma generation zone after its partial evaporation. This gives the constant diagram of distribution of accelerated plasma flows. In the plasma source the discharge ignition is executed by a discharge between the ignition electrodes 4 and 5, having the contact with thin film conductor 2 deposited on a dielectric 6. The solenoid 7 is used to increase the discharge stability ignition. The plasma source anode unit is composed by an anode 8 and a focusing solenoid 9. The assembly of generator units is effected by the clamps 10. A control semiconductor valve 11 is used for discharges commutation. The ignition capacitor 12 of 10-20μF is discharged by this valve. The pulse arc discharge is made by energy of capacitors battery 14 having a capacity of 2-4 thousand of microfarads.

The generator works in the next consecution. After obtaining in the vacuum chamber on which is fixed the generator the pressure less than 10-3 Pa, the capacitor bank 12 is charged up to a voltage of 500 - 800V, and the capacitors batteries 13 and 14 is charged up to 150-400V. The control signal going on the valve 11 perform the discharge of the capacitor bank 12. The appearing current pulse evaporates the film conductor 2 and creates the appearance of initiating plasma in the area of the localised electrical contact on the electrode 5 and cathode 1. The plasmoid creates a conductivity channel between the cathode 1 and the ignition electrode 5. This is excite the discharge of the capacitor13 and forming of the cathode spots. The material of evaporated in the cathode spot is almost fully ionised. The plasma jets expend in all directions and some fraction of the plasma makes contact with anode.

The further development of the initiating discharge bring to filling of the space between the cathode 1 and the anode 8 by the plasma what due to the beginning of a main discharge by the energy accumulated in the capacitors battery 14. The solenoid 9 create a magnetic field to focus and accelerate plasma. It is generate plasma flows of cathode material. The necessary coating is formed from deposited plasma flows on the surface of manufacturing articles.

The FIG.2 presents the oscillograms of alteration of discharge current between the plasma source electrodes in the process of one pulse. The curve 1 shows the discharge current alteration between the ignition electrodes (unit scale 100 A), the curve 2 shows the main discharge current alteration between the cathode and the anode (unit scale 1000A). The time of the ignition pulse is 25 μs, the time of

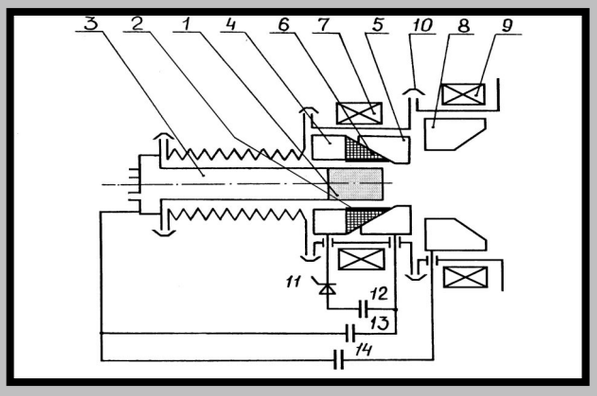

FIG. 1. Schematic illustration of the Hall's plasma accelerator used for pulsed arc deposition DLC coatings.

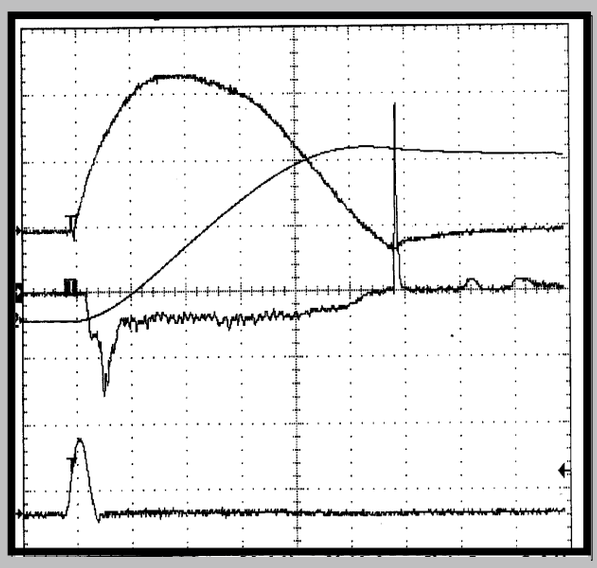

FIG. 2. Oscillogram of the parameters disharge

the main erosion pulse is 200 μs. The integral current between the cathode and the anode is determined by the curve 3.

The current of plasma going through Longmur probe sensor (the curve 4) is measured during the discharge. The contribution of ion current in the plasma flow is approximately 10% of the arc current. Electrons of plasma reach the probe in 8 μs after main pulse beginning and ions of plasma reach the probe only after 240μs. The electrical current is provided by a flow of electrons from the cathode to the anode which is significantly faster than the velocity of the ions. The electron velocity was 1.5×10^7cm/sec and the ion velocity was 0.5×10^6 cm/sec, difference 30 times.

the deposited DLC films have the same chemical composition as the graphite cathode. The DLC films have carbon 98% and oxygen 2%, but the graphite cathode has a little more oxygen.

The films have a low content of impurities. The total amount of impurities is ~3% on layers surface of a thickness of 5nm, and in deeper layers it is less than 2%. The main impurity was oxygen and while secondary impurity ion mass spectroscopy analysis showed the presence of traces of Cr,Fe,Ni, which probably concerns the sputtering of vacuum chamber parts.

The results of electron microscopy and diffraction analysis indicate that the quasiamorphous disordered phase contains crystalline inclusions of different carbon modifications, with size 5÷15 nm (FIG. 3). At the same time one can see larger crystalline inclusions with diamond structure. Crystalline inclusions have a comparatively small volume in films, therefore the quasiamorphous phase has the main influence on DLC-films properties.

Properties	Diamond films CVD	Hydrogenized films α-C:H	Arc plasma deposition films tα-C	Diamond (Type II)
Microhardness (GPa)	70-90	18-40	40-100	57-100
Young's modulus (GPa)	986-1050	50-150	450-600	1079
Density (g/cm^3)	3.5	1.8-2.4	2.4-3.4	3.52
Friction coefficient, up to	0.05	-	0.05	0.05
Resistivity (Ohm·cm)	up to 10^{12}	$10-10^{14}$	10^4-10^9	10^{14}
Thermal conductivity (W/m·°K)	600-1800	0.2-0.5	3-9	2000
Refraction index (λ=583nm)	2.4-2.45	1.7-2.3	2.4-2.7	2.44

TABLE 1. Properties of diamond and DLC films.

Our experiments have shown that the deposited DLC films have a good adhesion with different materials of substrate. The DLC films exhibited a density mass up to 3.4 g/cm^3, electrical specific resistance at different conditions is from 10^4 up to 10^9 Ohm×cm, the temperature of structural transformation to graphite was higher than 673°K [13]. TABLE 1 shows the results of comparison of some properties of DLC films with natural diamond and carbon films prepared by using other methods.

For explain the film properties we have conducted complex studies of their structure, chemical and phase composition by electron microscopy, Raman and photoelectron spectroscopies, nanohardness and nanotribology [13].

DLC films deposited on surface AHV components have thickness 0.5÷0.2μm. therefore for measurement of hardness it's necessary to use nanohardness. The result of measurements were shown that DLC films hardness depends from condition of deposition and achieves hardness of natural diamond up to 100GPa.

Chemical composition investigation performed by means of X-ray photoelectron spectroscopy method has shown that

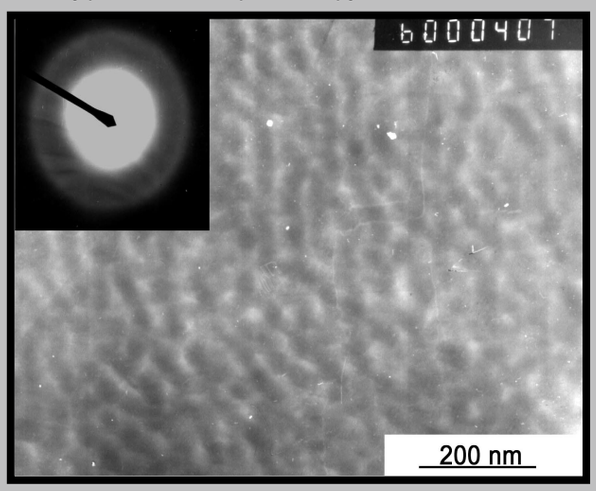

FIG. 3. TEM image and a diffraction pattern of nanostructure of the DLC film.

The electron diffraction patterns of the quasiamorphous phase in carbon films exhibits from two to six diffusive rings which may differ by their position, intensity and shape in various samples and can be described by that of small cluster models. It was found that DLC films deposited from pulsed vacuum plasma flows represent a nanostructural condensate with ordered nanoclasters of a size of about 0.5-2.5 nm with coherently dispersed electrons (FIG. 4) and have a diamond structure which organize clusters more larder sizes 5÷15 nm. Between these nanoregions there are carbon atoms located in disorder.

Different DLC films properties are due to different correlation of sp, sp^2 and sp^3 atomic bonds [14-16]. It was shown that possible changing the deposition conditions to obtain

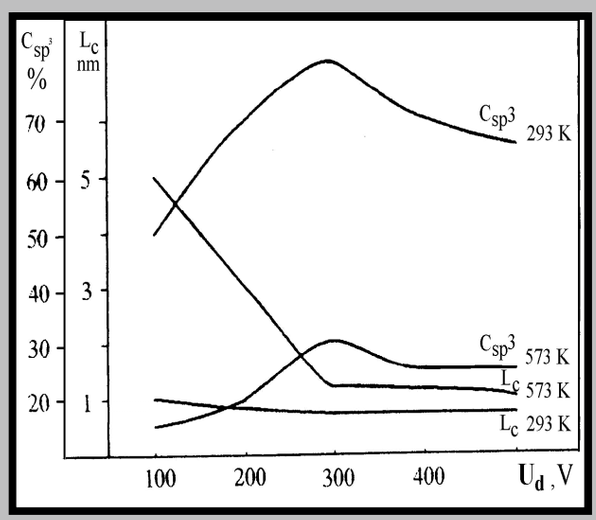

FIG. 4. The dependence of Csp^3 atomic bonds and Lc area size of coherent electron scattering on main discharge voltage Ud for substrate temperature of 293°K and 573°K.

Indices	Control group	After an AHV implantation						
		1-3 days		P	1 month		P_1 <	P_2<
	n=10	1 group (n=14)	2 group (n=10)		1 group (n=9)	2 group (n=7)		
Time of coagulation in non siliconized test-tube (sec)	491.0±12.l	347.2±13.8	660.0±ll.6	0.001	366.0±23.2	432.0±6.7	0.05	0.001
Time of coagulation in siliconized test-tube (sec)	688.5±12.5	412.2±80.8	780.0±8.9	0.05	532.0±66.2	794.0±18.5	0.05	0.5
Autocoagulogramme 8 min	13.8±0.3	15.2±0.9	13.0±0.6	0.5	12.0±0	20.6+0.6	0.001	0.001
10 min	16.7±0.3	15.6±1.2	14.0±l.2	0.05	12.3±0.8	24.6±0.8	0.001	0.001
PTI %	86.3±3.2	94.4±3.7	96.5+14.1	0.5	89.3±4.9	78.2±4.6	0.001	0.06
Fibrinogen A (mg)	96.6±4.7	296.0±35.9	126.6±l.0	0.05	371.6±35.6	123.0±4.7	0.05	0.001
Tolerance of plasma to heparine (sec)	231.0±3.2	112.0±10.8	188.0±22.0	0.1	100.0±56.3	147.4±6.2	0.008	0.06
Thrombus time (sec)	28.3±1.9	27.4±0.9	29.0±l.2	0.5	21.8±1.4	25.0±1.7	0.05	0.005
Fibronolisis euglobuline (sec)	3324±33	3442±48	3090±17	0.001	3412±41	2620±101	0.001	0.003
Hematocryte	45.0±0.9	47.8±5.2	41.0±0.6	0.05	48.3±4.2	40.4±l.0	0.05	0.5

where: P – truth of data comparison after 1-3 days and data of control group
P_1 - truth of data comparison after 1 month and data of control group
P_2- truth of data comparison after 1 month and 1-3 days after operation

TABLE 2. Coagulation data of the peripheral blood of dogs after implantation AHV with the DLC coating.

DLC films with the predominance of tetrahedral (sp^3-diamond) types of bonds between carbon atoms. Determination of bonds between carbon atoms C-C sp^3 and C-C sp^2 is realized using X-ray photoelectron and Raman spectroscopy. For example FIG. 4 shows the correlation of the number of sp^3 bonds on main discharge voltages for different substrate temperatures. One can see that this dependence has a non-linear behavior. Diamond type sp^3 bonds are most prevalent with main discharge voltage of 300V. It was ascertained that the properties of both DLC-films prepared by pulsed vacuum arc plasma deposition and all DLC film-titanium substrate samples have high chemically inert and biocompatible.

On the base of investigations of DLC coatings property dependence on deposition conditions there were chosen optimal parameters of cathodic-arc evaporation of graphite target with formation of carbon plasma flows and their condensation on surface of substrates from titanium alloys VT-16 and on components of AHV made of VT-16 alloy. The investigation results have shown that the deposition of DLC coatings increase considerably wear resistance and chemical fastness of researching alloys. DLC coatings of 0.08-0.1μm thickness were deposited on AHV components at different deposition modes and than was executed a medico-biological testing of AHV to determine their thrombogenity and biocompatible.

Comparative experiments with dogs were executed to discover the effectiveness of DLC-coating details AHV [17]. The AHV "PLANEX" was implanted to 14 dogs (1 group) and AHV "PLANEX" with DLC coatings was implanted to 10 dogs (2 group). For both groups autocoagulography coagulation period was defined in 8 and 10 minutes to determine the first hemostasia phase. The protrombin index, fibrinogen A level, the prothtrombin period of spontaneous and euglobulin fibripoliosis were defined to determine the second hemostasia phase.

The data of venous and aortic coagulography peripheric blood as well upper and bellow the AHV implantation were analyzed to expose the AHV influence on hemostasia system. TABLE 2 demonstrates the results of the investigations.

A month later after the implantation a well-noticeable hypercoagulation and increased level of fibrinogen A were observed in the peripheric blood of the dogs (group 1). Coagulation indexes approached the normal in the dogs (group 2) which were implanted AHV with DLC coatings. The coagulation period was increased, PTI index came back to initial state, the number of fibrinogen A and hematocritis figures were decreased. Thus brightly expressed thrombogenios influence of AHV "PLANEX" without DLC coatings on the blood coagulation system on both local and systematic levels was preserved for a month.

Conclusion

According to results of thrombogenity investigations there were optimized the conditions of DLC- coatings deposition on AHV components and there were prepared AHV which were implanted to animals. For determine the thrombogenity of AHV the blood for analysis was taken before and after implanted AHV. Coagulogramme was studied during one month. The obtained results have shown that the passing of blood through AHV leads to moderate activation of coagulation processes. The AHV with DLC coatings which prepared by pulsed cathodic arc plasma deposition have vastly less thrombogenity than the AHV without DLC coatings.

AHV with DLC coatings influenced much less expressively hypercoagulating on the central and peripherical blood stream starting with the first month in the body. Taking into consideration, all the above mentioned should be recommended preferably to apply in clinical practice.

References

[1] Y.P. Ostrovsky., Disk artificial hart valves Planex, J. Engen. Phys. and Thermophys., 69, 3, 478-488 (1996) (in Russion).
[2] Gotman, Characteristic of metals used in implant., J. Endourology Dec.11(6), 383-389 (1997).
[3] E.Knott, H. Reul, M. Knoch et.al., In vitro comparison of aortic heart valve prostheses, Part 1: Mechanical valves, J. Thorac. Cardiovasc. Surg., 96, 6, 952-961 (1998).
[4] H.S. Tran, M.M. Puc, C.W. Hewitt et al., Diamond-like carbon coatings and plasma or glow discharge treatment of mechanical heart valves, J. Invest. Surg., 12, 133-140 (1999).
[5] E.I. Tochitsky, O.G. Sviridovich, N.M. Beliavsky, Deposition of Biocompatible Thromboresistant Coatings from Pulsed Plasma on Artificial Heart Valves, VI Int. Conf. Plasma Physics and Plasma Technol.- Proceedings Book, 2, 471-474, Minsk, Belarus, September 15-19, 2003.

[6] Dion, C. Baquery, J.R. Monties, Diamond: the biomaterial of the 21st century, Inter. J. Art. Org., 16, 623-627 (1993).
[7] Dion, X.Roques, C. Baquey, et. al., Hemocompatibility of diamond-like carbon coating, Biomed. Mater. Eng., 3, 51-55 (1993).
[8] L.Lu., M.W. Jones, Diamond-like carbon as biological compatible material for cell culture and medical application, Biomed. Mater. Eng., 3, 223-228 (1993).
[9] L Tang, C.Tsai, W.W. Gerberich et. al., Biocompatibility of Chemical Vapour Deposited Diamon, Biomaterials, 16, 483-488 (1995).
[10] L.A. Thomson, F.C. Law, N. Rushton, Biocompatibility of diamond-like carbon coating, Biomaterials, 12, 37-40 (1991).
[11] M.I. Jones, I.R. McCol, D.M. Grant et.al., Hemocompatibility of DLC and TiC-TiN interlayers on titanium , Diamond and Related, 8, 457-462 (1999).
[12] E.I. Tochitsky, O.V. Selifanov, V.V. Akylich et.al., Electrical Erosion Pulsed Plasma Accelerators for preparing Diamond-like Carbon Coatings, Surf. and Coat. Techn., 47, 522-527(1991)
[13] E.I. Tochitsky, A.V. Stanishevskii, I.A. Kapustin, et.al., Structure and properties of carbon films prepared by pulsed vacuum arc deposition, Surf.and Coat. Techn., 47, 292-298 (1991).
[14] A.V. Stanishevsky, E.I. Tochitsky, Formation of Metastable Carbon Film Structure by pulsed Arc Plasma deposition in Vacuum, J of Chemical Vapor Depos., 4, 297-310 (1996).
[15] T.L. Parker, K.L. Parker, I.R. McColl et.al., The biocompatibility of low temperature diamond-like carbon films: transmission electron microscopy, scanning electron microscopy and cytotoxicity study, Diamond and Related Mater., 3, 1120-1123 (1994).
[16] Y.X. Leng, J.Y. Chen, P. Yang et.al., Mechanical properties and platelet adhesion behavior of diamond-like carbon films synthesized by pulsed vacuum arc plasma deposition, Surface Science, 531, 177-184 (2003).
[17] S.I. Korsak, Thrombogenous artificial vales Planex of dependence from type of surface coating, Zdravookhranenie, 8, 14-18 (1997) (in Russion).

THE CHLORINATED SYNTHETIC DIAMOND SURFACE INTERACTION WITH C-NUCLEOPHILES

V.V. Korolkov, B.N. Tarasevich, I.I. Kulakova, G.V. Lisichkin

Department of Chemistry,
Lomonosov Moscow State University,
Leninskie Gory 1, build.3, Moscow, 119992, Russia
E-mail: korolkov@list.ru

Abstract

Several reactions of C-nucleophiles with the chlorinated surface of two types of diamond were implemented. Detonating nanodiamond "UDA-SF" and synthetic diamond "DALAN" have been employed in the above procedures. The incorporation of butyl and nitrile groups has been achieved. However the incorporating of phenyl groups via reaction with PhLi is still a problem. For the first time NMR-H1 spectroscopy of suspension was used for elucidating structure of grafting compound was proposed.

Keywords: *nanodiamonds; grafting compounds; surface chemistry; chemical functionalization.*

[Engineering of Biomaterials, 56-57,(2006),16-19]

Introduction

There is an escalating interest in diamond chemistry to nanoscale diamonds in recent years [1]. It is due to several reasons. The first is that nanodiamonds (ND) became commercially available only in last ten years [2]. The second and obviously the most significant ones are their unique properties which combine mechanical, termic, radio and chemical stability of diamond as well as lability of functional cover of surface. The latter is determined by large value of specific surface area in ND. In various patterns of NDs specific surface area is about 300 m^2/g or less whereas in the case of natural or synthetic diamonds powders the value of specific surface area usually is about several metres per gram. Such large value of specific surface area of NDs substantially increases possibilities of their further chemical modification and moreover enlarges the field of potential application of diamond materials. Among the most attractive utilizations of NDs are biomedical applications (nanoparticles for drug carry in vivo) and development of new chromatographic materials, especially for HPLC.

Also stable hydro- and organosoles of NDs are required for many technological applications. Therefore the problem of chemical modification of ND particle surface is of current importance. Besides modification of ND surface is attractive as a technique for unification of surface chemical state.

Notwithstanding the fact that NDs is a promising material the number of works concerning chemical modification of its surface is rather modest [3,4,5]. Therefore investigations on controlled chemical creation of grafting compounds on the ND's surface are of fundamental and technological importance.

Experimental

In the present work two types of diamond were employed: detonation nanodiamond "UDA-SF" and synthetic diamond powder "DALAN". "UDA-SF" is typical nanodiamond with the size of aggre-gates no more then 0.04 μm and specific surface area 245 m^2/g (BET measurement). Synthetic diamond powder "Dalan" used represents itself a polydisperse powder with the size of particles from 5 nm up to 10 microns with a specific surface area of 22 m^2/g (BET measurement).

Chemical state of diamond particles was characterized using Fourier-transform spectroscopy (IR200 Thermonicolet), NMR-H1 - spectroscopy (Bruker-Avance-400).

Results and discussions

It is necessary to mention that in native state the surface of diamond powder is covered by different oxygen containing groups (for ex. alcohol, carboxyl, carbonyl and others that is firmly confirmed by infrared spectra [6,7]), i.e. the surface is polyfunctional. And this fact complicates any further chemical reactions on the diamond surface due to nonselectivity of their passing. Consequently the polyfunctionality arises the problem of unification of diamond surface in order to make reactions that are carried out on it to be selective.

The most common procedure of unification, and moreover the only one, consists in hydrogen stream treatment of diamond at 1073 or 1173 K for 4 or 5 hours. These conditions are sufficient to modify the diamond surface in a way of hydride group's layer formation (Scheme, FIG.1).

It should be noted that specific surface area of diamond powder is slightly affected by this treatment as determined by BET analysis. So, after such treatment we obtained a fully hydrogenated diamond surface that is confirmed by IR-spectra presented (FIG.2).

As we can see from spectra, after such treatment stretch-

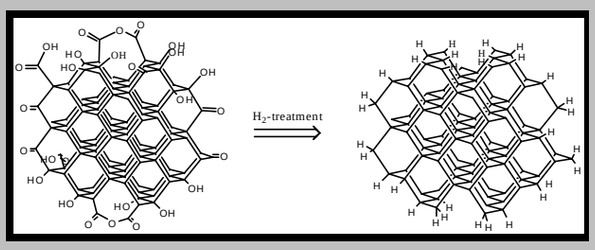

FIG. 1. Scheme. Reduction of diamond surface.

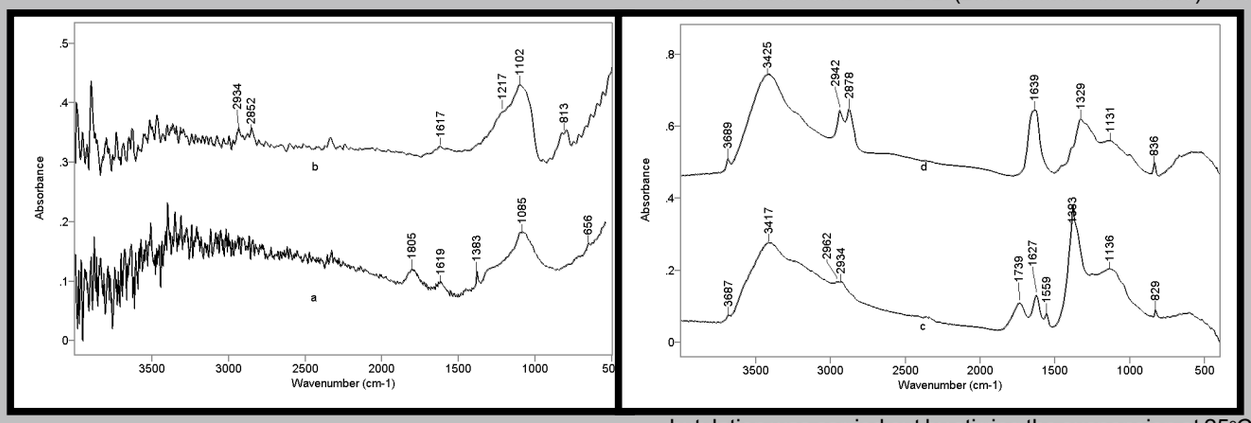

FIG. 2. FTIR spectra: a, c - pristine "DALAN" and "UDA-SF", b, d - the same diamonds after hydrogen stream treatment at 800°C for 5 h.

ing vibration related to C=O-group disappeared whereas two stretching vibrations of CH - bonds appeared. In the case of "UDA-SF" (FIG.3 spectra c and d) very strong adsorption of hydroxyl groups (3400-3500 cm^{-1}) is present even after hydrogen treatment.

By the way with the loss of polyfunctionality of the diamond surface we also have lost its reac-tion capacity within the formation of the CH-bonds on the surface.

In order to activate the surface in terms of electrophile center creation it was subjected to chlorination. Chlorination was performed in two ways. In case of "DALAN" chlorination was carried out by treating sample with sulfurylchloride in the presence of azobisisobutyronitrile (AIBN) in benzene in Ar ambient at 50-60°C. Photochemical chlorination by molecular chlorine dissolved in carbon tetrachloride was employed in case of "UDA-SF". As it was found by elemental analysis this treatment resulted in the ultimate chlorinated diamond surface formation. It is worth to point out that further treatment of "DALAN" with sulfurylchloride is yielded in sulfonylchloride group's layer

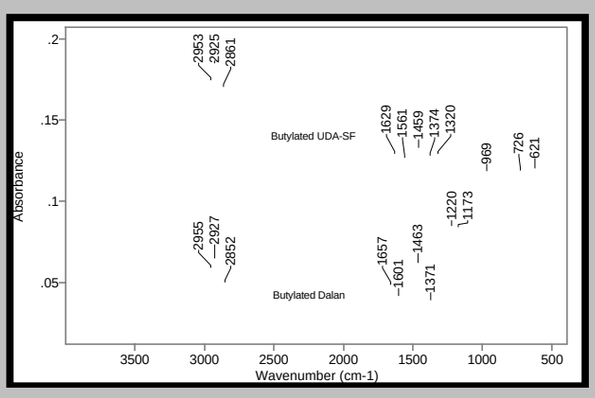

FIG. 3. FTIR spectra of butyklated samples of „DALAN" and „UDA-SI".

formation.

Speaking of chlorinated diamond powder one should always keeps in mind that "fully chlorin-ated" doesn't mean that all surface bonded hydrogen atoms are substituted by chlorine. It only means that no further chlorination is possible under described conditions and that is due to steric hindrance or repulsion between chlorine atoms on the surface.

Further reactions of chlorinated of both types of diamonds were carried out after an exhaustive vacuum evaporation of the reaction mixture. The chlorinated diamond powder was then treated with n-BuLi (2.5M solution in hexane). The butylation was carried out by stirring the suspension at 25°C for 24 h under an argon atmosphere. It should be noted that initially reaction mixture was subjected to ultrasonic treatment (50 Wh, 35±10% KHz) for 1.5 hours. The reaction was then terminated by adding water to the solution. The powder was then repeatedly washed with acetone, ether and water to remove LiCl and other organic by-products, and was dried in vacuum (<1 mm Hg.) for several hours and then characterized by FTIR spectroscopy.

This makes it possible to incorporate n-butyl groups onto the diamond surface which clearly seen from IR-spectra presented (FIG.3).

As it can be obviously seen from spectra presented the new vibrations appeared in the region of 3000-2800 and 1500-1300 reciprocal centimeters that are related to stretching and bending vibra-tions in alkyl chains, i.e. in butyl groups bonded to the diamond surface. Also frequencies assigned to stretching and bending vibrations of alcohol groups appeared too.

IR spectroscopy supplies us only with qualitative data. We can only see appearance or disap-pearance of certain bands in spectrum but very little can be gathered about the structure of grafted sub-stance. In order to precisely determine the structure of surface groups we have proposed a simple tech-nique utilizing NMR-H1 spectroscopy. We have collected NMR-H1 spectrum of suspension of n-Bu-UDA-SF in $CDCl_3$ (FIG.4). And it clearly indicates the presence of n-Bu group on the diamond sur-face.

Reaction of phenyl lithium (1.2M solution in Et_2O) with chlorinated diamond surface of "DALAN" was carried out in the same manner as with butyl lithium. FTIR spectra presented bellow (FIG.5).

But unfortunately the interpretation of IR-spectra of phenylated diamond surface isn't so vivid as with butylated diamond surface. For instance none of CH-bond stretching vibrations can be observed in spectra whereas bending vibrations (1488 and 1431 cm^{-1}, 1504 and 1434 cm^{-1}) are pre-sent. Thus in this case direct evidence of Ph-group grafting on to the diamond from IR-spectra cannot be obtained. In order to prove phenyl groups bonding to the diamond surface we treated phenylated diamond "Dalan" with nitrating mixture (hydrogenated diamond was also treated in the same way for comparison). In the case of phenylated diamond a

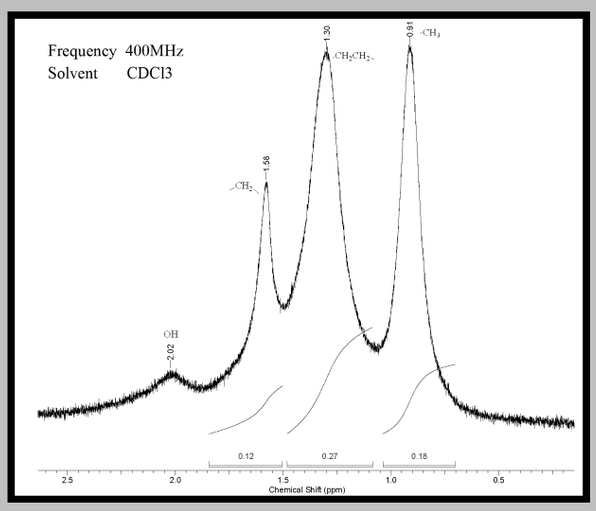

FIG. 4. Utilization of NMR-H1 spectroscopy of modified diamond suspension for elucidation structure of grafting compounds (by ex. of butylated UDA-SF).

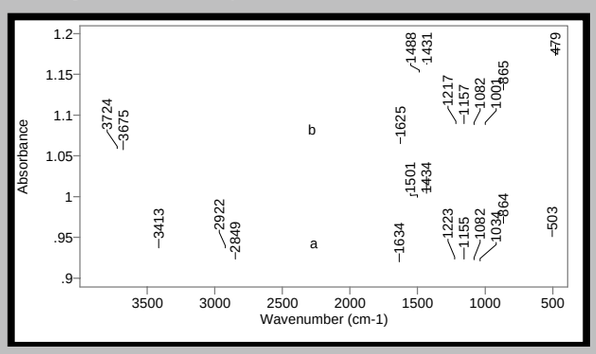

FIG. 5. FTIR spectra of phenylated „DALAN": a - sample was treated with SO_2Cl_2 for 22 hours and then treated with PhL obtained via exchange reaction n-BuLi+PhBr in Et_2O; b - sample was treated with SO_2Cl_2 for 8 hours and then treated with PhLi obtained via reaction of met. Li with PhBr in Et_2O.

new adsorption at 1536 and 1347 cm^{-1} has appeared and these are due to antysimmetrical and symmetrical vibrations in NO_2 - group in $-C_6H_4-NO_2$ - fragments formed during nitration (FIG.6). No adsorption at 1536 and 1347 cm^{-1} was found in the case of hydrogenated diamond.

Thus we get an indirect evidence of incorporation of phenyl groups onto the diamond surface.

Our attempts to incorporate phenyl groups onto the "UDA-SF" surface via reaction with PhLi obviously have failed. On FIG.7 one can see FTIR spectra for the pristine, hydrogen treated and subjected to phenylation "UDA-SF". Phenylation was performed by adding a solution of PhLi in Et_2O (obtained via exchange reaction: n-BuLi + PhBr) to photochemically chlorinated for 24 hours "UDA-SF". FTIR spectra of treated sample clearly indicates that no phenyl groups are incorporated onto the surface at appreciable concentration. The only result of such treatment is only additional hydroxylation of diamond surface.

Nitrile group on the diamond surface is very attractive due to various possible ways of its trans-formation. So as to incorporate cyanide groups on to the surface of "DALAN" and "UDA-SF" a solution of sodium cyanide in anhydrous dimethylsulfoxide was added to chlorinated diamond powder. The reaction was carried out by stirring the suspension

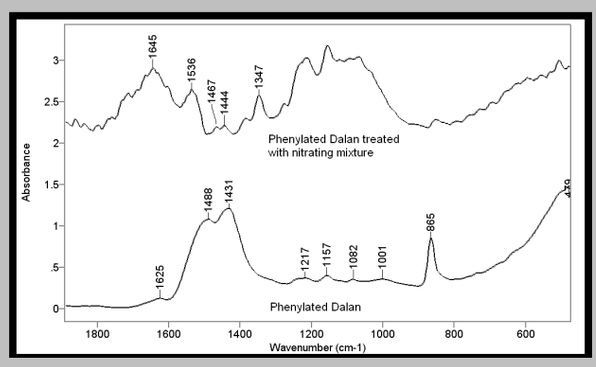

FIG. 6. FTIR spectra of phenylated „DALAN" and the same sample subjected to nitration by mixture of HNO_3 and H_2SO_4.

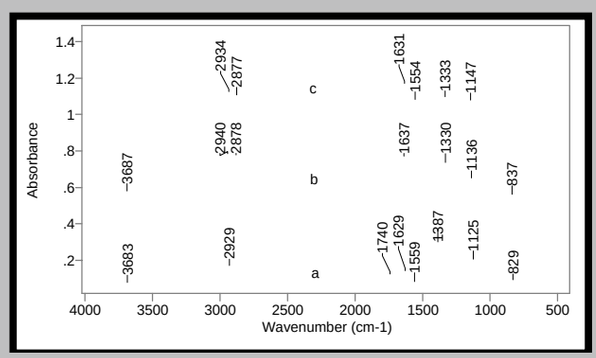

FIG. 7. FTIR spectra: a-pristine UDA-SF, b-hydrogen treated, c-"phenylated".

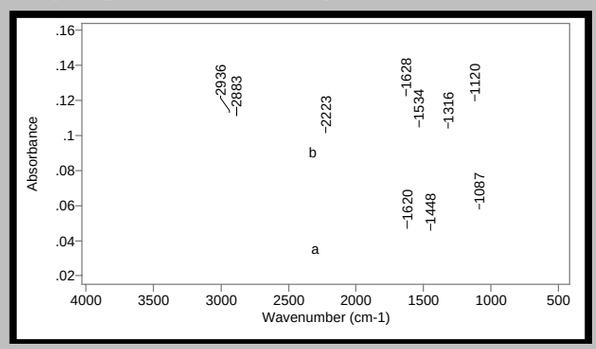

FIG. 8. FTIR spectra: a-NC-DALAN, b-NC-UDA-SF.

at room temperature for 24 h. The powder was then filtered, repeatedly washed with water and acetone, dried and characterized by FTIR spectroscopy (FIG.8). In both cases FTIR spectra showed strong disappearance of the CH-bond stretching vibrations but only in "UDA-SF's" spectrum new frequency ascribed to CN-group vibrations have appeared at 2223 cm^{-1}. The most evident reason explaining this fact is low concentration of nitrile groups on the surface of "DALAN" which has comparatively small specific surface area (22 m^2/g).

Conclusion

Reactions of several C-nucleophiles with chlorinated diamond surface were investigated and new modified diamonds with n-butyl and nitrile groups were obtained. For the first time NMR-H1 spectroscopy of suspension was proposed to elucidate structure of grafting compounds that can be helpful for fast and precise determination of organic functional groups on the surface.

References

[1] Dolmatov V. Yu. Detonation synthesis ultradispersed diamonds: properties and applications // Russ. Chem. Rev. - 2001. - 70, 7. - P. 607-626.
[2] V.V. Danilenko On the History of the Discovery of Nanodiamond Synthesis // Physics of the Solid State - 2004. - 46, 4. - P. 595-599.
[3] Y. Liu, Z. Gu, J. L. Margrave, V. N. Khabashesku Functionalization of Nanoscale Diamond Pow-der: Fluoro-, Alkyl-, Amino-, and Amino Acid-Nanodiamond Derivatives // Chem. Mater. - 2004. - 16, 20. - P. 3924-3930.
[4] Yu Liu, V. N. Khabashesku, N. J. Halas Fluorinated Nanodiamond as a Wet Chemistry Precursor for Diamond Coatings Covalently Bonded to Glass Surface // JACS. - 2005. 127, 11. - P. 3712-3713.
[5] A. Xiaoning, Z. Hanmin Functionalization of carbon nanobeads and their use as metal ion adsorb-ents // Carbon - 2003. - 41, 15. - P. 2889-2896.
[6] Jiang Tianlai, Xu Kang, Ji Shengfu FTIR studies on the spectral changes of the surface functional groups of ultradispersed diamond powder synthesized by explosive detonation after treatment in hydrogen, nitrogen, methane and air at different temperatures // J. Chem. Soc., Faraday Trans. - 1996. - 92, 18. - P. 3401-3406.
[7] T. Jiang, K. Xu FTIR study of ultradispersed diamond powder synthesized by explosive detonation // Carbon. - 1995. - 33. - P. 1663-1671.

GROWTH OF CELLS ON CARBON COATINGS MANUFACTURED IN NEW MW/RF REACTOR

I. Šubrtová*, L. Grausová, L. Bačáková**, W. Kaczorowski*****

*Department of Material Science, Technical University of Liberec, Czech Republic
**Institute of Physiology, Academy of Sciences of the Czech Republic, Prague, Czech Republic
***Institut of Material Science, Technical University of Lodz, Poland
E-mail: Irena.Subrtova@sezam.cz

Abstract

Due to unique physico-chemical properties and good biocompatibility are carbon layers considered to be promising material for wide field of biomedical applications. In this study, carbon films were manufaktured in microwave and radio frequency plasma reactor using dual frequency method (MW/RF PCVD - microwave and radio frequency plasma chemical deposition). Four various processes of deposition were used for preparation layers on substrates of medical stainless steel AISI 316 L. On samples of all four processes, growth and adhesion of cells were observed.

[Engineering of Biomaterials, 56-57,(2006),19-21]

Experimental details

Materials and deposition procedure

In the present study we have studied carbon coatings (NCD) prepared in microwave and radio frequency plasma reactor using dual frequency method MW/RF PCVD - microwave and radio frequency plasma chemical vapour deposition. Parameters of the deposition were optimised to get uniform films on the stainless steel AISI 316L. Stainless steel substrates used in the present study were shaped as 2,5 mm thick circular discs with diameter of 8 mm. Substrates were machined, electropolished, ultrasonically cleaned in methanol and dried. Prior to NCD deposition, the surface were cleaned in an argon inert plasma in the vacuum chamber for 10 minutes. [1] Four various processes of deposition were used TAB. 1. In present paper, coated samples were named after number of deposition process, uncoated were just AISI 316L.

Cells and cultures conditions

Coated and uncoated samples were sterilized in steam autoclave by temperature 120°C for 20 minutes, immersed in tissue water. All samples were placed into polystyrene multidishes (Costar, 24 wells, diameter 15 mm) and seeded with human osteosarcoma cell line MG 63 and Dulbecco medium at the initial density 30 000 cells/well. Glass coverslips and the polystyrene dish as control materials were used. Cells were cultured for one, three and seven days in the temperature of 37°C in atmosphere containing 5% of CO_2. On day one and three after seeding, the cells were rinsed in phosphate-buffered saline (PBS), fixed with 70% cold ethanol (-20°C, 5 min), vizualized by propidium iodide (5µg/ml, 5min). Their morphology was evaluated and documented using epifluorescence microscope IX 50 equipped with a digital camera DP 70 (Olympus, Japan). Fluorescent cell linker kit PHK 26 RED and propidium iodide for better vizual representation, were used. The number of adhering MG 63 cells was counted in 10-16 randomly selected mi-

PROCESS	Methane [%]	Bias [V]	Power [W]	Pressure [Pa]	Time [min]
1.	30	400	150	10-60	6
2.	30	500	250	10-30	3
3.	20	600	250	10-25	4
4.	15	700	250	10-30	5

TABLE 1. Parameters of deposition processes.

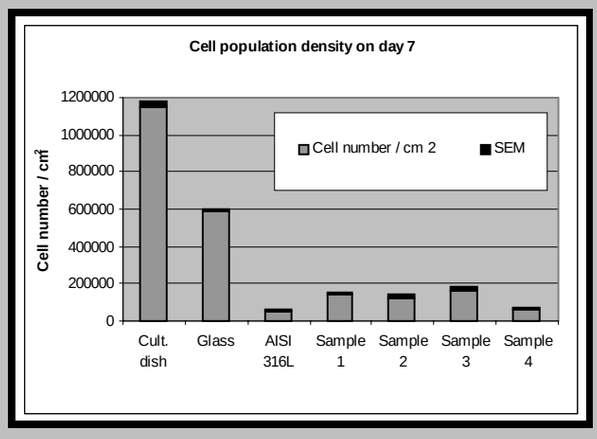

FIG. 1. Number of initially adhered osteoblast-like MG 63 cells on tissue culture polystyrene (Cult.dish), on glass coverslips (Glass), uncoated sample AISI 316 L, Sample 1, 2 , 3, 4 on day 7 after seeding. Average ±SEM from 10-16 measurements, statistical significance in comparison with values obtained on culture dish.

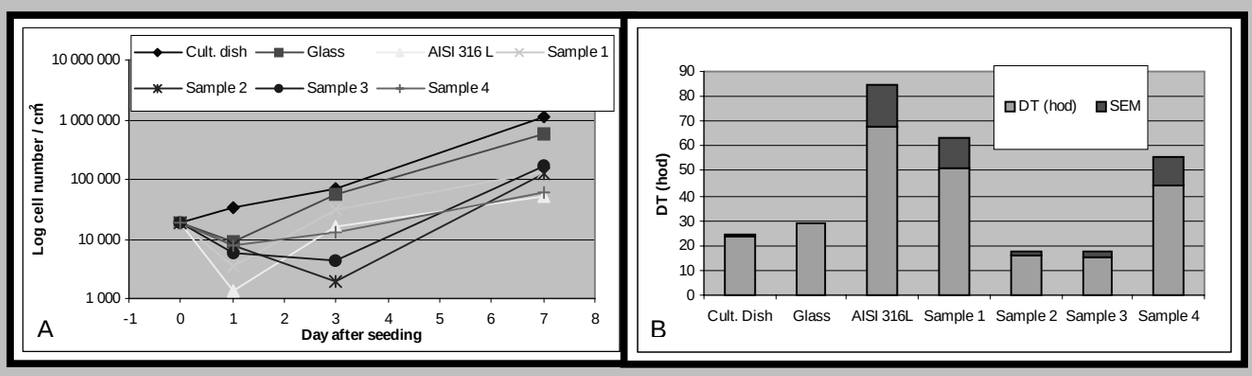

FIG. 2. Number of initial adhered osteoblast-like MG 63 cells (A) growth curves of these cells from day 0-7 (B) the population doubling time DT between days 3 and 7 after seeding on tissue culture polystyrene (Cult.dish), on glass coverslips (Glass), uncoated sample AISI 316L and coated Sample 1, 2 , 3, 4.

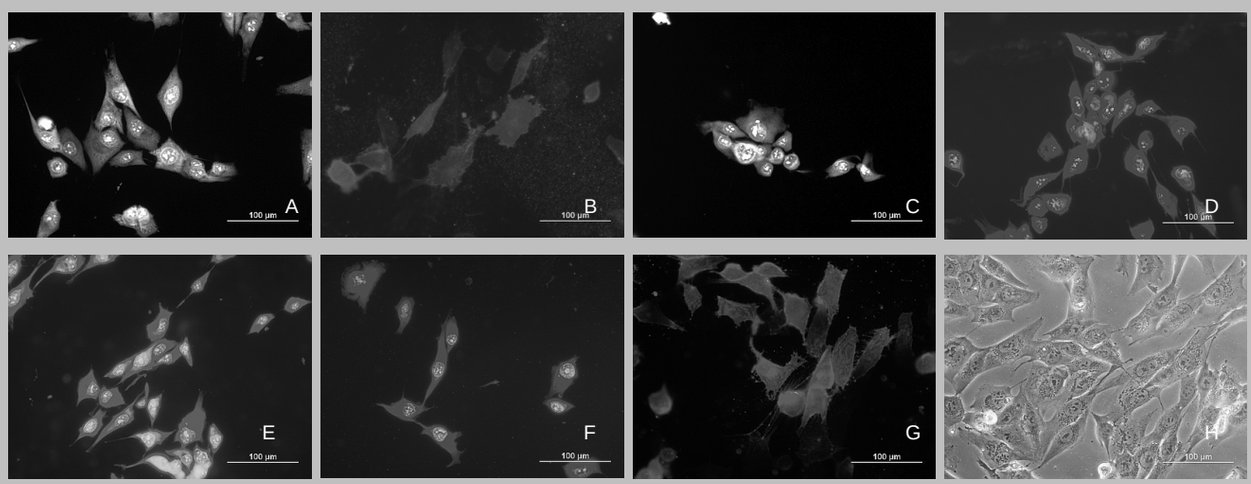

FIG. 3. Morphology of osteoblast-like MG 63 cells on day 1 after seeding, stained with propidium iodide or red fluorescent cell linker, epifluorescence (A) culture dish polystyrene (B) glass coverslips (C) sample 1 (D) sample 2 (E) sample 3 (F) sample 4, (G) AISI 316 L, (H) native cells in medium on culture dish.

croscopic fields (20x objective, 1 and 3 day after seeding). On day 7 after seeding, when the cell counting in microscopic field was disabled by a high cell population density and formation of multi-layered areas, the cells were detached by trypsin-EGTA for 5 min at 37°C and counted in a Bürker homeocytometer (18 measurements for each sample). [2,3]

Results

On day 1 after seeding, the number of cells initialy adhered on all samples was lower than found on conventional tissue culture polystyrene dishes and than on glass coverslips. In comparison with uncoated sample AISI 316 L was the number of cells on coated samples significantly higher. Morphology of osteoblast-like MG 63 cells on day 1 after seeding is represented in FIG.3. From day 1 to 3 after seeding, the cell number on all samples incresased in the following order: Polystyren > Glass > Sample 1 >AISI 316 L > Sample 4 > Sample 3 > Sample 2. On day 1 and 3 after seeding, clear preference of cell growth on edges of samples was observed. Clusters of cells on edge areas of samples were detected, but in the middles of samples only isolated cells were found. On day seven the higher proliferation activity of cells on the all coated samples in comparison to uncoated sample was observed. The most number of adhering cell were on polystyrene culture dish and on the glass coverslips. Non of our samples has better cell adhesion. In comparison with coated samples has higher number of cells the Sample 3 than Sample 2, Sample 1 and AISI 316L (FIG.1). Average cell numbers were compiled as growth curvers (FIG. 2A). The population doubling time DT of MG 63 cells between day 3-7 was shortest for Sample 3 (FIG. 2B), followed with Sample 2, Culture dish, Glass, Sample 4, Sample 1 and AISI 316L. Statistic data were presented as means ± S.E.M. from 10-16 measurements obtained from 1 sample for each experimental group. Statistical significance was evaluated by the Student's t-test in comparison with values obtained on polystyren culture dish.

SEM observation were performed in VEGA TS 5130 scanning electron microscope. The results of observation

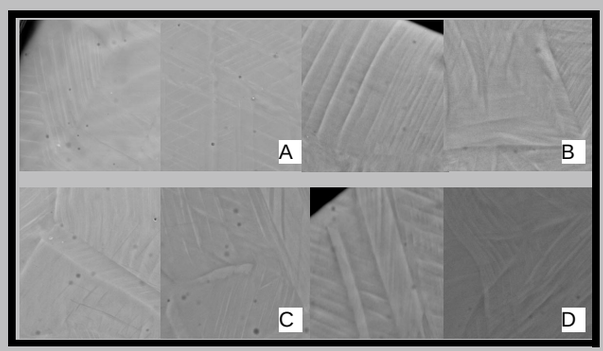

FIG. 4. SEM micrographs of surfaces of coated samples; photo on left side presents edge of sample, right is the middle of the sample (A) sample 1 (B) sample 2 (C) sample3 (D) sample 4

were presented in the FIG.4. Different surface morphology of layers on samples could be one of the reasons to growth preference of cells on individual samples. It may be the cause of the growth preference of cells on the edge areas of samples with comparison to the middle areas of samples, where on day 1 and 3 after seeding rather isolated cells were found.

Conclusion

In this study growth and proliferation of osteoblast-like cells MG 63 on four carbon films deposited under different process conditions in MW/RF reactor were investigated. In this paper the comparison of cell growth on coated, uncoated, glass and tissue culture polystyren was performed. We have noticed potential dependence of cell adhesion on surface morphology on edges and in the middle of sample. This study may be helpful in a selection of coating conditions in MW/RF reactor to create suitable carbon films for biological application.

Acknowledgements

We thank Mgr. Lubica Grausova for maintaining the cell line MG 63 in culture and excellent technical assistance by tests. Special thanks to MUDr. Lucie Bačáková, CSc. for making available test and for all support. We thank Ing. Witold Kazcorowski for preparing the carbon films. We would also like to thank Ing. Vladimír Kovačič and Ing. Jana Grabmüllerová (Department of textile materials, Technical University of Liberec) for observations on scanning electron microscope.

References

[1] Kaczorowski W., Niedzielski P., Mitura S.: Manufacture of carbon coating for biomedical applications in a new MW/RF reactor. Engineering of Biomaterials, 43-44, (2005), 28-31 ISSN 1429-7248.
[2] Bačáková L., Jungová I., Slosarczyk A., Zima A., Paszkiewicz Z.: Adhesion and growth on human osteoblast like MG 63 cells in cultures on calcium phosphate-based biomaterials. Engineering of Biomaterials, 38-43,(2004), 15-18.
[3] Bačáková L., Lapčíková M., Kubies D., Rypáček F.: Adhesion and growth of rat aortic smooth muscle cells on lactide-based polymers. Tissue Engineering, Stem Cells and Gene Therapies. Edited by Y. Murat Elçin, Kluwer Academic/Plenum Publishers, Volume 534, 2003, 179-189.

ELECTRIC POTENTIAL OF BIOMATERIALS COATED WITH DIELECTRIC CARBON LAYER AND NON-COATED IN WATER AND SERUM

S. Urbański*, P. Niedzielski*, S. Mitura*, T. Wierzchoń, A. Sokołowska***

*Institute of Materials Science and Engineering,
Technical University of Lodz;
90-924 Lodz, Stefanowskiego 1/15 Street, Poland
**Faculty of Materials Science,
Warsaw University of Technology;
02-507 Warsaw, Wołoska 141 Street, Poland
e-mail: piotrn@p.lodz.pl

Abstract

Electric potentials, established in water and human blood serum, of the electrodes made of platinum, graphite, Ti6Al4V alloy, TiN, AISi316L steel, oxidized steel and the materials coated with diamond like carbon layer (DLC) and a nanocrystalline-diamond layer (NCD) were determined. The values of the potentials of non-coated materials increased with increasing electron work function (Φ) of investigated materials in reasonable accordance. The difference between the potentials measured in serum and in water was ascribed to the differing molecular electron structure of the proteins in contact with the electrodes. Electrode potentials of different materials coated with the same thin dielectric carbon layer varied significantly depending on the Φ value of the substrate. In this way the selection of a substrate material permits influencing on the interaction between NCD (DLC) coating and serum compounds. The potential of an electrode has appeared to be a simple but sensitive indicator of the phenomena that take place on the biomaterial surface.

Keywords: *electrode potential, electron work function, Pt, TiN, carbon, Ti6Al4V, AISI316L, DLC, NCD.*
[Engineering of Biomaterials, 56-57,(2006),21-24]

Introduction

The bulk biocompatibility of implant materials (i.e., the similarity of their mechanical, magnetic etc. properties to the properties of the human body) can be evaluated in the macro-scale in a quite simple way by in vitro examinations. The interaction between the surface of the implant material and the tissues, blood and cells is usually examined in vitro by observing the phenomena in the microscopic scale using biological methods. The specific drawback of the biological methods carried out in vitro lies in the necessity of using certain additional substances, absent in the living organism, that ensure the stability of the specimen. Moreover, the results of biological examinations obtained by various investigators are difficult to compare. Simple physicochemical methods suitable for estimating macroscopically the biocompatibility of the implant surface are scarce. They primarily include corrosion examinations and tracing the presence of the markers of selected bio-chemical processes that proceed in blood.
M.J. Jones et al. [2], who examined the haemocompatibility

of Ti, TiC, TiN and DLC, combined a macroscopic physical measurement (surface tension in respect to water) and a chemical measurement (haemoglobine release into plasma) with microscopic biological examinations (platelets attachment). These three methods yielded similar results as to the ordering of the biocompatibilities of the materials examined. The measurement of the surface tension was the simplest and absolutely 'non-invasive'. Similar attempts at relating the surface tension with the haemocompatibility were made by J.A. McLaughlin et al. [3], X. Wang et al [4], and B.J. Hunt et al [5]. The relation between the hardness and the surface biocompatibility was studied by L.A. Thomson et al. [6].

In our previous work [1] we made an attempt to relate the electric potential of an electrode immersed in water (ε_{water}) with its electron work function (Φ_M). The preliminary results showed a reasonable agreement between ε_{water} and Φ_M, although the spread of the values was quite wide.

The present study was concerned with an attempt at utilizing the electric potential of an electrode made of the biomaterial examined as the indicator of the interaction between the components of a given biological medium and the electrode surface. Contrary to the common electrochemical corrosion investigation we only considered the effects of the electron transfer from the electrode into molecules of the surrounding medium. The materials whose ions passed into water were not examined, chiefly because they may be toxic for a living body. Therefore we did not used the equilibrium equation between a metal and its ion expressed as

$$\varphi_M - \varphi_R = \frac{\mu_M - \mu^{\oplus}_M}{zF} + \frac{RT}{zF}\ln a$$

where μ - electrochemical potential, F - Faraday number, a - activity

but we solely measured the contact potential V (Volta voltage) related to the electron work function (Φ_M) of the biomaterial and to the charge neutrality level (CNL) of the molecule, given by

$$\Phi_M = E_F + electron \quad surface \quad states$$
$$V = \Phi_M - CNL$$

The contact potential between solids has been described for electronic purposes using the band model theory (7). The same theory was used for describing the solid-molecule contact [8]. Although the band structure of a molecule differs from the band structure of a solid, it has been proved that the effects that occur at the solid-molecule contact are analogous to those that take place between two different solids. When examining the Au-perylene-tetra-carboxylic-dianhydride molecule contact, these authors observed a broadening of molecular bands at the contact with the metal and ascribed this to the electron hopping interaction Φ_{Au6S}-Φ_{mol}. The mechanism associated with the formation of Me-Molecule interface barrier involves the charge transfer between the two materials due to a weak chemical interaction. As a result an electrostatic interface dipole is formed, which tends to align the metal Fermi level and the molecule charge neutrality level.

For example, J.Ristein et al [9] described the contact potential of an H-terminated diamond surface with H_2O at pH6 to be a result of the electro-chemical potentials of the two bodies becoming equilibrated. Since, under these conditions, C- H shows a negative electron affinity, diamond functions as an electro-donor in this contact.

Investigated biomaterial	Φ_M [eV]	References
Platinum	5,32-6,35	[15]
Graphite	4,0-4,7	[15]
AlSi316L	Fe-4,31	[15]
Ti6Al4V	Ti-3,9	[15]
Fe_2O_3	3,8	[15]
TiN	3,75	[17]
NCD/DLC	3,0	[16]
Investigated fluid		
H_2O		
Srerum		

TABLE 1.

Experiments

Measuring method

The potential of the electrode in the liquid examined was determined by measuring the voltage established between the reference electrode, which was an EK602 calomel minielectrode of a potential of +223 ±5 mV, with respect to the potential of the saturated chinhydron electrode considered to be equal to zero according to the Geneva Convention.

The voltage was measured using a MERAU722A electronic voltemeter with the inner resistance $R_W=10^9\Omega$ and a sensitivity of 10mV.]

Materials

The liquids examined were de-ionized water and a fresh human blood serum obtained from drug-free volunteers, at pH=7.2 and a temperature of 300K.

The examinations included biomaterials whose significance seemed prospective for the applications where the implants were to be in contact with blood. Polymer materials were omitted, chiefly because their effectiveness depends on the 'micro-architecture' of the implant made of them [10]. The electrode materials used in the experiments are given in TABLE 1.

TiN was formed on a Ti6Al4V alloy substrate by subjecting it to glow discharge assisted d.c. nitriding in nitrogen at a temperature of 1123K, as described in [13]. Diamond-like carbon (DLC) was produced on a Ti6Al4V alloy substrate by the pyrolysis of methane in an r.f.-frequency plasma at a temperature of 573K. The nanocrystalline diamond (NCD) layer was produced on a Ti6Al4V alloy substrate using the pyrolysis of methane in an r.f.-frequency plasma at a temperature of 873K as described in [14]. The AISI316L steel was oxidized by heating at 728K in air as described [11].

Results and discussion

FIG. 1 shows the results of measurements of the electrode potentials in H_2O (ε_{water}) and the values of the electron work function (Φ) of the non-coated materials. The results classify the materials according to growing ε_{water} as follows: Pt>graphite>oxidized steel>TiN. The same sequence is true when ordering according to increasing Φ.

The Ti6Al4V alloy and AISI316L steel differed from the other materials. The value of their ε_{water} depended strongly on the time for which the electrode was immersed in water (FIG. 2). This observation seems to suggest that the metallic ions have passed to the water and confirms that electrochemical corrosion occurs in both materials [11,12]. ε_{water} of oxidized steel remained constant, which confirms the results obtained by Chun-Che Shih et al. [11]. The measurement of ε_{water} permitted us to reveal, quickly and immedi-

ately, any metal dissolution, an effect very undesirable when dealing with biomaterials.

The values of non-coated electrode potentials in serum, ε_{serum}, are shown in FIG. 3. When immersed in serum, the electrodes behaved in a similar way as in water. Although the electric potentials ε_{serum} of the individual electrode materials were changed, the sequence according to growing ε_{serum} followed the increase of Φ and ε_{water} values.

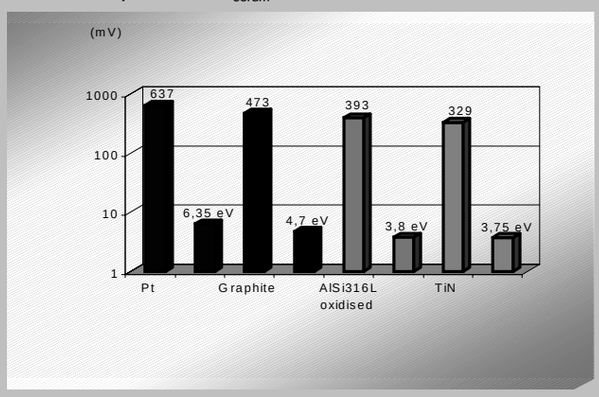

FIG. 1. Electrode potentials in water ε_{water} and electron work function Φ of noncoated materials.

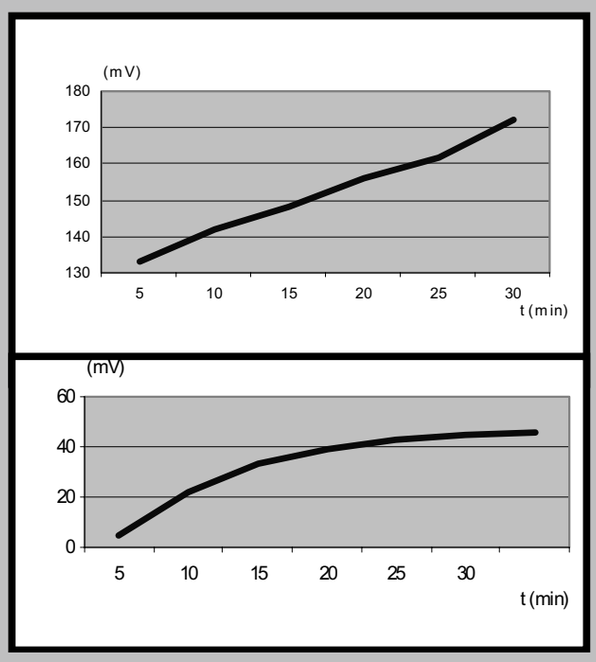

FIG. 2. Electrode potentials in water ε_{water} of: a)Ti6Al4V, b)AlSl316L.

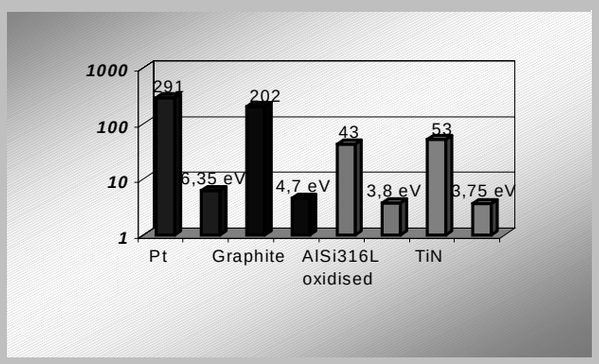

FIG. 3. Electrode potentials in serum ε_{serum} of noncoated materials.

The potential difference ε_{serum} - ε_{water} should be an expression of the phenomena that occur at the biomaterial-serum components boundary. As shown in FIG.4, the electrodes made of various materials differed in their ε_{serum} - ε_{water} value roughly in accordance with the increase of their ε_{water}. The difference (ε_{serum}-ε_{water}) of Pt was the largest. The (ε_{serum}- ε_{water}) of graphite and TiN were smaller, but almost the same, and did not follow the ε_{water} sequence. Therefore, TiN appeared to be an exceptionally surface-active biomaterial.

The results may be described in terms of the existence of the contact potential at a solid-protein junction and the space charge built of negatively charged ions similar to the

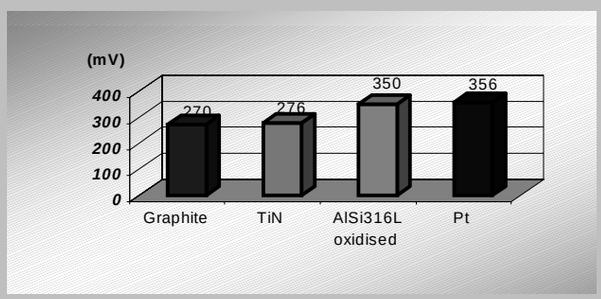

FIG. 4. ε_{serum} - ε_{water} of noncoated materials.

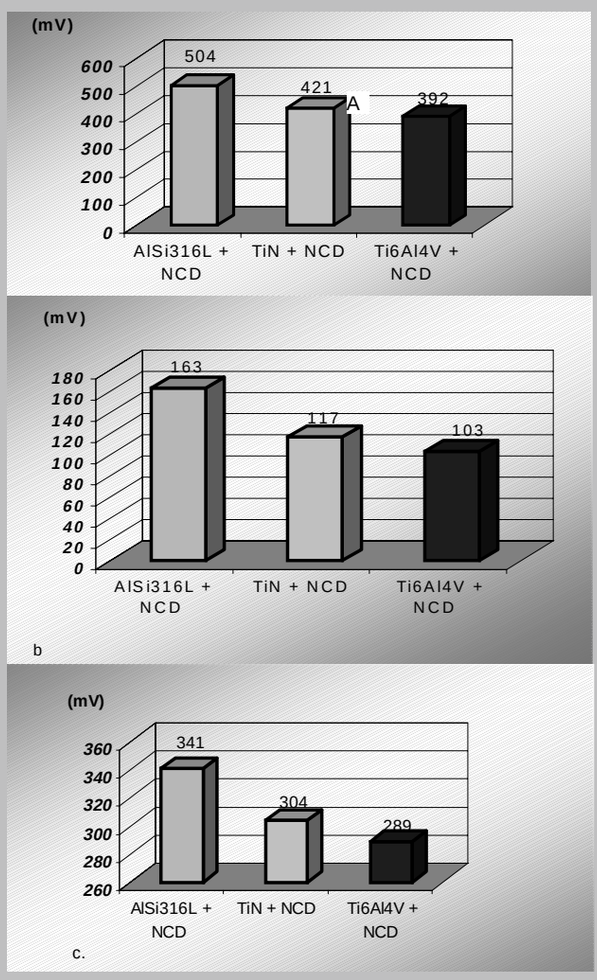

FIG. 5. Electrode potentials of carbon NCD layer coated materials: a) ε_{water} of NCD, b) ε_{serum} of NCD, c) ε_{water} - ε_{serum} of NCD.

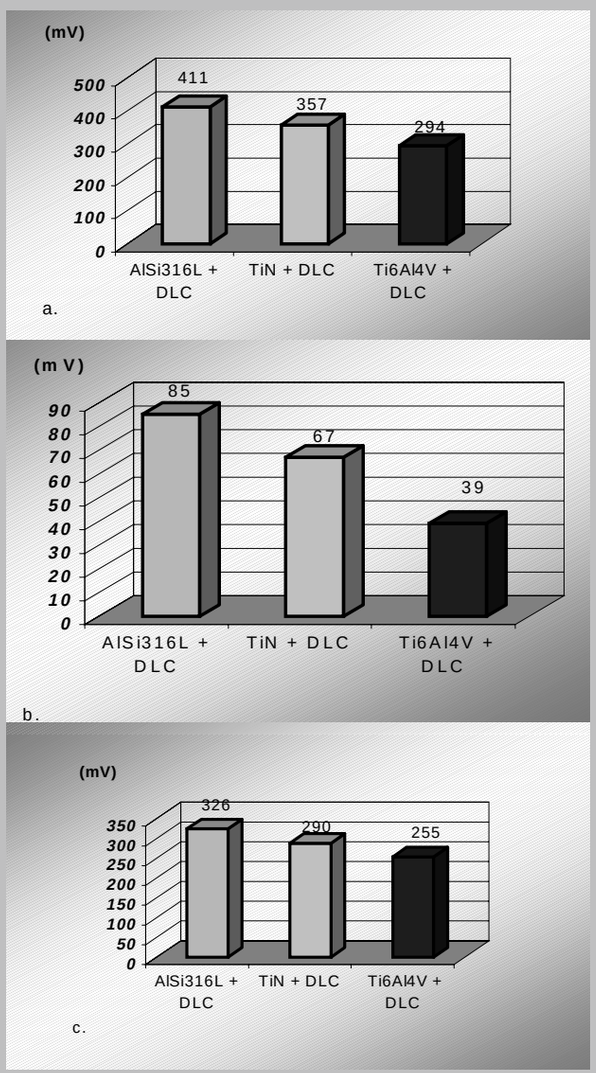

FIG. 6. Electrode potentials of carbon DLC layer coated materials: a) ε_{water} of DLC, b) ε_{serum} of DLC, c) ε_{water} - ε_{serum} of DLC.

Helmholtz-Stern layer.

The electrodes made of the metals coated with thin dielectric layers (NCD, DLC) behaved in different way as the non-coated electrodes (FIG. 5, 6). Their ε depended first of all on the kind of the substrate materials in particular on its Φ and not on the Φ value of NCD, DLC. So it appeared, that a selection of a substrate metal permits changing the interaction between NCD, DLC layer surface and serum components.

Conclusion

The measurements of the electric potential ε of various electrodes immersed in water and human serum show that this parameter (ε) is sensitive to the dissolution of the metal and to the electron energy structure of the solid-molecule contact. Therefore, the value of ε seems to be a quick and simple preliminary indicator of the biocompatibility of a material.

The measurements of ε of thin dielectric carbon layers (DLC, NCD) deposited on various conducting materials show, that the surface biocompatibility of NCD, DLC coatings can be affected by electron properties of their substrates.

References

[1] A.Sokołowska, S.Mitura, T.Wierzchoń, P.Niedzielski, K.Orlińska, P.Sawosz, Inżynieria Biomateriałowa 7 (2004), 55.
[2] M.J. Jones, I.R. Mc Coll, D.M Grant., T.L. Parker: Diamond Relat. Mater. 8 (1999) 457.
[3] I.A. Mc Laughlin., B.Meenan, P.Maguire, N.Janieson: Diamond Relat. Mater. 5 (1996) 486.
[4] X. Wang, F.Zhang, Ch.Liu, Zh.Zheng, X.Liu, A.Chen, Zh. Jiang, Surf a Coat, Tech. 128-129 (2000) 36
[5] B.J. Hunt, R.Paratt, M.Cable, D.Finch, M.Yacomb, Blood Coagul. Fibrinolysis 8 (1997) 223.
[6] L.A.Thomson, F.C.Law, N.Rushton, J.Franks, Biomaterials 12 (1991) 37.
[7] E.Spenke, Elektronische Halbleiter, Springer Vrlg., Berlin, Heidelberg, N.Y. 1965.
[8] H.Vazquez, F.Flores, R.Oszwaldowski, J.Ortega, R.Perez, A.Kahn, Appl. Surface Science 234 (2004) 107.
[9] I.Ristein, M.Riedel, F.Maier, B.F.Mantel, M.Stammler, L.Ley, J.Phys, Surface of diamond, Condens. Matter 13 (2001) 8979.
[10] L.Siemiński, K.J.Goch, Biomaterial - interactions, Biomaterials 21 (2001) 2233.
[11] Chun-Che Shih, Chun-Ming Shih, Yea-Yang Su, Lin Hui Julie Su, Man-Song Chang, Shing Jong Lin, Corrosion Science 46 (2004) 427.
[12] D.F.Williams, Titanium: Epitome of biocompatibility or caux for concern, J. Bone Joint. Surg. 76 (1994) 348.
[13] E.Czarnowska, T.Wierzchoń, A.Maranda, E.Kaczmarewicz, J.Mater. Sci.: Mat. In Med. 11 (2000) 73.
[14] S.Mitura, E.Mitura, A.Mitura, Diamond a Rel. Mat. 4 (1995) 302
[15] W.Formienko, Emisjonnyje swojstwa materjałow - sprawoćnik, Kijew, Naukowaja Dumka, 1970.
[16] R.J.Nemanich, P.K.Bauman, M.C.Benjamin, O.-H.Nam, A.T.Sowers, B.L.Ward, H.Ade, R.F.Davis, Appl. Surf. Sci. 130 (1998) 694.
[17] G.V.Samsonov , J.M.Vinitskij: " Hamdbok of Refractive Compounds" J.S.J Plenum 1980.

CARBON FIBRE-BASED POSTS WITH CEMENTIT UNIVERSAL RESIN CEMENTATION SYSTEM AS A MATERIAL FOR RESTORATION OF ENDODONTICALLY COMPROMISED TEETH - SEM EVALUATION OF SEALING

Banaszek Katarzyna*, Klimek Leszek**

*Department of Endodontics, Medical University of Łódź, ul Pomorska 251, 92-213 Łódź, Poland
**Institute of Materials Engineering, Technical University of Łódź, Stefanowskiego 1/15, 90-924 Łódź, Poland
Email: kemilk@p.lodz.pl

[Engineering of Biomaterials, 56-57,(2006),24-27]

Introduction

Dental caries or mechanical injuries can result in substantial loss of hard tissues of the tooth crown. Teeth with partially or completely destroyed coronary structure can still function in the oral cavity provided they undergo root canal treatment and prosthodontic reconstruction with posts and

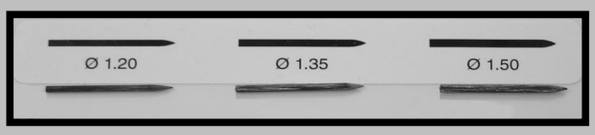

FIG. 1. Kit of carbon fibre posts for tooth

cores and prosthetic crowns [9,12]. Endodontically treated teeth may be restored with prefabricated posts made of stainless steel, gold, titanium, nickel-chromium-cobalt or iridium-platinum alloys, ceramics or custom-made cast posts produced in the prosthetic laboratory [1,12].

For the last two years, new carbon fibre-based systems for restoration of lost hard tissues in endodontically treated teeth have been available on the market as an alternative to metallic and ceramic post and cores [2,3,8,10].

These posts contain reinforcing carbon fibres embedded in an epoxy resin matrix, which keeps them together. The fibres have similar physical properties as the dentin. The content of carbon fibers constitutes approximately 40-65% of the post depending on different manufacturer. When inserted into the root canal of the tooth they adjust to the root's work in the alveolar bone during mastication (10).

The objective of the study

The objective of the study was SEM evaluation of Carbonite carbon fibre post adhesion using universal resin cementation system - Cement-It.

Material and methods

Fifteen human teeth - maxillary and mandibular canines and incisors extracted for periodontal reasons and stored in 10% formalin solution - were evaluated in the study. The teeth were divided into 3 groups, each one consisting of 5 teeth, according to the size and width of the root: group A with maxillary lateral incisors, group B with maxillary central incisors, and group C with mandibular canines. Dental crowns, after removing carious lesions, were cut off 1-2mm above the cemento-enamel junction. The root canals of teeth were instrumented with K-files and next irrigated using 15% sodium versenate, 5.25% sodium hypochloride, and finally distilled water. Teeth divided into groups were prepared with special fibre post reamers (Harald Nordin S.A., Switzerland) according to the canal width and adjusted to the size of the carbon fibre post, Carbonite, (Harald Nordin s.a., Switzerland), to be used. The root canals prepared with reamers were irrigated once again with endondontic irrigants and distilled water, dried and checked for post fitting in root canals. Then, the dentinal surface was etched with 37% phosphoric acid, prior to adhesion of the bonding system. The acid was rinsed with 5ml of distilled water and root canals dried with paper points. Resin cementation system (Pentron, Wallington, USA) consisting of one-component bonding resin, Bond 1, and a composite cement, Cement-It, was used to fix carbon fibre posts. Root canal instrumentation and post surface preparation were carried out according to the manufacturer's recommendations. After post insertion, each tooth was additionally light-cured for 40s to bond completely the material in the root canal. The filled teeth were stored in physiological saline and incubated for 72 hours at 37°C.

In order to qualitatively assess specimens they were ground to half their thickness in the labio-lingual direction and coated with gold layer of several dozen nanometers. The prepared specimens were viewed in the Hitachi S-3000N SEM.

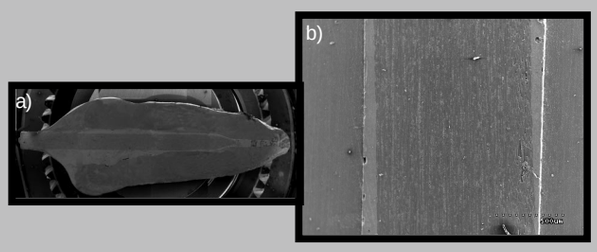

FIG. 2. Longitudinal section of the restored tooth with the carbon fibre post (a) and a magnified fragment of the post (b).

The evaluation of sealing was performed in the apical part of the post by determining the width of the gap between the carbon fibre post and the resin cement, as well as the post and the root canal dentin.

For the obtained results, arithmetic mean and standard deviations were calculated. To verify the formulated hypotheses the parametric test of significance based on small samples was used.

Additionally, the analysis of the carbon fibre post structure was performed in the light microscope basing on longitudinal sections and cross-sections of the posts.

Results

The general view of the restored tooth is presented in FIG.2a, while FIG.2b shows a magnified fragment of the carbon fibre post.

The results of gap width measurements in the examined teeth restored with carbon fibre posts are depicted in TABLE 1.

In the teeth studied the adhesion between the post and the resin cement as well as between the resin cement and the dentin was very good (FIG. 3). Only in same places, the presence of a few-micrometer gaps was sporadically observed (FIG. 4).

Type of the post	Gap width [μm]			
	resin cement–carbon fibre post		Dentin-resin cement	
	Mean	Standard deviation	Mean	Standard deviation
Large - ϕ 1.5 mm	0.5	1.1	0.8	1.8
Medium-ϕ 1.35 mm	0.5	1.0	0.7	1.2
Small - ϕ 1.2 mm	0.6	1.1	0.8	1.6

TABLE 1. Gap widths in restored teeth.

Photomicrographs of longitudinal sections and cross-sections of carbon fibre posts are demonstrated in FIG. 5.

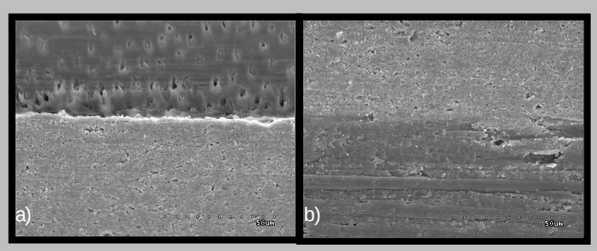

FIG. 3. Adequate adhesion of the post-restored tooth system: a) resin cement-dentin, b) resin cement-carbon fibre post.

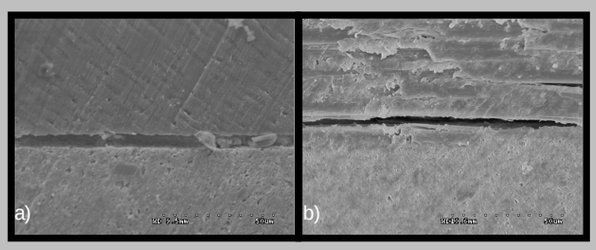

FIG. 4. A gap in the post-restored tooth system: a) resin cement-dentin, b) resin cement-carbon fibre post.

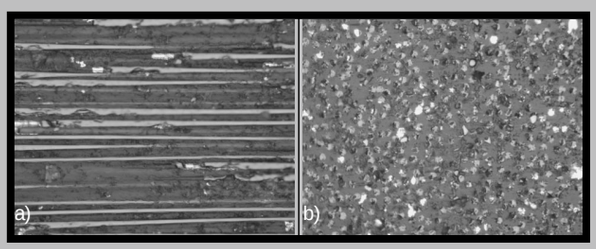

FIG. 5. The structure of carbon fibre posts: a) longitudinal section, b) cross-section.

Discussion of the results

Carbon fibre posts, Carbonite, have smooth walls and are similar in shape to a pin with a tapered end. They are available in 3 sizes adjusted to different sizes of the root canal.

Carbonite posts, in compliance with the manufacturer's certification, contain approximately 65% of longitudinal carbon fibres with braided plait arrangement in an epoxy resin matrix. However, SEM investigations (FIG.5) have revealed that fibre content is lower, and they are not arranged in the form of braided plait but parallel

In reconstruction of the endodontically compromised teeth with posts, besides the type of the material used, shape of the post, the amount of the removed root canal dentin and more precisely the amount of the dentin left after canal preparation have a significant impact on vertical fractures. The greater amount of the removed dentin while instrumenting the canal, the higher risk of endodontically compromised tooth fracture. The highest stresses occur in tooth tissues prepared for a post and core but not restored with a post [7]. The material with higher resistance i.e., chromium-cobalt or chromium-nickel alloys, reduces stresses induced in tissues of the tooth reconstructed with prosthodontic appliance. However, when we use the material whose Young module is lower than that of the dentin, then stresses generated in the root are higher than in the dentin of the healthy tooth [7]. Thus, the higher the Young module in the material, the lower stresses appear in the tooth restored with the post. As regards the post shape, it is known that optimal distribution and the least stress values occur when the root segment of a post is taper-shaped and has parallel walls in relation to root canal walls [4]. Dejak and Młotkowski in their study have revealed that stresses in the vicinity of the tooth cervix decrease along with the increase in the thickness of the metallic post, while thinner and longer posts, by 2/3 of root length, do not reduce stresses around the dental cervix but generate higher stresses in the apical region [5]. The above considerations indicate that the most optimal post would be the one made of metal with a high Young module e.g., chromium-cobalt, chromium-nickel, of a medium size in relation to the root size and taper-shaped with walls parallel to root walls as ideal adhesion to the dental root surface [4, 5, 7]. Also, elasticity (flexibility) of the post used is as important. Carbon fibres and adhesive system have elasticity parameters close to dentin properties [3, 10]. Since carbon fibres and the epoxy resin matrix are elastic, stresses are transmitted to the dental tissues.

Subsequently, the next problem arises which is associated with the materials used for post cementation inside the root. These materials are less resistant than those metal cast posts are made of. Lack of precision in fabricating a post causes production of stresses in the root while biting and chewing, which leads to chipping off resin cement and negatively affects resistance of the remaining tooth structure [6].

The most crucial element of prosthetic restoration with a post is adhesion between the post, cement and root dentin to form an integral whole.

Failure resulting in lack of seal in teeth with composite or prosthetic crowns can be caused by iatrogenic errors during both endodontic treatment and prosthetic build-up due to marginal leakage of the reconstructed tooth crown. This microleakage is of considerable importance in necrotic teeth after the endodontic procedure, and particularly in the case of teeth subject to root canal retreatment [11].

Due to lack of sealing, bacteria pass to hard dental tissues and induce secondary caries i.e., bacterial infection, subsequently leading to further complications. Microleakage permits wet oral environment to contact with the inside of the already filled root canal. Such a situation can become the reason for failure of endodontic and prosthodontic treatment and makes the clinicist retreat the tooth endodontically. However, retreatment is often difficult or impossible to perform so the clinicist is forced to carry out an endodontic surgical procedure, which, when fails, can in consequence lead to tooth loss. That is why, sealing is of great significance in adhesive dentistry used for reconstruction of endodontically treated teeth.

In the teeth studied the presence of small, a few-micrometer gaps was only sporadically observed. They occurred at the dentine/resin cement and resin cement/post interfaces. The maximal gap size was 5 μm. Lack of sealing in root canals can result from rapid bonding of the resin cement used to fix the post. In most cases there was no discontinuity in the specimens studied.

Thus, we can presume that the use of post and cores reinforced with carbon fibres embedded in epoxy matrix and cemented in the root canal with adhesive techniques enables the tooth to maintain its durability and functioning in the masticatory system.

It can be concluded that the applied method of non-vital tooth restoration will be satisfactory as far as sealing and protection against microbial penetration into the dental tissues are concerned.

Conclusion

Carbon fibre post system with adhesive techniques can be an alternative to restoration of endodontically treated teeth.

References

[1] Combe E. C. , Wstęp do materiałoznawstwa stomatologicznego, Warszawa 1997, Wydawnictwo Medyczne SANMEDICA.
[2] da Silva R.S., de Almeida Antunes R.P., Ferraz C.C., Orsi I.A. : The effect of the use of 2% chlorhexidine gel in post-space preparation on carbon fiber post retention. Oral Surg Oral Med Oral

Pathol Oral Radiology Endod, 2005, Vol.99, 3, 372-377.
[3] De Santis R., Prisco D., Apicella A., Ambrosio L., Rengo S., Nicolais L. : Carbon fiber post adhesion to resin luting cement in the restoration of endodontically treated teeth. Journal of materials science, 2000, Apr., Vol. 11(4), 201-6.
[4] Dejak B., Józefowicz W. " Wpływ różnych kształtów wkładów koronowo-korzeniowych na naprężenia w tkankach zęba" (Influence of different designs of post and core on stresses in the tissues of teeth) Prot.Stomat.XLIV,1994,5,248-250.
[5] Dejak B., Młotkowski A." Badanie naprężeń w zębach w zależności od wielkości części korzeniowej wkładów" (Evaluation of stresses in the teeth depending on size of the posts) Stomatologia Współczesna, vol.2,nr 5,1995,410-419.
[6] Dejak B." Wpływ braku przylegania wkładu koronowo-korzeniowego do niektórych części korzenia na naprężenia występujące w strukturach odbudowanego zęba" (Influence of inaccuracy in adjustment of a post and core on the stresses in the tissues of teeth) Prot.Stomat. 2000,L, 1,30-37.
[7] Dejak. B. "Badania naprężeń w zębach odbudowanych wkładami koronowo-korzeniowymi z różnych materiałów" (Evaluation of stresses in the teeth restored with dowels made of different materials) Stomatologia Współczesna, vol. 2, nr 1, 1995, 35?40.
[8] Iglesia-Puig M.A., Arellano-Cabornero A. : Fiber- reinforced post and core adapted to a previous metal ceramic crown.. J Prosthet Dent, 2004, vol.91, 2, 191-194.
[9] Kupka T., Tanasiewicz M., Ilewicz L.: Zachowawcza odbudowa całkowicie zniszczonej korony zęba bocznego z użyciem standardowego wkładu koronowo-korzeniowego oraz wypełnienia kompozytowo- amalgamatowego (Conservative restoration of the totally destroyed crown of a posterior tooth with the use of a standard post and combined composite - amalgam restoration) Czas. Stomat., 2001, LIV, 6, 349 - 356.
[10] Lassila L.V., Tanner J., Le Bell A.M., Narva K., Vallitu P.K.: Flexural properties of fiber reinforced root canal posts, Dental Materials 2004, Vol. 20, 1, 29-36.
[11] Mannocci F., Ferrari M., Watson T.F. : Microleakage of endodontically treated teeth restored with fiber posts and composite cores after cyclic loading : A confocal microscopic study ; J Prosthet Dent , 2001, Vol.85, 3, 284-291.
[12] Spiechowicz E., Protetyka Stomatologiczna, Warszawa 1992, Państwowy Zakład Wydawnictw Lekarskich.

MODIFYING ELECTROPHYSICAL PROPERTIES OF SI-CBN INTERFACE BY INTRODUCTION OF ULTRATHIN DIELECTRIC LAYER

Firek P., Mroczyński R., Szmidt J., Beck R.B., Werbowy A.

Institute of Microelectronics & Optoelectronics, Warsaw University of Technology, Poland
Email: pfirek@elka.pw.edu.pl

Abstract

This study concerns modifications of Si - c-BN interface (with and without dielectric underlayer). c-BN films produced on p-type <100> Si substrates by means of Radio Frequency (RF) CVD process. Silicon nitride and oxynitride were deposited by Plasma Enhanced Chemical Vapour Deposition technique and used as a dielectric underlayer. MIS devices were fabricated to allow electrical characterisation. Moreover, the influence of underlayers on adhesion of c-BN to silicon substrate was examined.

[Engineering of Biomaterials, 56-57,(2006),27-29]

Introduction

Several properties of cubic boron nitride (c-BN) like wide bandgap width, good thermal stability, good thermal conductivity, or chemical and mechanical resistance make this material, in combination with other wide bandgap materials, the potential candidate for certain microelectronics and optoelectronics applications, particularly in the field of high-temperature and high-power devices [1-3].

Experiment

The silicon substrates used in these experiments were: p-type <100>, 4-7Ωcm. Substrates were cleaned by the RCA method before the experiments. Then different dielectric underlayers were deposited by PECVD technique on two samples: sample 1 - silicon nitride, sample 2 - silicon oxynitride. After their deposition, samples were transferred to the (RF) CVD reactor and on top of them c-BN films were produced. Additionally, for the purpose of comparison, c-BN films were also deposited directly on silicon. The parameters of the processes are presented in TABLE 1. The thicknesses of the obtained c-BN/dielectric underlayer were measured elipsometrically by Gaertner L117B, λ=632,4 nm.

In order to enable electrical characterisation of the obtained system, round dot metal electrodes (Al) were evaporated on top of the structures and thus metal-insulator-semiconductor (MIS) capacitors were obtained. Subsequently their capacitance-voltage (C-V) and current-voltage (I-V) characteristics were measured. C-V characteristics allowed extraction of the basic parameters (effective charge density (Q_{eff}), flat band voltage (U_{FB}) or mid-bands interface trap density (D_{itmb})) of investigated systems.

At the end, adhesion of c-BN films to silicon was examined, as well as the influence of the underlayer on this parameter. The mechanical scriber technique was used to perform these investigations. Typical method of improving the adhesion is deposition of thin h-BN layer between Si and c-BN film[4-5]. The application of Si_3N_4 and SiO_xN_y interlayers was investigated in this work.

	PECVD		RF CVD	
Number of sample	*parameters*	*thickness [Å]*	*parameters*	*thickness [Å]*
1	Underlayer - Si_3N_4 Power - 10W Pressure - 45 Pa, Time - 30s, Flows: SiH_4 – 95sccm NH_3 – 60sccm	38	Voltage - 105V Time - 45s Pressure - 30 Pa Flow: N_2=20sccm Source of boron: $(C_2H_5)_3B$	~1500
2	Underlayer - SiO_xN_y Power - 10W Pressure - 65 Pa Time - 20s Flows: SiH_4 – 150sccm NH_3 – 32sccm N_2O – 16sccm	36		
3	-	-		

TABLE 1. Process' parameters and thickness of layers used in the experiments.

Results

FIG.1 shows exemplary C-V characteristics of BN films directly deposited onto silicon substrate. The curves were measured in two directions: from inversion to accumulation ("I-A" - see FIG.1) and from accumulation to inversion ("A-I"). The hysteresis loop could be a result of big amount of charge that is collected in a c-BN film. Table 2 shows basic electrophysical parameters that were extracted from C-V

Parameter	Value
ε_i	4,2
U_{FB}	- 2,44 [V]
U_{MB}	- 0,266 [V]
Q_{eff}/q	2,41 E+11
D_{itmb}	4,66 E+11

TABLE 2. Basic electrophysical parameters of the c-BN layer extracted from the C-V measurements.

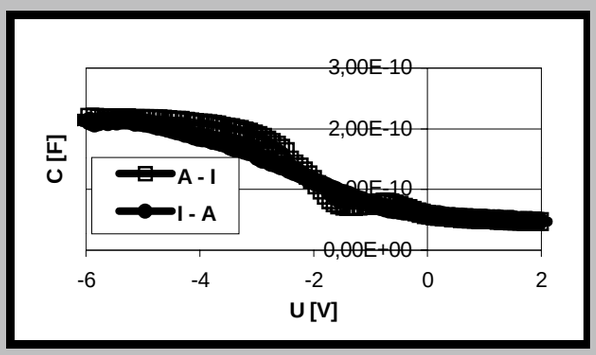

FIG. 1. Exemplary high-frequency (1 MHz) C-V curves of the c-BN/silicon structure.

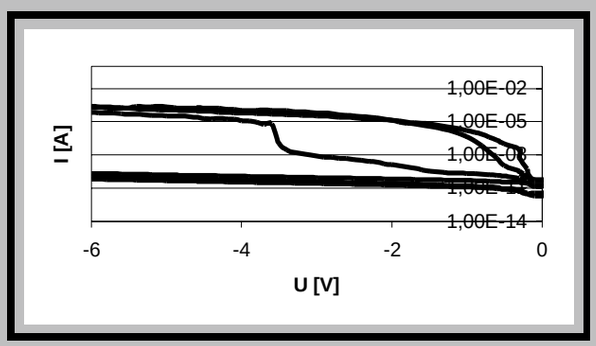

FIG. 2. Current-voltage characteristics of MIS structures with c-BN produced directly on the silicon substrate.

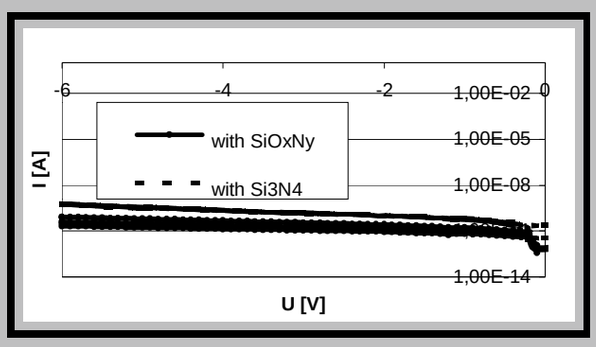

FIG. 3. Current-voltage characteristics of MIS structures with ultrathin dielectric undelayer and c-BN.

curve. The parameters of investigated layers are situated in typical range for this material (depending on method and parameters of deposition [6-8]).

The current-voltage (I-V) characteristics c-BN/silicon system are presented on the FIG. 2. There are two groups of curves. The first group represents structures, that have a break-down for quite low voltage values and high leakage The second group represents structures with a very good isolating properties (see FIG.2).

Next diagram (FIG. 3) shows I-V characteristics of the structures with ultrathin dielectric underlayer. In both cases it can be noticed that after use of ultrathin dielectric underlayer, I-V characteristics look more reproducible. Moreover, silicon oxynitride makes the dual dielectric system more effective as an insulator - there is a visible change in a current flow.

As it was mentioned above, part of this study was the investigation of adhesion. In order to perform these examinations, the samples with and without ultrathin dielectric underlayer were used.

FIG. 4 presents scratches on the c-BN surface which were made using the same weight for all investigated samples. Even without any particular load (it was used only the weight of a diamond scribe holder only) there is a noticeable scratch reaching almost to the silicon substrate. From these figures the following conclusion can be drown: the dielectric undelayer did not improve adhesion of c-BN film to the silicon substrate. Further research focused on improving adhesion, for example high temperature annealing of dielectric film, will be necessary.

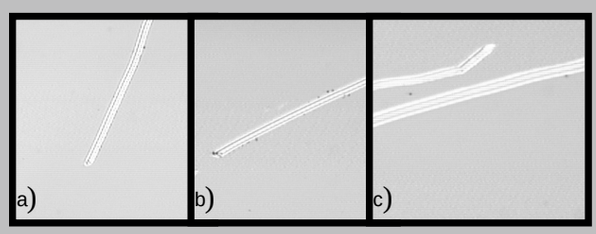

FIG. 4. Pictures of investigated layers - influence on adhesion a. BN without underlayer; b. BN with Si_3N_4 underlayers; c. BN with SiO_xN_y underlayer.

Conclusions

C-BN films were grown on the p-type <100> silicon substrates at the same technological process conditions. Ultrathin dielectric layers were introduced to the dielectric/semiconductor system. Boron nitride film was also deposited directly onto silicon substrate, for comparison. Although hysteresis loop is significant, interface state density value (in the middle of forbidden silicon band) do not exceed $4{,}66e10^{11}$ for the c-BN/silicon system. The current-voltage characteristics became more repeatable and more stable after the introduction of ultrathin dielectric underlayer introducing.

The c-BN/silicon oxynitride/silicon system indicates also a small decrease in current flow, comparing to c-BN/silicon system. Introducing dielectric underlayer did not improve adhesion of boron nitride films to the silicon substrates. Further technological process will be necessary.

References

[1] R. Kirschmann (ed.), High-Temperature Electronics, IEEE Press, Piscataway, 1999.
[2] P.J. Gielisse, "Wide Bandgap Materials in Future Electronic Applications", IMAPS POLAND Conference 2000.
[3] S. Noor Mohammad, Solid-State Electronics, 46 (2002) 203.
[4] S. Kurooka, T. Ikeda, A. Tanaka, Nuclear Instruments and Methods in Physics Research B, 206 (2003), 1088-1091.
[5] H.Walter, K. Bewilogua, A. Schutze, T. Maassen, Diamond and Related Materials, 8 (1999), 110-113.

[6] J. Smidt, Chaos, Solitons & Fractals Vol. 10, No 12, pp 2099-2152, 1999.
[7] A. Werbowy, P. Firek, J. Szmidt, M. Gałązka, A. Olszyna, Journal of Wide Bandgap Materials, SAGE Publ., vol. 9, No. 3 (2002) pp. 169-176.
[8] J. Szmidt, A. Sokołowska, A. Olszyna, A. Werbowy, P. Pawłowski, Diamond and Related Materials 8, (1999), 391-397.

THE EFFECT OF PARTICLES, INCLUDING NANOPARTICLES, ON MACROPHAGES *IN VITRO* AND *IN VIVO*

P.A. Revell*, H. Altaf*, T. McFarlane*, D. Bociaga, K. Mitura****

*Eastman Dental Institute, UCL, London, England
**Technical University of Lodz, Poland.
Email: bakowicz@p.lodz.pl

Abstract

Macrophages remove foreign material from the body and are recruited to sites were there are particles present. Multinucleate giant cells form by the fusion of macrophages. In the presence of particles, macrophages produce various chemical mediators, known as cytokines, as well as enzymes. Some of the cytokines are pro-inflammatory (for example, IL1ß, IL6 and TNFα) while others promote giant cell formation (GM-CSF, M-CSF, TGF). The presence of these cellular products can be shown by examining tissue sections with immunohistochemistry and by western blotting. The message (mRNA) for the synthesis of these molecules can be demonstrated by in situ hybridization and the polymerase chain reaction.

Macrophages process ingested material and present it as antigen to lymphocytes. Antigen-presenting macrophages play an important part in the initiation of metal sensitization. Surface receptors and their counterligands are expressed on macrophages and lymphocytes during antigen presentation.

The particles present in tissues around joint prostheses have been isolated and characterized. Over 95% of these are less than 1 micron (ECD) in size. Transmission electron microscopy has revealed nanoparticles of metal in the range 15-20 nm. Such particles are too small to be phagocytosed. Hydroxyapatite, diamond-like carbon (nano-diamond) and metal particles are being studied and results compared with those of particles in the micrometre range. There is a different response to different nanoparticles.

Key words: *Macrophage; lymphocyte; particles; cytokines; immunity; sensitization; nanodiamond.*
[Engineering of Biomaterials, 56-57,(2006),29-31]

Introduction

After the acute phase of inflammation, macrophages and multinucleate giant cells (MNGC) are responsible for removing foreign material, micro-organisms and dead tissue from the body. MNGC are formed by fusion of macrophages. Both of these cells are recruited to sites were there are particles, for example, wear debris around prosthetic joints. Macrophages are derived from circulating monocytes, migrating from vessels. In the presence of particles, macrophages and MNGC produce chemical mediators, known as cytokines. These can be demonstrated in situ and their production can be induced in cell culture when macrophages are incubated with particles.

It is clear from in vitro studies that macrophages are induced to produce these factors when they phagocytose (engulf) particles. Recognition of foreign material depends on a variety of mechanisms including surface receptors for the Fc component of immunoglobulin and for complement. The particles found adjacent to prosthetic joint components are derived mainly from the load-bearing surfaces and shed into the synovial fluid. It is likely that particles in the body become rapidly coated with proteins, including albumin, globulins, and complement components.

An important function of some macrophages is the processing of ingested material and its presentation as antigen to lymphocytes, the specific mediator cells in immune responses. Antigen-presenting macrophages are found in relation to particles in vivo, and these cells play an important part in the initiation of the process of sensitization to metal. Surface receptors and counterligands are expressed on macrophages and lymphocytes and can be detected in cell culture and in tissue sections. Macrophages and MNGC also contain nitric oxide synthase (iNOS) which gives rise to nitric oxide, a signalling molecule, and superoxide dismutase (SOD), involved in oxygen free radical production. Acid phosphatase (AcP) and non-specific esterase (NSE) play a part in the breakdown of ingested biological material, though there is no intracellular mechanism for intracellular breakdown of particles of man-made materials, such as metal or polyethylene.

The particles present in tissues around joint prostheses have been isolated and characterized. While there are occasional large shards visible by light microscopy, over 95% of particles are less than 1 micron (ECD) in size [1-3]. Transmission electron microscopy has also revealed the presence in some samples of nanoparticles of metal, in the range 15-20 nm. Such particles could not be taken into the cells by the usual phagocytosis process and might be pinocytosed. The study of the effects of nanoparticles on inflammatory cells is at a preliminary phase. Hydroxyapatite, diamond-like carbon (nanodiamond) and metal particles are being studied and results compared with those of particles in the micrometre range.

Materials and methods

Detailed materials and methods are not provided here in this short review. The effect of micro- and nanoparticles on macrophages has been studied in tissue retrieved from man after revision surgery for prosthesis loosening and from animals after experimental procedures. Cell culture studies use primary monocytes and lymphocytes derived from peripheral blood (PBM, PBL) as well as cell lines. Methods of investigation include immunocytochemistry (IHC) with monoclonal antibodies (mab), western blotting, in situ hibridisation (ISH), polymerase chain reaction (PCR) and reverse transcriptase PCR (RT-PCR) as well as ELISA, biochemical assays (eg citrulline- arginine for iNOS) and enzyme histochemistry (eg for AcP and NSE).

Results and discussion

Macrophages and MNGCs

Examination of tissue sections from patients undergoing

revision surgery for aseptic loosening, shows the presence of a cellular infiltrate composed of macrophages, MNGCs and lymphocytes [4-6], though there are also mast cells, fibroblasts and endothelial cells forming new blood vessels. This description will concern itself only with the phagocytic cells and their relationship to lymphocytes. The macrophages and MNGCs can be labelled with mab CD68. When activated, these cells express HLA-DR and integrins (CD11a,b,c) at their surface membrane [7-9]. Double-labelling fluorescence immunocytochemisty shows that these activated cells contain a number of cytokines. Such cytokine production can be demonstrated in functional studies of PBM and the human monocyte/ macrophage cell line U937, using IHC and western blotting to demonstrate each cytokine in tissue and cells, ELISA to show the levels of cytokine released into tissue culture fluid and PCR for the mRNA of each cytokine in cells either in culture or in tissue. The various cytokines known to be produced on microparticle phagocytosis in culture or in vivo are shown in FIGURE 1 [9-17]. Some of these promote the inflammatory process (IL1ß, IL6, TNFα), some are anti-inflammatory (IL10), yet others promote MNGC or ostoeoclast formation (GM-CSF,M-CSF,TGFα -directly; IL1, TNF -indirectly).

Macrophage-lymphocyte interactions

The presence of lymphocytes intermingled with the macrophages and MNGCs was reported over a decade ago [18]. Accumulating evidence points to an immunologically mediated process in the reaction to wear particles [18-21]. There is clinical evidence of metal sensitization in some cases, while others with aseptic loosening show features of a T cell mediated process on immunohistological examination and cell culture. An important function of phagocytic cells is presentation of antigen to lymphocytes. Markers of antigen-presenting cells have been demonstrated on interface macrophages in aseptic loosening (RFD1, CD80, CD86) with the counterligand (CD28) found on the accompanying T helper (CD4) lymphocytes [21-24]. Other ligands and counterligands (HLA-DR, TCR; CD40, CD40L; ICAM, LFA-1) known to be expressed in antigen-presentation are present on the macrophages and lymphocytes associated with particles in situ [25]. Furthermore, the interaction between macrophages phagocytosing particles and T lymphocytes has been modelled in cell culture experiments. T lymphocyte activation and proliferation requires the presence of IL2 or IL15. The latter is present abundantly in the particle-related macrophage infiltrate and its production can be stimulated on phagocytosis of particles in cultured U937 cells [7, 26, 27].

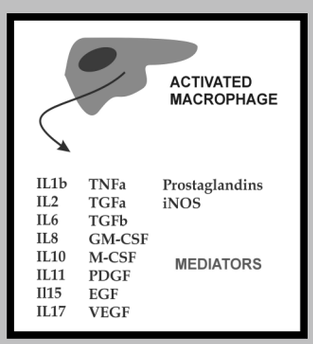

FIG.1. Cytokines and other mediators produced by actived macrophages.

Microparticles and nanoparticles

The studies described above refer to microparticles (>0.1µm diam). However, nanoparticles of titanium (15-20 nm diam) have been noted in cells from the implant interface by transmission electron microscopy in our own laboratory and by researchers in the USA. Little is known of how these nanoparticles enter the cell or of their effect on cell function, which has prompted our preliminary studies in this area. A recently reported experiment showed that nanoparticles of hydroxyapatite (nanoHA) increased the proliferation of Jurkatt T cells when cocultured with U937 cells. This effect was not due to IL15 production by U937 cells. More recent collaborative research has compared the effects of microparticles of CoCr alloy (1.3-2.4µm) with three different nanodiamond particles (0.15-0.81µm; 0.5-1.2µm aggregates; 0.2-0.6µm aggregates) on culture with U937 cells. The expression of HLA-DR, a sign of activation, and CD80, CD86 and CD40, indicators of antigen presentation, were measured using a FACS method. Positive control was provided by lipopolysaccharide (LPS) and negative control by culturing the cells in culture medium alone. CoCr, diamond particles (D1,DB) caused HLA-DR expression. CD86 was expressed with one of these diamond particles and CoCr. There was insignificant HLA-DR or CD86 expression the smallest diamond (D2). The results for CD40 are shown in FIGURE 2. All values are the means with standard errors (3 replicates for each macrophage stimulant). There was expression of CD40 by cells incubated with CoCr and the largest diamond particles (DB) after 24 hrs. This was respectively 3 and 4.5 times greater than CD40 expression in positive controls. There was much less CD40 expression in the case of the D1 and D2 nanodiamond particles. The results are normalized to the mean value for the negative controls, which contained no added particles or LPS.

Conclusions

Particles in the micrometre range (0.1-2.5µm) are phagocytosed by macrophages and cause activation of these cells on the evidence of tissue examination and cell culture studies. Some macrophages fuse to form giant cells (MNGC). Macrophages and MNGC produce numerous mediators and present antigen to lymphocytes upon activation. Particles in the nanometre range (<100nm) are also found in macrophages in tissue. Relatively little is known of their effects on cells but evidence is presented from preliminary studies that macrophage activation and antigen presentation is less with nanoparticles than that seen with microparticles.

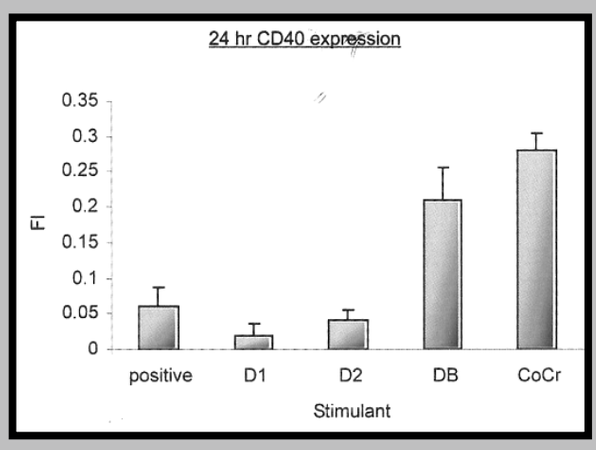

FIG. 2. Expression of CD 40 by U937 cells after incubation with different particles for 24 hrs. CoCr, cobalt chromium; DB, D1, D2, diamond; positive, LPS.

References

[1] Yamac T, The extraction and characterisation of wear particles from tissues around failed orthopaedic implants of different designs PhD Thesis, University of London; 1999.
[2] Kobayashi A, Bonfield W, Kadoya Y, Yamac T, Freeman MAR, Scott G and Revell PA, The size and shape of particulate polyethylene wear debris in total joint replacements. Proc Instn Mech Engrs [H] 211, 11-15; 1997.
[3] Maloney WJ, Smith RL, Schmalzreid TP, Chiba J, Huene D and Rubash H, Isolation and characterisation of wear particles generated in patients who have had failure of hip arthroplasty without cement. J Bone Jt Surg 77A, 1301-1310; 1995.
[4] Revell PA. Tissue reactions to joint prostheses and the products of wear and corrosion. Curr Top Pathol 71, 73-101; 1982
[5] Revell PA, Al-Saffar N and Kobayashi A. Biological reaction to debris in relation to joint prostheses. Proc Instn Mech Engrs 211H, 187-197; 1997.
[6] Al-Saffar N and Revell PA, Pathology of the Bone-Implant Interfaces. J Long-term Effects of Medical Implants 9, 319-347; 1999
[7] Revell PA and Jellie SE. Interleukin 15 production by macrophages in the implant interface membrane of aseptically loosened joint replacements. J Mater Sci; Mater in Med 9, 727-730;1998.
[8] Clarke SA and Revell PA. Expression of ß2 integrins at the bone/biomaterial interface. Proc Soc Biomat, San Diego, California;1998.
[9] Clarke SA. Integrin expression at the bone biomaterial interface. PhD Thesis, University of London, 1999
[10] Al-Saffar N and Revell PA, Pathology of the Bone-Implant Interfaces. J Long-term Effects of Medical Implants 9, 319-347; 1999.
[11] Al-Saffar N and Revell PA. Interleukin-1 production by activated macrophages surrounding loosened orthopaedic implants: a potential role in osteolysis. Br J Rheumatol 33, 309-316: 1994.
[12] Al-Saffar N and Revell PA. Differential expressioin of transforming growth factor-α and macrophage colony-stimulating factor/colony stimulating factor-1R (c-fms) by multinucleated gian cells involved in pathological bone resorption at the site of orthopaedic implants. J Orthop Res 18, 800-807; 2000.
[13] Chiba J, Rhubash HE, Kim KJ and Iwaki Y. The characterization of cytokines in the interface tissue obtained from failed cementless total hip arthroplasty with and without femoral osteolysis. Clin Orthop 300, 304-312; 1994.
[14] Al-Saffar N, Revell PA, Khwaja HA and Bonfield W. Assessment of the role of cytokines in bone resorption in patients with total hip replacement. J Mater Sci; Mater in Med 6, 762-767; 1995.
[15] Al-Saffar N, Revell PA, Khwaja HA and Kadoya Y. Assessment of the role of GM-CSF in the cellular transformation and the development of erosive lesions around orthopaedic implants. Am J Clin Pathol 105, 628-639; 1996.
[16] Xu JW, Kontinnen YT, Li TF, Waris TF, Lassus J, Matucci-Cerinic M, Sorsa T and Snatavirta TS. Production of platelet-derived growth factor in aseptic loosening of total hip replacement. Rheumatol Int 17, 215-221; 1998.
[17] Hercus B, Saeed S and Revell PA. Expression profile of T cell associated molecules in the interfacial tissue of aseptically loosened prosthetic joints. J Mater Sci: Mater Med 13, 1153-1156; 2002.
[18] Lalor PA, Revell PA, Gray AB, Wright S, Railton GT and Freeman MAR. Sensitivity to titanium. A cause for implant failure? J Bone Jt Surg 73B, 25-28; 1991.
[19] Weyand CM, Geisler A, Brack ME, Bolander ME and Goronzy JJ. Oligoclonal T-cell proliferation and interferon-gamma production in periprosthetic inflammation. Lab Invest 78, 677- 685; 1998
[20] Hercus B and Revell PA. Phenotypic characteristics of T lymphocytes in the interfacial tissue of aseptically loosened prosthetic joints. J Mater Sci: Mater Med 12,1063-1067; 2001.
[21] Bainbridge JA, Revell PA and Al-Saffar N. Costimulatory molecule expression following exposure to orthopaedic implants wear debris. J Biomed Mater Res 54, 328-334; 2001.
[22] Al-Saffar N, Revell PA and Kobayashi A. Modulation of the phenotypic and functional properties of phagocytic macrophages by wear particles from orthopaedic implants. J Mater Sci: Mater Med 8, 641-648; 1997.
[23] Altaf H, Saeed S, Bhatt R and Revell PA. The assessment of antigen presenting cells in the bone-implant interface. Biomaterialen 4, 86; 2003.
[24] Altaf H and Revell PA. The characterisation of antigen presenting cells in the bone implant interface & in response to biomaterials. Proc 7th World Biomaterials Congress, Sydney, Australia, 686; 2004.
[25] Bhatt R, Saeed S, Altaf H and Revell PA. In vitro assessment of interactions between T-cells and antigen-presenting cells (Apcs) when challenged with biomaterials: the CD40-CD40L interaction. Proc 7th World Biomaterials Congress, Sydney, Australia, 488; 2004.
[26] Saeed S anad Revell PA. Production and distribution of interleukin 15 and its receptors (IL-15R? and IL-R2ß) in the implant interface tissues obtained during revision of failed total joint replacement. Int J Exp Path 82, 201-209; 2001.
[27] Saeed S, Al-Saffar N and Revell PA. Expression of interleukin-15 (IL-15) and its receptors by U937 cells stimulated by metal wear particles retrieved from periprosthetic tissue. Proc 6th World Biomaterials Congress, Hawaii, 401; 2000.

THE INFLUENCE OF NANOCRYSTALLINE DIAMOND LAYERS OBTAINED BY MW/RF PECVD METHOD ON SURFACE PROPERTIES OF AISI 316 L STEEL

Tadeusz Blaszczyk*, Barbara Burnat*, Henryk Scholl*
Piotr Niedzielski , Witold Kaczorowski****

*University of Lodz, Faculty of Physics and Chemistry,
Department of General and Inorganic Chemistry, 90-136
Lodz, Narutowicza 68, Poland
**Technical University of Lodz,
Institute of Materials Science,
Department of Biomedical Engineering,
90-924 Lodz, Stefanowskiego 1/15, Poland
e-mail: tebe@chemul.uni.lodz.pl

Abstract

Determination of corrosion parameters of AISI 316 L with nanocrystalline diamond (NCD) layers deposited by means of new Microwave / Radio Frequency Plasma Enhanced Chemical Vapor Deposition (MW/RF PECVD) method in testing solution 0.5 M NaCl was a basic aim of presented work. We measured corrosion potentials, potentiodynamic characteristics, breakdown and repassivation potentials, corrosion resistance and impedance characteristics of AISI 316 L samples with- and without NCD layers. Summarizing obtained results it can be stated that NCD layers improve corrosion features of AISI 316 L and that surface preparation techniques have insignificant influence on these features.

Keywords: *biomaterials, austenitic steel AISI 316 L, NCD layers, electrochemistry, corrosion*
[Engineering of Biomaterials, 56-57,(2006),31-34]

Introduction

Since 1986 S. Mitura and co-workers from Technical University in Lodz have produced nanocrystalline diamond (NCD) layers on different substrates by means of Radio Frequency Plasma Enhanced Chemical Vapor Deposition Method (RF PECVD) [1-3]. In 2004 a new dual frequency - Microwave and Radio Frequency PECVD method was there applied for NCD layers deposition [4]. Dual frequency

method was in details described by L. Martinu et al. [5] for deposition of P-SiOx films, J. E. Klemberg-Sapieha et.al. [6] for silicon nitride (P-SiN) and amorphous hydrogenerated silicon (a-Si:H) films, and A. Raveh et. al. [7] and P. Reineke et. al. [8] for amorphous diamond-like carbon layers. This method was used also in Technical University of Lodz for NCD layers deposition onto AISI 316 L stainless steel. AISI 316 L has good mechanical properties. That's why it is one of the most frequently used materials as bone-implants placed for short time [9,10]. The improvement both mechanical and corrosion features as result of using NCD layers was mentioned by S. Mitura in earlier publications [11] and in details described by J. Marciniak [9]. Corrosion parameters are different in a lot of publications. The reason lies in preparation processes of samples' surface.

The aim of this work is to presentation of corrosion measurement results of austenitic AISI 316 L prepared by mechanical polishing with abrasive paper SiC and additionally with Al_2O_3, with and without NCD layers. NCD layers were deposited by means of a new MW/RF PECVD method. The following corrosion measurement's results are presented in this work: corrosion potential E_{cor} in open circuit (OCP), polarization resistance R_p using Stern-Geary method, breakdown E_b and repassivation E_{rep} potentials and impedance characteristics (EIS) in 0.5 M NaCl solution.

Experimental methodology

The investigated AISI 316 L samples had cylindrical shapes with 8 mm diameter and ca. 3 mm height. The samples were prepared in two different ways. One part of samples was polished with abrasive paper SiC from 500 to 2000 grit only, rinsed with distilled water and ethanol, and dried with argon (99.999). The other part of samples was additionally polished with Al_2O_3 and next rinsed with distilled water and ethanol, and dried with argon. The surfaces of samples were controlled using optical metallographic microscope.

On such prepared samples' surface NCD layers using MW/RF PECVD method were deposited. Deposition process of NCD layers consisted of two steps: 1) surface etching (power of MW=150 W and RF= 120 W, autopolarization potential V_b=-700V and duration of t=3 min,); 2) NCD layers deposition (MW=150 W and RF=120 W, V_b=-700V, flow of CH_4 50 sccm, and duration of t=2 min). According to above given parameters can estimate a thickness of NCD layers at ca. 1µm.

Electrochemical corrosion measurements were carried out in a glass electrolytic cell (volume ca. 2cm^3) in potentiostatic conditions using potentiostat / galvanostat PGSTAT 30 (EcoChemie AUTOLAB). Internal diameter of rubber ring gasket was a 0.6 cm and hence the active surface area (in contact with solution) was ca 0.28cm^2. During the measurements. temperature was $25^0\pm1^0$C and the solution was mechanically stirred and deoxidized with argon. Special miniature calomel electrode in saturated NaCl solution (standard potential E^0=0.243 V) was used as reference electrode - all potentials in this work are given versus this electrode. All measurements were carried out in cycle described in [12]. This cycle consisted of following steps: 1) corrosion potential measurement Ecor in open circuit potential (OCP) method, 2) current - potential characteristic measurement in potential range from E_{cor}-0.020V to E_{cor}+0.020V according to Stern-Geary method with scan rate 0.5 mV•s^{-1}, 3) impedance characteristic measurement at E_{cor} potential in frequency range from 0.04Hz to 10^4 Hz using sinusoidal signal with E_{AC}=5mV, 4) potentiodynamic characteristic measurement with scan rate 1 mV•s^{-1} from start potential E_{cor} - 0.200V to potential in which the measured current reached to programmed value. Then the scan direction was inversed and the measurement was carried out to the start potential. Steps from 1 to 3 were repeated in post-corrosion and fresh solutions.

Optical metallographic microscope was used for investigation of corroded samples. Scanning electron microscopy HITACHI S-3000N with an X-Ray microprobe analyzer EDX THERMO NORAN was used for structure and elements composition measurements.

Results

Corrosion potentials E_{cor}

For each sample we measured potential E vs time t. A final stable potential was considered as corrosion potential E_{cor}. Average values of E_{cor} and standard deviation are presented in TABLE 1.

It can be stated that E_{cor} values of AISI 316 L without NCD layers are independent from preparation method. A potential E_{cor} of AISI 316 L samples with NCD layers is more anodic in comparison with AISI 316 L samples without NCD layers. This potential depends on preparation technique and can be attributed with changes, which take place in structure of layer's surface during NCD deposition. After anodic polarization (designated "After corrosion") Ecor potentials did not monotonically change. The interpretation of observed E_{cor} changes is difficult. The most significant is a comparison of E_{cor} values in the same conditions i.e. before and after corrosion in fresh solution. Post-corrosion solutions can have different concentrations of corrosion products for each examined sample, which lead to large results dispersion (higher standard deviation). These results can be helpful with analysis of AISI 316 L implant's behavior in contact with human body - products of corrosion can accumulate in tissue nearby implant and cause situations close to second period of presented measurement.

Breakdown potentials E_b and repassivation potentials E_{rep}.

The preparation technique of AISI 316 L surface had a negligible influence on its potentiodynamic characteristics. FIGg.1 present example of potentiodynamic characteristics of samples (prepared with SiC abrasive papers) with and without NCD layers. It is important to notice that breakdown potentials E_b were difficult to detect from these characteristics - increase of measured current was not so sharp as for example in corrosion processes of Ti in KBr solutions [13]. Crevice and pitting corrosion occurred simultaneously near rubber gasket and it is a reason of this current - potential characteristic shape. That's why there is a great possibility to make error by determining the E_b value.

FIG. 2 shows fundamental difference between features of both samples - pits which emerged on surface of AISI 316 L without NCD developed in wide range of polarization potential up to potential close corrosion potential E_{cor}. In con-

Sample	Preparation	Before corrosion		After corrosion		After corrosion (in fresh solution)	
		E_{cor} [V]	ΔE_{cor}[V]	E_{cor} [V]	ΔE_{cor}[V]	E_{cor} [V]	ΔE_{cor}[V]
AISI	SiC	-0.17	0.01	-0.24	0.12	-0.15	0.09
AISI	SiC + Al_2O_3	-0.17	0.05	-0.31	0.12	-0.26	0.07
AISI with NCD	SiC	-0.10	0.05	-0.12	0.04	-0.17	0.06
AISI with NCD	SiC + Al_2O_3	0.01	0.05	0.13	0.16	-0.15	0.10

TABLE 1. Corrosion potentials E_{cor} of investigated samples.

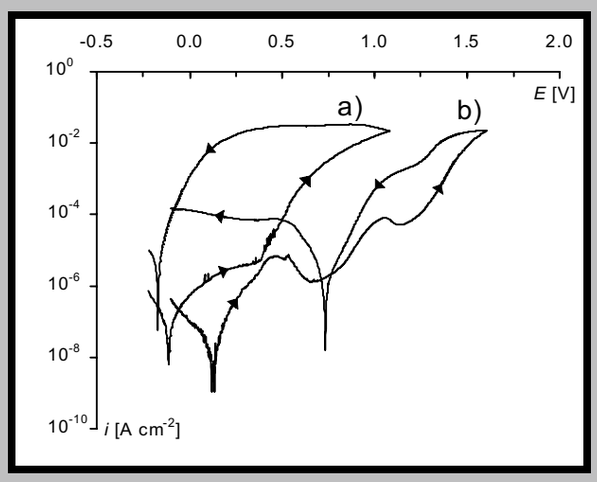

FIG. 1. Potentiodynamic characteristics for a) AISI 316 L and b) AISI 316 L with NCD layers; samples polishing with SiC.

trary - pits which emerged on surface of AISI 316 L with NCD layers repassivated in potential ca. 0.2 V that is more cathodic than breakdown potential E_{cor}. The same behavior is observed for AISI 316 L samples after polishing with Al_2O_3. E_b and E_{rep} potentials are more positive for AISI 316 L with NCD layers in the range from 0.7V to ca. 1V than AISI 316L without NCD. These potentials depend little on preparation technique (FIG.2). It means that possible differences of layers' surface connected with the different preparation technique, which were mentioned with corrosion potential analysis, have no influence on pits creation. Crevice and pitting corrosion were detected by microscopic investigations of samples' surface.

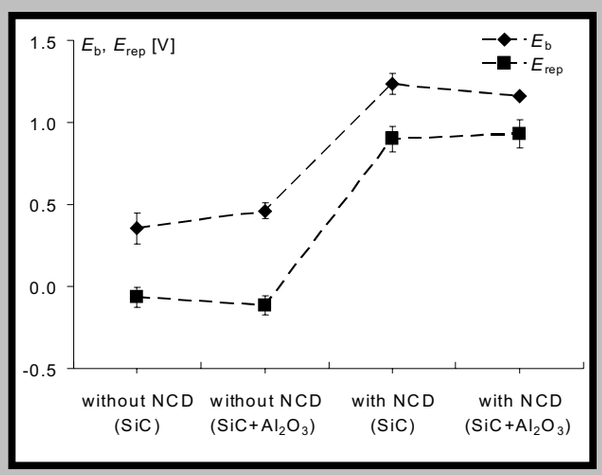

FIG. 2. Breakdown E_b and repassivation E_{rep} potentials vs. samples preparation and NCD layers presence.

Corrosion resistance Rp and corrosion current icor

The R_p resistance and corrosion current icor were calculated from Stern-Geary linear characteristics (see TABLE 2).

Analyzing obtained results it can be stated that before anodic polarization of AISI 316 L with NCD layers the polarization resistance R_p is 1.5÷2.0 times higher than the resistance R_p of the same samples without NCD. A corrosion current icor behaves reversely. A preparation technique of

Sample	Preparation	R_p [Ω cm^2]	ΔR_p [Ω cm^2]	i_{cor} [A cm^{-2}]	Δi_{cor} [A cm^{-2}]
AISI	SiC	$1.28 \cdot 10^5$	$0.43 \cdot 10^5$	$2.22 \cdot 10^{-7}$	$0.72 \cdot 10^{-7}$
AISI	SiC + Al_2O_3	$1.85 \cdot 10^5$	$0.37 \cdot 10^5$	$1.46 \cdot 10^{-7}$	$0.31 \cdot 10^{-7}$
AISI with NCD	SiC	$1.92 \cdot 10^5$	$0.95 \cdot 10^5$	$1.59 \cdot 10^{-7}$	$0.69 \cdot 10^{-7}$
AISI with NCD	SiC + Al_2O_3	$3.75 \cdot 10^5$	$1.48 \cdot 10^5$	$7.84 \cdot 10^{-8}$	$3.44 \cdot 10^{-8}$

TABLE 2. Polarization resistance R_p and corrosion current icor before anodic polarization.

sample surface has influence on both values - R_p is higher for samples, which are polished with Al_2O_3 in comparison with samples, which are polished with SiC. It is connected with surface roughness - after polishing with SiC there are a large quantity of scratches on sample's surface, which enlarge an "electrochemical" surface. This fact has high influence on corrosion processes. Rp resistance of samples with NCD layers decreases drastically after anodic polarization independently of surface preparation technique.

Impedance characteristics

Impedance characteristics of AISI 316 L without and with NCD layers after polishing with abrasive papers SiC and additionally with Al_2O_3 before anodic polarization as Bode plot shows FIG.3a. Electrical equivalent circuit used for fitting the experimental characteristics is presented in FIG.3b.

All presented characteristics in FIG.3a. are similar and therefore they are not designated. Electrical equivalent cir-

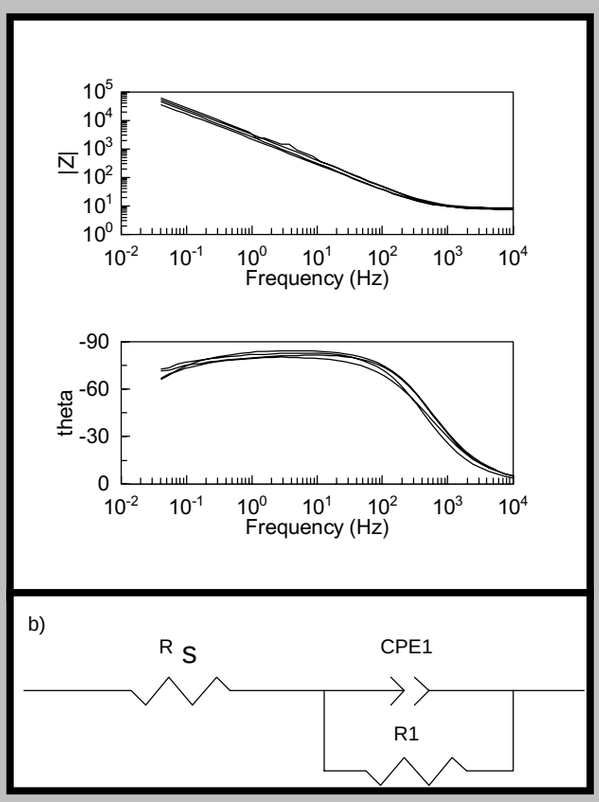

FIG. 3. Impedance characteristics of AISI 316 L without and with NCD layers;
a) Bode plots (see text), b) electrical equivalent. circuit.

cuit contains uncompensated electrolyte resistance, i.e. the resistance of electrolyte between working electrode and reference one, Rs¨7.4÷8.2 W·cm^2, constant phase element CPE1-T¨(5.5÷8.8)·10^{-5}, CPE1-P¨0.89÷0.94 and reaction resistance R1¨(0.4÷1.9)·10^4 Ω·cm^2. Constant phase element corresponds to the double layer capacity (CPE1-P is close 1) and includes information about the surface roughness.

Conclusions

Summarizing results presented above it can be stated that NCD layers: 1) shift a corrosion potential E_{cor} in more positive values but surface preparation method has negligible influence on E_{cor} potential; 2) shift breakdown E_b and repassivation E_{rep} potentials in more anodic values and decrease a potential range in which occurs pitting corrosion; 3) increase polarization resistance R_p and decrease corrosion current icor in corrosion potential E_{cor} but R_p and i_{cor} values depend on surface preparation; 4) have no influence on impedance characteristics. In final conclusions it can be stated that NCD layers improve corrosion features of AISI 316 L and that surface preparation techniques have insignificant influence on these features.

Acknowledgements

This work was supported by the MS&IST grant No. 3 T08C 036 27.

References

[1] Mitura E., Niedzielska A., Niedzielski P., Mitura S. The properties of carbon layers deposited onto titanium substrates. // Diamond and Related Materials - 1996. -5. - P. 998-1001.
[2] Mitura S. Nanotechnology in Materials Science. - Amsterdam: Pergamon - Elsevier Science Ltd, 2000
[3] Mitura S., Mitura A., Niedzielski P., Couvrat P. Nanocrystalline Diamond Coatings. // Journal of Chaos, Solitons and Fractals (Special Issue) - 1999. - 10(12). - P. 2165-2177.
[4] Kaczorowski W., Niedzielski P., Mitura S. Manufacture of carbon coating for biomedical applications in a new MW/RF reactor. // Eng. of Biomaterials -2005. -43-44. - P. 28-31.
[5] Martinu L., Klemberg-Sapieha J. E., Wertheimer M. R. Dual-mode microwave / radio frequency plasma deposition of dielectric thin films // Appl. Phys. Lett. - 1989. - 54. - P. 2645-2647.
[6] Klemberg-Sapieha J. E., Kuttel O. M., Martinu L., Wertheimer M.R. Dual microwave - R.F. plasma deposition of functional coatings. // Thin Solid Films - 1990. - 193/194. - P. 965-972.
[7] Raveh A., Martinu L., Hawthorne H.M., Wertheimer M.R. Mechanical Properties of Dual-Frequency Plasma Deposited Diamond-like Carbon // Surf. Coat. Technol. - 1993. - 58. - P. 45-55.
[8] Reinke P., Klemberg-Sapieha J.E., Martinu L. Effect of Amorphous Carbon Layers on the Growth of Diamond in Dual-Frequency Plasma // J. Appl. Phys. - 1994. - 76. - P. 5754-5759.
[9] Marciniak J. Biomateriały. - Gliwice: Wydawnictwo Politechniki Śląskiej, 2002 P. 493.
[10] Laskawiec J., Michalik R. Zagadnienia teoretyczne i aplikacyjne w implantach. - Gliwice: Wydawnictwo Politechniki Śląskiej, 2002 P. 170.
[11] Couvrat P., Denis M., Langer M., Mitura S., Niedzielski P., Marciniak J. The corrosion tests of amorphous carbon coatings deposited by r.f. dense plasma onto steel with different chromium contents. // Diamond and Related Materials - 1995. - 4. - P. 1251.
[12] Boguslawski G., Blaszczyk T., Scholl H. Electrochemical corrosion of Ti6Al4V alloy with nanocrystalline diamond coatings. // Eng. of Biomaterials - 2004. - 38-42. - P. 160-163.
[13] Scholl H., Blaszczyk T., Niedzielski P., Gralewski J. Biomaterials in nanoelectrochemistry - corrosion investigations of Titanium and Titanium with NCD layers. // Eng. of Biomaterials - 2004. - 35-36. - P. 45-53.

CORROSIVE FEATURES OF Ti WITH NANOCRYSTALLINE DIAMOND LAYERS OBTAINED BY MEANS RADIO FREQUENCY AND MICROWAVE / RADIO FREQUENCY PLASMA CHEMICAL VAPOR DEPOSITION METHODS

Barbara Burnat*, Witold Kaczorowski, Grzegorz Boguslawski**, Tadeusz Blaszczyk*, Henryk Scholl***

*University of Lodz, Faculty of Physics and Chemistry,
Department of General and Inorganic Chemistry,
90-136 Lodz, Narutowicza 68
**Technical University of Lodz,
Institute of Materials Science,
Department of Biomedical Engineering,
90-924 Lodz, Stefanowskiego 1/15
e-mail: burnat@op.pl

Abstract

A new dual-mode microwave / radio frequency (MW/RF) plasma reactor for deposition of nanocrystalline diamond (NCD) coatings has been developed in Technical University of Lodz. In this work we present the results of investigations concerning influence of NCD layers deposition method on corrosive features of Ti in Tyrode's solution. NCD layers were produced by means of Radio Frequency and Microwave / Radio Frequency Plasma Chemical Vapor Deposition (RF PCVD and MW/RF PCVD). Electrochemical investigations show that both NCD coatings improve some corrosive features of Ti. However obtained results show that pitting corrosion did not occur on Ti/NCD RF samples, but it occur on Ti/NCD MW/RF despite of thicker NCD layers.

Keywords: *Ti; nanocrystalline diamond (NCD); NCD deposition methods; RF PCVD; MW/RF PCVD; electrochemical measurements; corrosion parameters.*
[Engineering of Biomaterials, 56-57 ,(2006),34-37

Introduction

Ti and its alloys play an important role in medical applications as implants [1]. Materials used in human body, as medical implants, must be characterized by: good biocompatibility, chemical stability, biostability, good adhesion and excellent mechanical characteristics [2]. In order to enhance mechanical properties, corrosion resistance and biocompatibility of biomaterials a deposition of different carbon coatings is used. Diamond-like carbon (DLC) and nanocrystalline diamond (NCD) are the most often used carbon coatings. DLC films contain 80% sp^3-bonded carbon [3,4]. NCD coatings, as Mitura reported in [5], have a thickness of about 0.5-1 μm and are composed of 97% diamond. One of the latest works about Microwave Plasma Chemical Vapor Deposition (MPCVD) technique signalizes a possibility of producing a new form of diamond film called ultrananocrystalline diamond (UNCD) which consist of crystalline grains of 95% sp^3-bonded carbon that are 3-5 nm in size [4]. DLC, NCD and UNCD layers are produced in different chemical vapor deposition processes: Radio Fre-

quency Plasma Chemical Vapor Deposition (RF PCVD) [5], Microwave Plasma Chemical Vapor Deposition (MPCVD) [4] and Microwave / Radio Frequency Plasma Chemical Vapor Deposition (MW/RF PCVD) [6-8].

In Technical University of Lodz are available RF PCVD and MW/RF PCVD methods for NCD layers deposition. The aim of this study was to compare an influence of these deposition methods on corrosive features of Ti in Tyrode's solution, especially an oxidation of sp^2-bonded carbon, breakdown potential, repassivation potential, polarization resistance, corrosion rate and type of corrosion. Obtained differences in corrosive features may be joined with changing of surface layers different for used deposition techniques

.

Experimental

All measurements were done using cylindrically shaped samples of Ti (99.99 - Aldrich) with a diameter of 6.35 mm. Preparation of Ti electrodes consisted of sequential wet polishing with 1000 and 2000 grit SiC paper, polishing with diamond gel 1 μm and chemical etching in Kroll's solution ($HF:HNO_3:H_2O$ in volume ratio 1:3:5 respectively). Finally, the samples were rinsed with distilled water and dried in argon. The surface appearance was verified using optical metallographic microscope. Such prepared Ti samples were covered by NCD using two different methods: RF PCVD and MW/RF PCVD. RF generator was connected to working electrode with Ti samples. MW power was applied through a quartz tube mounted in opposite to working electrode [8]. The main parameters of NCD deposition processes are shown in TABLE 1.

According to parameters given in TABLE 1 a thickness of NCD layers can be estimated at ca. 0.5 μm for RF PCVD and even four-times higher for MW/RF PCVD.

Electrochemical measurements were carried out in a glass electrolytic cell with a volume of ca. 2 cm^3 [9]. All corrosion measurements were carried out in a typical three-electrode system. Calomel electrode in saturated NaCl solution was used as a reference electrode. Tyrode's solution (0.8 g NaCl, 0.02 g $CaCl_2$, 0.02 g KCl, 0.1 g $NaHCO_3$, 0.1 g D-glucose, 0.1 $MgCl_2$, 0.005 g NaH_2PO_4 and H_2O in 100 cm^3 solution) [10] was prepared from chemical reagents POCh S.A. (Polish Chemical Reagents) and Aldrich - with purity "for analysis" - without additional purification. Following electrochemical methods were used in corrosion measurements according to [11]: open-circuit potential (OCP) for corrosion potential E_{corr} detection, Stern-Geary's method for polarization resistance R_p and corrosion rate CR detection, potentiodynamic curves for breakdown potential E_b and repassivation potential E_{rep} detection and electrochemical impedance spectroscopy (EIS) which allowed to determine properties of phase boundary electrolyte solution / sample [12].

The surface appearance before and after the corrosion process was verified using optical metallographic microscope. Surface structure and elements composition analysis of samples after corrosion process were performed using scanning electron microscopy with X-ray analysis (SEM-EDX) method.

Parameters		RF PCVD	MW/RF PCVD
Ion etching	Gas	Ar	Ar
	Bias voltage	-800 V	-700 V
	RF power	2.5 kW	320 W
	MW power	-	150 W
	Time of etching	2 min	10 min
Deposition of NCD layers	Gas	CH_4	CH_4
	Bias voltage	-800 V	-700 V
	RF power	2.5 kW	500 W
	MW power	-	150 W
	Gas stream velocity	25 sccm	20 sccm
	Time of deposition	10 min	12 min

TABLE 1. The main parameters of NCD deposition processes.

Sample	E_{corr} [V]	E_b [V]	E_{rep} [V]
Ti	-0.383±0.026	no exist	no exist
Ti/NCD (RF PCVD)	0.165±0.001	no exist	no exist
Ti/NCD (MW/RF PCVD)	0.065±0.040	3.38±0.33	3.22±0.28

TABLE 2. Corrosion, breakdown and repassivation potentials.

Results and discussion

Electrochemical measurements

Values of open circuit potential E vs. time t were collected for each sample. Time of registration was from 2000s till 6000s. Stabilized electrode potential was established as corrosion potential E_{corr}. Averaged values and standard deviations of E_{corr} are presented in TABLE 2. Potentiodynamic characteristics dependence of current density j=I/A (I - measured current [A], A - sample surface [cm^2]) versus polarization potential E [V] are presented in FIG.1. Breakdown potential E_b and repassivation potential E_{rep} values obtained from these characteristics are also presented in TABLE 2. In case of Ti electrodes with NCD layers deposited by RF PCVD method pitting corrosion did not occur, and therefore E_b and E_{rep} values were impossible to detect.

Analyzing data presented in TABLE 2 it can be stated that NCD layers cause increase of corrosion potential Ecorr form -0.383 V to 0.165 V (ca. 0.45 V) in case of RF PCVD and form -0.383 V to 0.065 V (ca. 0.55 V) in case of MW/RF PCVD deposition methods. In case of Ti without NCD and Ti with NCD layers deposited using plasma vapor deposition method with radio frequency (called Ti/NCD RF) there was no breakdown in Tyrode's solution. Oxidation peak current was observed in potential range 1-3 V on the obtained potentiodynamic characteristics for Ti/NCD RF. This oxidation peak was joined with intensive gas bubbling on sample surface, and it can be attributed to presence of graphitic (sp^2) material on deposited NCD layers [13]. For Ti samples with NCD layers deposited using dual frequency plasma vapor deposition method (called Ti/NCD MW/RF) breakdown potential E_b was close to 3.4 V. Repassivation

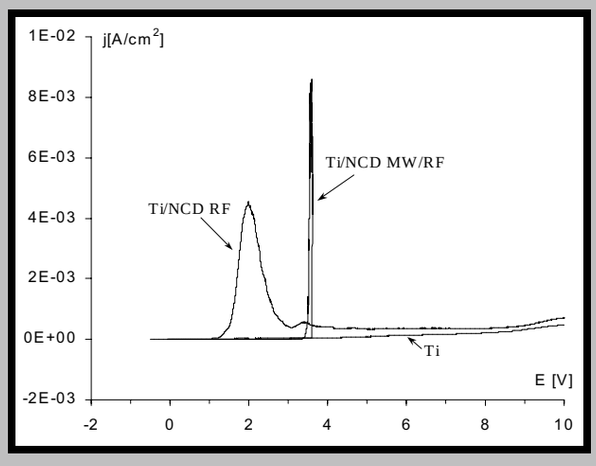

FIG. 1. Potentiodynamic characteristics of investigated electrodes in Tyrode's solution.

Sample	CR [mmPY]	Rp [Mohm·cm^2]
Ti	(5.65±0.46)·10^{-5}	4.0±0.3
Ti/NCD (RF PCVD)	(3.49±0.18)·10^{-6}	64.7±3.6
Ti/NCD (MW/RF PCVD)	(4.18±0.66)·10^{-6}	54.6±8.6

TABLE 3. Averaged values of corrosion rate CR and polarization resistance R_p.

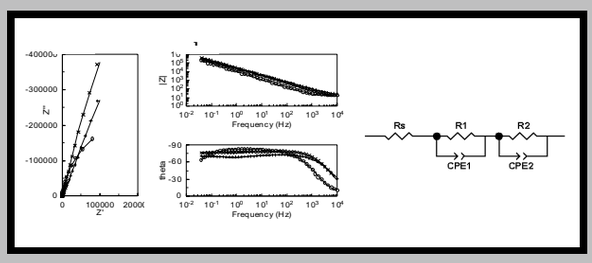

FIG. 2. Nyquist (a) and Bode (b) plots for Ti (o), Ti/NCD RF (´) and Ti/NCD MW/RF (+); electrical equivalent circuit (c).

Sample	Rs [ohm·cm^2]	R1 [ohm·cm^2]	CPE1-T	CPE1-P	R2 [ohm·cm^2]	CPE2-T	CPE2-P
Ti	14.4	64	8.53·10^{-4}	0.657	5.28·10^5	1.77·10^{-5}	0.928
Ti/NCD RF	12.1	2498	5.63·10^{-5}	0.897	5.11·10^6	8.37·10^{-6}	0.886
Ti/NCD MW/RF	17.3	7246	2.96·10^{-5}	0.821	4.48·10^6	1.06·10^{-5}	0.829

TABLE 4. Elements' values of electrical equivalent circuit.

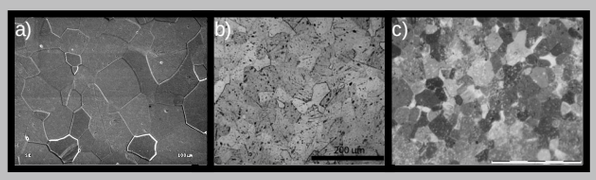

FIG. 3. SEM picture of Ti without NCD (a), optical microscope images of Ti/NCD RF (b) and Ti/NCD MW/RF (c).

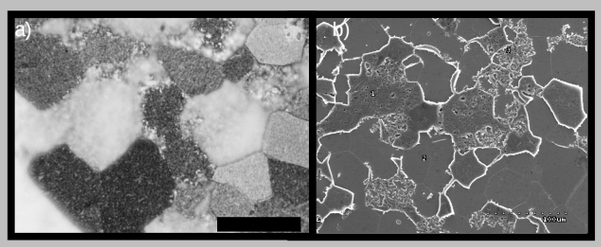

FIG. 4. Pitting corrosion on Ti/NCD MW/RF: optical microscope image (a), SEM picture (b).

	Point 1		Point 2		Point 3	
	Atom %	El. Wt. %	Atom %	El. Wt. %	Atom %	El. Wt. %
Ti	36.88	60.53	87.08	95.50	36.75	60.47
C	5.02	2.06	2.58	0.71	6.46	2.67
O	48.45	26.57	10.34	3.79	46.99	25.82
Na	1.65	1.30	-	-	1.65	1.30
Mg	0.84	0.70	-	-	0.86	0.72
P	0.90	0.95	-	-	1.18	1.25
Cl	4.56	5.54	-	-	4.00	4.87
Ca	1.71	2.34	-	-	2.11	2.91

TABLE 5. SEM-EDX element composition of Ti/NCD MW/RF surface after corrosion.

potential $E_{re}p$ was ca. 3.2 V for these samples. Oxidation peak was not observed on these samples. That's why the presence of graphitic (sp^2) material on surface of Ti/NCD MW/RF may be negligible.

Polarization resistance R_p and corrosion rate CR were calculated from Stern-Geary's characteristics using CorrView program. The Stern-Geary's characteristics were registered with scan rate 0.5 mV/s in potential range from E_{corr} -20 mV to E_{corr} +20 mV. Averaged values of these parameters are presented in TABLE 3.

Analyzing data presented in TABLE 3 it can be stated that NCD layers deposition on Ti causes more than ten-times increasing of R_p values. Corrosion rates for Ti with NCD layers, independent of deposition method, are order of magnitude smaller than for Ti without NCD.

Impedance characteristics EIS were registered at Ecorr potential in wide frequency range from 10 kHz to 40 mHz, with a harmonic signal E_{AC} =5 mV. Examples of characteristics for investigated samples and electrical equivalent circuit fitting obtained experimental data are presented in FIG.2.

The circuit was the same for all investigated samples. It contained uncompensated electrolyte resistor Rs, two identical branches CPE1 || R1 and CPE2 || R2 connected in series. The first branch CPE1 || R1 describes impedance characteristics in high frequency range, while the second branch CPE2 || R2 describes them in low frequency range. CPE1-T element corresponds to differential double layer capacity of phase boundary solution / sample, while CPE1-P values corresponds to surface roughness. Resistance R1 describes corrosion processes. R1 value significantly increases after NCD layers deposition, what can be joined with decreasing of corrosion reaction rate. Simultaneously decreases differential double layer capacity (CPE1-T). Physicochemical meaning of CPE2 and R2 is equivocal - these elements may correspond to phase boundary titanium oxide / titanium features [14].

Microscopic measurements - surface structure and elements composition analysis

SEM picture of Ti without NCD and optical microscopes images for Ti with NCD layers are presented in FIG.3. Changes caused by pitting corrosion on Ti/NCD MW/RF are shown in FIG. 4. Elements composition for three points of corroded surface marked on FIG.4b are presented in TABLE 5.

On Ti surface without NCD layers and after NCD layers deposition the crystallites of the substrate are clearly visible (FIG. 3). NCD layers deposited using RF PCVD method change the sample color form metallic-silver to yellow (FIG. 3b), while layers deposited by means MW/RF PCVD method give blue color (FIG. 3c). FIG.4a shows that corrosion processes for Ti/NCD MW/RF take place on whole crystallites surface with preferable orientation (areas out of focus). This effect is confirmed by SEM picture (FIG. 4b). Elements composition data from TABLE 5 show that Ti, O and C are present in any point of this surface. Moreover the presence of other elements such as Na, Mg, P, Cl and Ca was found in points 1 and 3 and it may be joined with corrosion processes in Tyrode's solution. Smooth region with point 2 is a region of crystallites which did not corrode. Making a comparison of C contents in analyzed points it can be found that in points 1 and 3 the contents of C are unexpectedly higher than in point 2. This fact can be explain by the appearance of C from glucose existing in Tyrode's solution.

Summary and conclusions

Electrochemical investigations show that both NCD coatings improve some corrosive features of Ti. In case of Ti

with NCD layers the shift of corrosion potential was observed in more positive values. Moreover the corrosion rates of Ti with both NCD layers are order of magnitude smaller than for Ti without NCD. The both NCD coatings have comparable values of corrosion rate and polarization resistance. Investigated samples with different NCD coatings have similar impedance characteristics and the same equivalent electrical circuit.

Obtained electrochemical results show different corrosive features of NCD layers deposited on Ti using two different techniques - pitting corrosion did not occur on Ti/NCD RF samples, but it occur on Ti/NCD MW/RF despite of thicker NCD layers. Microscopic investigations made for Ti/NCD MW/RF show that localized corrosion process is joined with surface microstructure - pitting corrosion take place on whole crystallites surface with preferable orientation. These differences in corrosive features may be joined with changing of surface layers different for used deposition techniques. In electrochemical aspect the new method MW/RF PCVD (despite of existing breakdown at 3.4V) is better in comparison with RF PCVD, because there is no anodic peak in potential range 1-3V. Therefore it can be supposed that the presence of graphitic (sp2) material on NCD layers deposited by MW/RF PCVD method is smaller.

Summarizing obtained results can be stated that MW/RF PCVD technique requires subsequent improvement of the main parameters of NCD deposition processes on Ti so that the breakdown will be eliminate or the breakdown potential will be shifted to maximum value.

References

[1] Marciniak J. Biomaterialy. - Gliwice: Wydawnictwo Politechniki Śląskiej, 2002

[2] Long M., Rack H.J. Titanium alloys in total joint replacement - a materials science perspective // Biomaterials - 1998. - 19. - P. 1621-1639.

[3] Friedmann T.A., Sullivan J.P., Knapp J.A., Tallant D.R., Follstaedt D.M. Medlin D.L., Mirkarimi P.B. Thick stress-free amorphous-tetrahedral carbon films with hardness near that of diamond // Appl. Phys. Lett. - 1997. - 71. - P. 3820-3822.

[4] Carlise J.A., Auciello O. Ultracrystalline Diamond. Properties and Applications in Biomedical Devices // Interface - 2003. - 12. - P. 28-31.

[5] Mitura S. Nanotechnology in Materials Science. - Amsterdam: Pergamon - Elsevier Science Ltd, 2000

[6] Raveh A., Martinu L., Hawthorne H.M., Wertheimer M.R. Mechanical Properties of Dual-Frequency Plasma Deposited Diamond-like Carbon // Surf. Coat. Technol. - 1993. - 58. - P. 45-55.

[7] Reinke P., Klemberg-Sapieha J.E., Martinu L. Effect of Amorphous Carbon Layers on the Growth of Diamond in Dual-Frequency Plasma // J. Appl. Phys. - 1994. - 76. - P. 5754-5759.

[8] Kaczorowski W., Niedzielski P., Mitura S. Manufacture of carbon coatings for biomedical applications in a new MW/RF reactor / / Eng. of Biomaterials - 2005. - 43-44. - P. 28-31.

[9] Boguslawski G., Blaszczyk T., Scholl H. Electrochemical corrosion of Ti6Al4V alloy with nanocrystalline diamond coatings // Eng. of Biomaterials - 2004. - 38-42. - P. 160-163.

[10] Bell E., Wingate R.J.T., Eddison M.,Toole L. Segmental identity and cerebellar granule cell induction in rhombomere 1. - BMC Biology - 2004. - 2 (14). - ISSN 1741-7007.

[11] ASTM G 102-89 (Reapproved 2004) Standard Practice for Calculation of Corrosion Rates and Related Information from Electrochemical Measurements.

[12] Bard A.J. Electrochemical methods. Fundamentals and applications. - John Wiley & Sons, Inc., New York, 1980

[13] Hian L.C., Grehan K.J., Compton R.G., Foord J.S., Marken F. Nanodiamond thin films on titanium substrates // J.Electrochem.Soc. - 2003. - 150. N 1. - P. E59-E63.

[14] Kolman D.G., Scully J.R. Electrochemistry and passivity of a Ti-15Mo-3Nb-3Al beta-titanium alloy in ambient temperature aqueous chloride solutions // J.Electrochem.Soc. - 1993. - 140. - P. 2771-2779.

PROPERTIES OF NiTi - SHAPE MEMORY ALLOY AFTER MODIFICATION BY RF PCVD METHOD

M.Czerniak-Reczulska*, P.Couvrat, J.Grabaczyk*, P.Niedzielski***

*Biomedical Engineering Division,
Institute of Materials Science and Engineering,
Technical University of Lodz, Poland
**Materials Department,
Ecole Catholique D'Arts et Metiers, Lyon, France
e-mail :gosiacze@p.lodz.pl

Abstract

The DLC (diamond-like carbon) and NCD (nanocrystalline diamond) layers coat made implants of medical steel 316 L, titanium and titanium alloys [1]. These layers have excellent properties such as: high hardness, good biocompatibility to various types of cells, good adhesion to implants [2], wheres implants with diamond layer have good corrosion resistance in body fluids. Result received for these materials are encourage to modification other materials for example shape memory alloy NiTi. Nitinol is often used material in interventional cardiology, orthodontics and urology [3]. Shape memory alloy charackterizes of return to designed shape, superelasticity, thermomechanical behavior [3]. This phenomenons are proceeded thanks to the martensite transformation. Modification in high temperature perhaps cause failure martensite transformation which influence on the material properties change.

***Key words**: nitinol, diamond layer, RF PCVD method*

[Engineering of Biomaterials, 56-57,(2006),37-39]

Introduction

Nitinol - equatomic shape memory alloy is often used material to production of vascular stents, filters, implants in orthopedics and orthodontics [3]. NiTi is characterized by an unique combination of properties, superelasticity, thermomechanical behavior, low density and shape memory. These are very favourable phenomenons taking into account the difference of size of blood-vessels where the implants are predicted to be introduced. Phenomenons in NiTi are proceeded thanks to martensitc transformation. The term martensitic phase transformation describes the formation during cooling or during loading with an external stress of the austenite high temperature phase [9]. In this phenomenon occurs atoms re-organise. This transformation dose not change the chemical composition. Results of this transformation are new crystal lattice.

All materials, which are implanted, should fulfill many factors, they could not cause allergic response or inflammatory reaction. They must exhibit biocompatibility - the ability of the human body to endure the implants without destruction of the tissue. They must have a specific system of mechanical properties - good adhesion, good corrosion resistance in body fluids.

Although studies have demonstrated the good corrosion resistance and biocompatibility of Nitinol [4], but the high nickel content at this alloy (54,5 to 57% weight) makes pos-

sible dissolution by corrosion and it still remains a concern. The corrosion ions caused failure cells and allergic response. In this emergency implants is rejected.

Due to assure biocompatibility implants on NiTi investigations over modification NiTi [3] are conducted. Our investigation qualifies NiTi properties after coated it them with nanocrystalline diamond layer manufactured by RF PCVD (Radio Frequency Plasma Chemical Vapour Deposition) method [5]. Idea of this method has consists in the process of activated of dense plasma in methane in a radio frequency filed 13,56 MHz. Manufacturing process of diamond layers consisted of two stages: ion etching of surface NiTi and diamond layer deposition on this surface.

NCD layer manufactured by RF PCVD is biocompatibility [6]. It does not cause allergic reactions and it does not contribute inflammation. Implants with NCD layer have good corrosion resistance in body fluids.

Materials and methods

In these tests were used NiTi samples delivered by Memory Metalle (Germany) such as:
- disks (diameter = 4,6 mm and thickness - 2 mm)
- ribbons (thickness - 0,63 mm, width -3,34 mm and lenght - 40 mm). Surface ribbons preparation dark grey oxide.

On this samples were manufactured diamond layer by RFPCVD (Radio Frequency Plasma Chemical Vapour Deposition) method [5]. Parameters of coating process shows TABLE 1. Before the RF PCVD process samples were mechanical polished and ultrasonic cleaned.

Samples' surface and structure after test was observed on the metallographic microscope and scanning electron microscope SEM. The microhardness of pure NiTi and NiTi with diamond layer were also examined. It was bending strength measurement pure NiTi and NiTi coated diamond layer.

Results and discussion

Before and after the NiTi samples coating by diamond layer X-ray analysis were made samples surface were observed by SEM.

FIG. 1a. shows results of clear disks analysis and in the table is range of content of elemenets. It can be seen that Ni and Ti are principals elements of this alloy. Surface of NiTi disk shows FIGURE 1b.

FIG. 2a. shows results of clear ribbons analysis and in the table is range of content of elemenets. It can be seen that Ni and Ti and O are principals elements of this alloy. Surface of NiTi ribbon shows FIGURE 2b.

FIG. 3a. shows analysis results of disks with diamond layer and in the table is range of content of elemenets. Surface of NiTi disks with diamond layer shows FIGURE 3b.

FIG. 4a. shows analysis results of ribbon with diamond layer and in the table is range of content of elemenets. Surface of NiTi riboon with diamond layer shows figure 4b. It can be seen that diamond layers is constant and uniformity.

NiTi structure

Structure of NiTi disks and ribbons was observed by metallographic microscope.

The view of pure NiTi disk structure shows FIG.5a. On the FIG. 5b was showed structure of NiTi disk after RF PCVD process. It can be seen that diamond layer on the NiTi ribbon is constant.

	ETCHING		COATING		
	Potential [V]	Time t [min]	Potential [V]	Time t [min]	Flow of gas process [cm^3/min]
NiTi disks	840-860	5 - 8	700-750	6 - 9	20-30
NiTi ribbons	700-740	4 - 7	680-720	3 - 5	20-30

TABLE 1. Parameters of RF PCVD process.

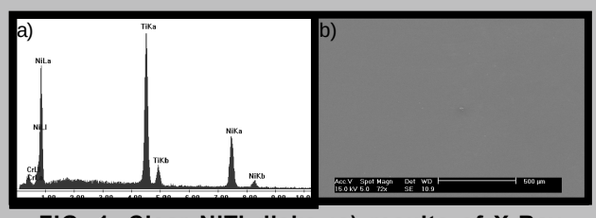

FIG. 1. Clear NiTi disks :a) results of X-Ray analysis, b) SEM view.

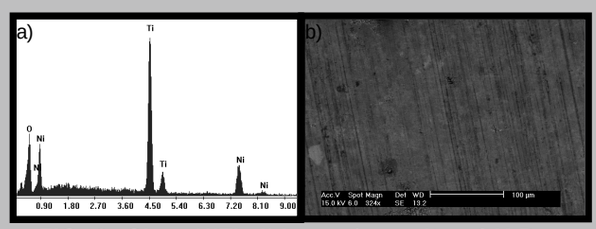

FIG. 2. Clear NiTi ribbon: a) results of X-Ray analysis, b) SEM view.

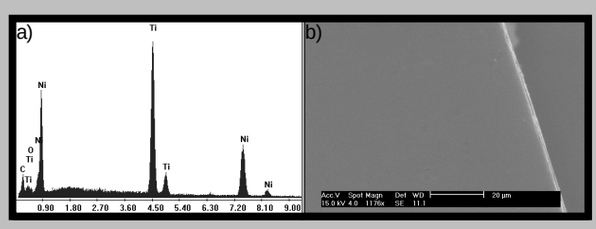

FIG. 3. NiTi disk with diamond layer: a)result of X-Ray analysis, b) SEM view.

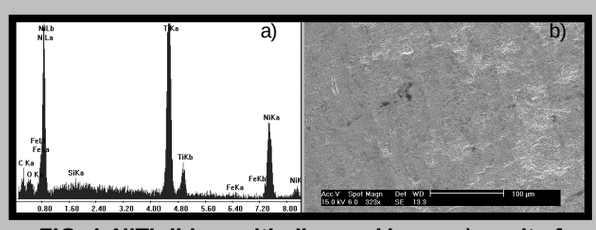

FIG. 4. NiTi ribbon with diamond layer: a)result of X-Ray analysis, b) SEM view.

The view of NiTi disk structure pure ribbon shows FIG.6a. On the FIG.6b was showed structure of NiTi ribbon after RF PCVD process.

Pictures show that structure of disks and ribbon after coating changed.

Microhardness

Was mesurement before and after RF PCVD process microhardness of NiTi.. Microhardness was made on the 6 clear NiTi samples and 6 samples with diamond layer. Results of these tests are shown in TABLE 2. It can be seen that microhardness after coating changed. During the RF PCVD process followed strengthen material.

Bending

Clear NiTi ribbon and NiTi ribbon with diamond layer were bending. FIG.7,8 show results of these test. It can be seen that NiTi samples after RF PCVD process did not return to original shape. Structrue of NiTi change. RF PCVD process makes the plasticity properties lower.

Differential Scaning Calorimetry

On the clear NiTi and NiTi with diamond layer were made differential scanning calorimetry (DSC). Measurements were made in range temperatures from -50 to 250°C. The flow gas in the time test was 50ml/min. FIG.9 shows curve DSC

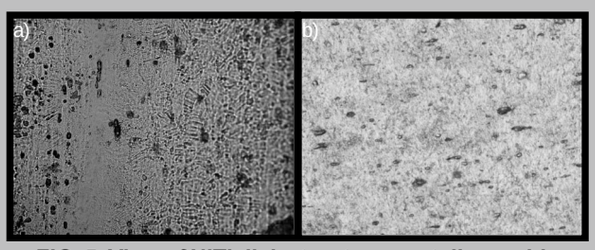

FIG. 5. View of NiTi disk structure- metallographic microscope - magnification 275x: a)clear NiTi, b) NiTi with NCD.

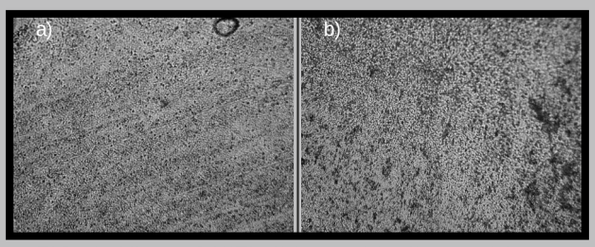

FIG. 6. View of NiTi ribbon with diamond layer structure - metallographic microscope -275x: a)clear ribbon, b) ribbon with NCD.

clear NiTi under heating and cooling. It can be seen that temperatures transformation Ap upon heating to amount 10°C and temperature transformation Mp upon cooling to amount 20°C.

FIG.10 shows NiTi curve DSC with diamond layer under heating and cooling. It can be seen that temperature transformation Ap upon heating to amount 30°C and temperature transformation Mp upon cooling to amount 10°C.

Microhardness NiTi– average for 6 samples	
Before RF PCVD	After RF PCVD
291 HV	370 HV

TABLE 2. Microhardness NiTi- average for 6 samples.

Conclusions

Investigations results show that modification by Radio Frequncy Plasma Chemical Deposition method NiTi does not satisfy expectations. Modification NiTi caused lower mechanical properties instead high them. The SEM images of diamond layer on the NiTi surface shows that layer is homogeneous and coats surface of NiTi samples very good but structure tests of NiTi shows that RF PCVD process caused material's change. High temperature during the process coating that's the problem, which destroits shape memory. phenomenon. Test DCS showed that RF PCVD process changes transformation temperatures upon heating an upon cooling. This is very unfavourably phenomenos. Material after RF PCVD does not good shape memory and superelasticity.

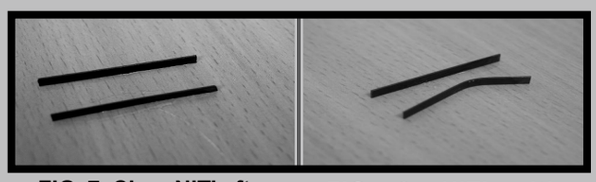

FIG. 7. Clear NiTi after bending.

FIG. 8. NiTi with diamond layer after

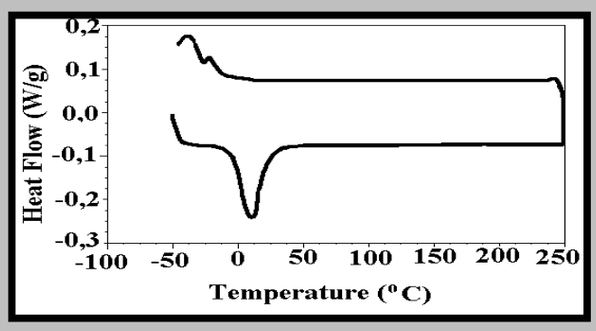

FIG. 9. Curve DSC clear NiTi.

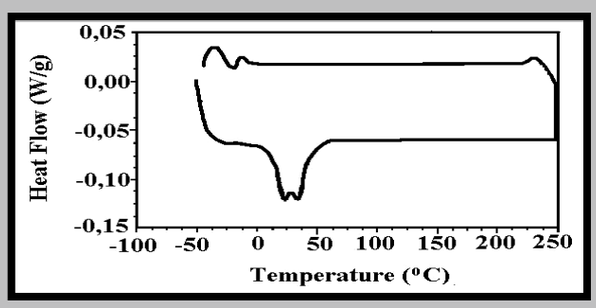

FIG. 10. NiTi DSC curve after RF PCVD process.

References

[1] B.P. McNamara, H. Murphy, M.M. Morshed: "Adhesion properties of diamond-like coated orthopedic biomaterials"; Diamond and Related Materials: 10 2001 1098-1102.
[2] G. Heinrich, B. Rinne, R. Thull, S.M. Rosiwal, R.F. Singer, "Characterization of CVD diamond-coated titanium base compounds for biomedical applications," Biomed. Tech. (Berl.) 43(1998):382-383 (Suppl).
[3] C.D.J.Barras and K.A.Myers "Nitinol-its use in vascular surgery and other application"; Eur Jvasc Endovasc Surg 19,564-569 (2000).
[4] P. Rocher, L. El Medawar, J.-C. Hornez, M. Traisnel, J. Breme, H.F. Hildebrand: "Biocorrosion and cytocompatibility assessment of NiTi shape memory alloys" ; Scripta Materialia 50 (2004) 255-260
[5] S.Mitura, A.Mitura, P.Niedzielski, P.Couvrat: "Nanocrystalline diamond coatings" Biomaterials: Volume: 17, Issue:6, 1996, pp. 587-595
[6] Bakowicz K., Mitura S.: "Biocompatybility of NCD";Journal of Wide Bandgap Materials,Vol.9, No.4 (2002)261-2711.
[7] Duerig T., Peton A.Stockel D. "An overview of nitinol medical applications" Materials Science and Engineering Volume:273-275, December 15, 1999, pp. 149-160.
[8] M.F.Chen, X.J.Yang, R.X.Hu, Z.D.Cui, H.C.Man: "Bioactive NiTi shape memory alloy used as bone bonding implants" ;Materials Science and Engineering C 24-20.
[9] http://herkules.oulu.fi

BIOMATERIAŁY W LECZENIU POURAZOWYCH UBYTKÓW NERWÓW OBWODOWYCH – PRZEGLĄD METOD I MATERIAŁÓW

Dariusz Szarek, Włodzimierz Jarmundowicz*, Aneta Frączek***, Stanisław Błażewicz*****

*Katedra i Klinika Neurochirurgii Akademii Medycznej,
ul. Traugutta 166, Wrocław
**Zakład Chorób Układu Nerwowego,
Akademia Medyczna we Wrocławiu,
ul. Traugutta 116, Wrocław
***AGH - Akademia Górniczo-Hutnicza,
Katedra Biomateriałów,
al. Mickiewicza 30, 30-059 Kraków
E-mail: dariuszszarek@wp.pl

Streszczenie

Niniejsza praca stanowi przegląd literaturowy metod, sposobów, a także materiałów stosowanych oraz będących sferze badań do konstrukcji protez do regeneracji obwodowego układu nerwowego. Zawiera również opis anatomicznych i fizjologicznych procesów przebiegających podczas regeneracji nerwów, a także zestawienie ich własności biomechanicznych.

Słowa kluiczowe: *regeneracja nerwów, technika operacyjna, biomateriały*

[Inżynieria Biomateriałów, 56-57,(2006),40-53]

Wstęp

Urazowe uszkodzenia nerwów obwodowych są poważnym problemem zarówno z punktu widzenia klinicznego jak i społecznego. Stosowane obecnie metody leczenia, w tym operacyjnego, pozwalają na uzyskanie względnie dobrych, lecz zwykle nie do końca zadowalających wyników leczenia. Leczenie jest żmudne i często obarczone koniecznością pobrania innego zdrowego nerwu skórnego dla naprawy uszkodzenia. Urazowe uszkodzenia obwodowego układu nerwowego są przyczyną dużej ilości interwencji chirurgicznych.

W 1995 roku w Stanach Zjednoczonych przeprowadzono ponad 50,000 operacji z powodu urazowych uszkodzeń nerwów obwodowych [1]. Liczba zabiegów wykonywanych w kilku ośrodkach w Polsce wynosi ponad 100 rocznie w każdym z nich [2]. Urazy z reguły dotyczą osób w dwóch grupach wiekowych: młodzież do 15 lat oraz osób w wieku 30-50 lat [3]. Prowadzi to do znacznej absencji chorobowej a niekiedy stanowi przyczynę poważnego kalectwa.

Jedną z głównych trudności w operacyjnym leczeniu urazowych uszkodzeń nerwów obwodowych jest wykonanie zespolenia przerwanego nerwu w przypadkach z dużym ubytkiem pomiędzy przeciętymi końcami [3,4]. Trójwymiarowe materiały używane obecnie jako skafoldy dla regeneracji tkanek mogą zastąpić obecnie stosowaną w takich przypadkach klasyczną metodę, jaką jest zespolenia kikutów nerwu z zastosowaniem allograftów lub autografów pobranych nerwów skórnych [5]. Metoda klasyczna jest związana z szeregiem ograniczeń takich jak dostępność i długość pobranego nerwu celem przeszczepienia, odnerwienie pola skórnego zaopatrywanego przez pobrany nerw, drugie miejsce operacyjne, ryzyko infekcji w miejscu po-

BIOMATERIALS IN THE TREATMENT OF PERIPHERAL NERVE INJURIES – AN OVERVIEW OF METHODS AND MATERIALS

Dariusz Szarek, Włodzimierz Jarmundowicz*, Aneta Frączek***, Stanisław Błażewicz*****

*Medical University of Wroclaw,
Department of Neurosurgery,
ul. Traugutta 166, Wroclaw
**Medical University of Wroclaw,
Institute of Nervous System Disease,
ul. Traugutta 116, Wroclaw
***AGH-UST, Department of Biomaterials,
al. Mickiewicza 30, 30-059 Cracow
E-mail: dariuszszarek@wp.pl

Abstract

The work presents the state of the art in the area of methods and materials used in peripheral nerve treatmend. Anatomical and physiological aspects of peripheral nerves their biomechanical properties and their treatment are presented.

Keywords: *nerve regeneration, operation procedure, biomaterials*

[Engineering of Biomaterials, 56-57,(2006),40-53]

Introduction

Peripheral nerve injuries are serious clinical and social problems. Current applied treatment methods, including operative, ones give relatively good, however not fully satisfacting effects. Treatment is long lasting and often harvesting of healthy cutaneus nerve is necessary. Traumatic peripheral nervous system injuries are the reason of great number of surgical interventions. In 1995, there were more than 50,000 peripheral nerve repair procedures performed in USA [1]. Number of surgical procedures performed in several centers in Poland is over 100 a year in every one of them [2]. Patients are typically in two age groups: young people till the age of 15 and middle-aged between 30 and 50 [3]. It causes significant disease absence and even may lead to serious disability.

One of the major problems in surgical treatment of the peripheral nerve injuries is ends coaptation in the case of large loss of nerve tissue [3,4]. Three dimensional materials in the form of scaffolds for tissue regeneration may replace currently applied classical technique, namely nerve coaptation with the use of cutaneous nerve allo and autographs [5]. There are many disadvantages of classic method such as limited availability and length of donor nerve tissue, skin denervation in area related to harvested nerve, second operative location, and risk of infection in the region of nerve harvesting [6]. Several types of materials have been proposed as peripheral nerve substitutes, for example: synthetic materials such as silicon, polylactic acid and polyglicolic acid, natural polymers such as chitosan, alginates, collagen, laminin, fibronectin, and others [7].

Anatomical and physiological aspects of peripheral nerve regeneration

Peripheral nerve consists of bunches of nerve fibers con

brania nerwu [6]. Szereg materiałów może mieć potencjalne zastosowanie dla uzupełnienia ubytków nerwów, np.: materiały syntetyczne takie jak silikon, poliglikolid, polilaktyd, naturalne polimery jak chitozan, alginiany, kolagen, laminina oraz fibronektyna i inne [7].

Anatomiczne i fizjologiczne aspekty regeneracji nerwów obwodowych

Nerw obwodowy zbudowany jest z grup włókien nerwowych połączonych warstwami osłonek łącznotkankowych. Włókno nerwowe tworzy wypustka komórki nerwowej pokryta osłonką mielinową wytworzoną przez specjalne komórki zwane komórkami Schwanna.

Nerwy, ze względu na charakter przewodzonych bodźców nerwowych, dzielą się na ruchowe - przewodzące impulsy odśrodkowe i czuciowe - przewodzące impulsy dośrodkowe z receptorów czuciowych. Ponadto w obrębie nerwów przebiegają włókna układu autonomicznego. Większość nerwów ma charakter mieszany, przewodzą włókna nerwowe wszystkich typów.

Komórki nerwowe, których wypustki tworzą nerwy obwodowe, leżą w obrębie rogów przednich rdzenia kręgowego oraz w zwojach międzykręgowych. Wytwarzane przez nie włókna nerwowe po opuszczeniu kanału kręgowego grupują się tworząc nerwy rdzeniowe.

W początkowym przebiegu nerwy te z reguły łączą się tworząc sploty, w obrębie których dochodzi do wymiany włókien nerwowych pomiędzy poszczególnymi pniami nerwowymi. Ze splotów wychodzą nerwy, które unerwiają właściwe dla nich mięśnie, skórę, ścięgna, stawy. Nerwy obwodowe mają kształt walca, przebiegają często wspólnie z naczyniami krwionośnymi.

Włókna nerwowe grupują się tworząc pęczki. Pęczki pokryte są osłonką łącznotkankową - perineurium. Przestrzeń pomiędzy poszczególnymi włóknami wypełniona jest luźną tkanką - endoneurium. Pęczki stanowią wewnętrzną makroskopową architekturę nerwu, przebiegają spiralnie i w sposób sfałdowany. Taki układ pozwala na swobodne wydłużenie się nerwu w czasie jego rozciągania [8]. W obrębie jednego nerwu przebiega z reguły kilka pęczków. Pokryte są one wspólna osłonką - epineurium, z którą są luźno związane. Stanowi ona zewnętrzną osłonę nerwu. Pośredniczy ona między wewnętrznymi strukturami nerwu, a środowiskiem zewnętrznym, chroni jego wnętrze przed urazami mechanicznymi, przewodzi większą część naprężeń podczas naciągania nerwu [8].

Dla prawidłowego funkcjonowania nerwu konieczna jest ciągłość anatomiczna włókien nerwowych oraz sprawne połączenie synaptyczne włókna nerwowego z jego efektorem. Wyróżniane są trzy główne stopnie uszkodzenia nerwu:
· Neurapraxis - przejściowe zablokowanie funkcji nerwu spowodowane np. jego uciśnięciem i niedokrwieniem
· Aksonotmesis - przerwanie włókien nerwowych bez uszkodzenia osłonek łącznotkankowych
· Neurotmesis - całkowite przecięcie nerwu.

W stopniu pierwszym i drugim regeneracja zachodzi spontanicznie z dobrym rokowaniem dla wyników leczenia. W stopniu trzecim niemożliwa jest spontaniczna regeneracja, dla uzyskania powrotu funkcji nerwu konieczna jest interwencja chirurgiczna i zespolenie przeciętych kikutów nerwu.

Regeneracja nerwu różni się zasadniczo od procesów gojenia się charakterystycznych dla wszystkich innych tkanek. Dla przywrócenia funkcji nerwukonieczna jest regeneracja ("odrośnięcie") włókna nerwowego od miejsca uszkodzenia aż do efektora i odbudowaniez nim połączenia synaptycznego.

nected by connective tissue-sheets. Nerve fiber is created by nerve cell process covered with myelin sheet produced by special cells called Schwann cells.

Nerves, depending on the type of conducted nerve impulses, are divided into motional - conducting anterograde impulses, sensational - conducting retrograde impulses from sensory receptors. A nerve also consists of fibers of autonomic system. Most of the nerves are mixed, they consist of nerve fibers of all types.

Nerve cells creating processes for peripheral nerves fibers are located in the front horns of spinal cord or in intervertebral ganglions. Nerve fibers after leaving vertebral canal group and create spinal nerves. Proximal parts of nerves connect and build the structures called nervous plexus, where fibers exchange between particular nerves takes place. Nerves leaving these structures innervate characteristic muscles, skin, tendons and joints. Peripheral nerves are cylinder in shape, they often run together with blood vessels.

Nerve fibers group into structures called fascicles. Fascicles are covered with connective tissue sheath - perineurium. Space between the fibers is filled with lose connective tissue - endoneurium. Fascicles are internal macroscopic nerve architecture with spiral and fold molding. Such a shape enables the nerve elongation during its stretching [8]. In one nerve there are usually few fascicles. They are covered with common sheath - epineurium, loosely connected with. It is an external nerve cover. It mediates between internal nerve structures and external environment, protects nerve internal structures from mechanical injury and conducts biggest part of tension during nerve tightening [8].

Normal nerve functioning requires anatomic integrity of nerve fibers and functioning synaptic connection of nerve fiber with its efector. There are three main types of nerve injuries:
· Neurapraxis - transient block of nerve function inflicted by for example pressure and nerve blood flow dysfunction
· Aksonotmesis - nerve fibers disruption without damage of connective tissue sheaths
· Neurotmesis - complete nerve cut

At the first and the second stage of injury nerve regeneration occurs spontaneously with good treatment prognosis. At the third stage of injury spontaneous regeneration is impossible, surgical intervention and nerve end coaptation is necessary for nerve function restoration.

Nerve regeneration greatly differs from healing processes characteristic for all other tissues. For nerve function restoration nerve fibers regeneration ("regrowth in") is necessary from injury site to efector and rebuild of synaptic connection.

Nerve regeneration process runs in few phases. During the first phase multiple pathophysiologic events occur described as Wallerian degeneration. This process is connected with myelin sheaths and nerve fibers break up that greatly depends on cells called macrophages. These cells besides phagocytic properties play an important role in supporting nerve fibers reconstruction process, called regeneration. They produce multiple substances called cytokines. Cytokines, for example REG 1, stimulate Schwann cells proliferation and also production of neurotrofic substances such like NGF (Nerve Growth Factor). These substances with retrograde axonal transport reach cell body and stimulate expression of genes responsible for protein production for axonal regeneration. Schwann cells build characteristic bands or tubes of Büngner, within of which regrowing axons growths in. [9,10].

Without anatomic nerve fiber reconstruction from injury

Proces regeneracji nerwu przebiega w kilku fazach. W pierwszej fazie dochodzi do szeregu zjawisk patofizjologicznych określanych jako degeneracja Wallera. U podstawy tych zjawisk leży rozpad osłonek mielinowych oraz wypustek nerwowych, w których istotną rolę odgrywają komórki zwane makrofagami. Komórki te oprócz właściwości żernych odgrywają również ważną rolę we wspomaganiu procesu odbudowy włókien nerwowych, który określamy regeneracją. Wytwarzają one szereg substancji zwanych cytokinami. Cytokiny, np. cytokina REG 1, stymulują komórki Schwanna do proliferacji, jak również do produkcji substancji neurotroficznych takich jak NGF (Nerve Growth Factor). Substancje te drogą wstecznego transportu aksonalnego docierają do ciała komórkowego i pobudzają ekspresję genów odpowiedzialnych za produkcję białek koniecznych dla regeneracji aksonu. W tym czasie komórki Schwanna wytwarzają charakterystyczne pasma lub rurki Büngnera, w które wrastają odrastające aksony. Proces regeneracji kończy się momentem wytworzenia połączeń synaptycznych oraz osłonek mielinowych wokół odrastających aksonów [9,10].

Bez anatomicznego odbudowania włókna nerwowego od miejsca urazowego przecięcia do narządu docelowego, wytworzenia z nim funkcjonalnej synapsy i odbudowania osłonki mielinowej niemożliwy jest powrót funkcji nerwu. Stosowane metody leczenia, zarówno klasyczne jak i eksperymentalne dążą do wykorzystania powyższego procesu celem uzyskania jak najskuteczniejszego wyniku regeneracji nerwu. Zespala się kikuty nerwu koniec do końca, co stwarza warunki by odrastające włókna nerwowe z kikuta proksymalnego mogły wrosnąć w kikut dystalny. W przypadkach urazów, w których dochodzi do ubytku nerwu konieczne jest wypełnienie ubytku przeszczepami nerwów. W ostatnich latach próbuje się wykorzystywać w tym celu inne materiały pochodzenia sztucznego.

Własności biomechaniczne nerwów obwodowych

Nerwy obwodowe zbudowane są z włókien nerwowych oraz osłonek nerwowych zbudowanych z tkanki łącznej o różnych właściwościach mechanicznych. Ze względu na rozmieszczenie tkanki łącznej oraz cylindrycznej konfiguracji włókien nerwowych, nerwy obwodowe posiadają własności anizotropowe. W przypadku nerwów trudno jest oszacować ich odpowiedź na działanie sił zewnętrznych ze względu na ich skomplikowaną budowę. Głównym elementem składowym nerwów obwodowych odpowiedzialnym za ich elastyczność oraz wytrzymałość na rozciąganie jest epineurium [11]. Warstwy epineurium nie ulegają przerwaniu w jednym, konkretnym punkcie na powierzchni nerwów, ale wzdłuż nerwu na pewnym jego odcinku. Dlatego też uszkodzenie nerwów obwodowych na skutek rozciągania nie jest zjawiskiem zlokalizowanym [12]. Materiały, które znajdują zastosowanie w regeneracji nerwów obwodowych muszą charakteryzować się dostateczną wytrzymałością na rozciąganie oraz odpornością na obciążenia dynamiczne tak, aby zdolne były przeciwdziałać siłom działającym w środowisku "in vivo". Badania nad własnościami mechanicznymi są niezbędnym krokiem w dalszym rozwoju materiałów stosowanych dla regeneracji nerwów obwodowych [7]. Właściwości mechaniczne takie jak naprężenie i odkształcenie graniczne, wydłużenie graniczne, moduł Younga, praca zniszczenia są niezbędne do dokonania charakterystyki materiałów przeznaczonych na implanty.

Dla nerwów piszczelowych królika wytrzymałość na rozciąganie oraz odkształcenie graniczne wynosi odpowiednio 11,7±0,7MPa i 38,5±2,0%. Osiągnięcie "górnej granicy

to target organ, synaptic connection reconstruction and reconstruction of myelin sheath nerve function restoration is impossible. Actually applied treatment methods, classical and experimental utilize this process to achieve an optimal nerve regeneration effect. Nerve stumps reconnection creates conditions for regrowing axons from the proximal stump to growth into the distal stump. In cases of great nerve tissue loss reconstruction with nerve autografts is necessary. Recently, for this purpose synthetic materials are being explored.

Biomechanical properties of peripheral nerves

A peripheral nerve consists of nerve fibers and connective tissue of different mechanical properties. Because of the arrangement of connective tissue and the tubular configuration of nerve fibers, the nerves are anisotropic and almost transversely isotropic. It is difficult to estimate the response of nerves to external forces due to their small size and complicated architecture. The main peripheral nerve component responsible for the elasticity and tensile strength of an intact nerve is epineurium [11]. The epineurial sheath does not rupture at one given point in the nerve, but rather along the nerve over some distance. Therefore, stretch injuries to peripheral nerve may not be localized phenomenon [12]. The materials used for supporting peripheral nerve regeneration have to have sufficient tensile strength and mechanical toughness to withstand in vivo mechanical forces. Investigation of tensile properties is a requisite step in the further development of peripheral nerve substitutes [7]. The mechanical parameters like ultimate stress and strain, ultimate elongation, Young's modulus, work to failure, viscoelastic behavior are necessary to evaluate such characteristics of any material designed for implantation in patients.

For rabbit tibial nerve, the tensile strength and ultimate strain are found to be 11,7±0,7 MPa and 38,5±2,0%, respectively. The strain at the "elastic limit" ranged from 8% to 20%, and the maximal strain at failure was approximately 30%. These ranges of variation were thought to be due to the nonhomogenous structure of nerve trunks, which consist of a complex variety of elements with different strength and elasticity [12]. The rabbit tibial nerve has an ultimate elongation of 16,3±0,7mm and ultimate load of 9,52±0,47N. For human ulnar nerves the ultimate load is reported to be 65 to 155 N human median nerve 73 to 220N [12,13].

Peripheral nerves exhibit highly nonlinear stress-strain behavior. The nerve may stretch up to 15% strain under minimal stress of internal structures.

These mechanical properties of peripheral nerve are determined by special interal nerve architecture that enables an optimal tensile stress load. Inside epineurium fascicles run freely and are loosely connected with it. They run in a spiral, wavy way along to longitudinal nerve axis. Thus, there is an excess of length of fascicles in relation to epineurium. During nerve stretching tensile stress is transferred by epineurium and fascicles straightening. Further stretching may cause epi, perineurium and nerve fibers disruption [8,12]. These data are similar to in vivo observations of intraneural blood flow in the rabbit tibial nerve. During gradual stretching venular blood flow significantly decreases when nerve is stretched to 8% beyond in vivo length. Complete intraneural ischemia was induced at 15% beyond in vivo length [1,11,12].

The estimated mean Young's modulus of the rabbit sciatic nerves in the transverse direction was 66.9±8.0 kPa, and the longitudinal direction was 580±150kPa [7,11]. The

elastyczności" nerwów ma miejsce przy odkształceniu od 8% do 20%, a maksymalne odkształcenie do zniszczenia oszacowane zostało na około 30%. Rozbieżności w wartościach odkształcenia mogą być spowodowane brakiem homogeniczności w strukturze pnia nerwu, który zawiera złożone składniki charakteryzujące się odmienną elastycznością oraz wytrzymałością [12]. Dla nerwów piszczelowych królika wydłużenie graniczne wynosi 16,3±0,7mm, a obciążenie graniczne 9,52±0,47N. Dla ludzkich nerwów łokciowych obciążenie graniczne jest oszacowane pomiędzy 65N, a 155N, a dla nerwów pośrodkowych od 73 do 220N [12,13].

Nerwy obwodowe wykazują silną nielinearną charakterystykę naprężenie-odkształcenie. Nerw może być rozciągany do 15% wartości odkształcenia przy minimalnym naprężeniu struktur wewnętrznych.

Powyższe właściwości mechaniczne nerwu są determinowane specjalną budową wewnętrzną nerwu, która zapewnia najoptymalniejsze przenoszenie naprężeń. W obrębie epineurium pęczki są ułożone swobodnie i luźno z nim związane. Ich przebieg jest pofałdowany w stosunku do osi długiej nerwu. Daje to nadmiar długości pęczków w stosunku do długości epineurium. Podczas rozciągania nerwu dochodzi do powstawania naprężeń, które w większości są przenoszone na epineurium i prostowania pęczków. Dalsze rozciąganie może spowodować przerwanie osłonek epi i perineurium oraz rozerwanie włókien nerwowych [8,12]. Wyniki tych badań potwierdzają obserwacje in vivo przepływu krwi w naczyniach nerwu. Ukrwienie nerwu królika znacząco spada przy zwiększeniu przyżyciowym długości o 8%. Kompletne zatrzymanie krążenia w nerwie następuje przy rozciągnięciu powyżej 15% [1,11,12].

Oszacowana wartość modułu Younga dla nerwów kulszowych królika w kierunku poprzecznym wynosi 66.9±8.0kPa, natomiast w kierunku podłużnym 580±150kPa [7,11]. Znajomość parametrów mechanicznych nerwów obwodowych jest konieczna z punktu widzenia ochrony pęczków nerwów, a także zachowania ich prawidłowej funkcji fizjologicznych. Tkanka łączna spełnia również bardzo ważną funkcję w utrzymaniu odpowiedniego środowiska w obrębie śródnerwia poprzez utrzymanie bariery dyfuzji dla różnorodnych makrocząsteczek. Zmiany w parametrach dyfuzji oraz uszkodzenia struktury powstałe na skutek naprężeń rozciągających, mogą powodować długotrwałe, a nawet stałe, upośledzenie funkcji nerwu [12].

Metody leczenia

W przypadku przecięcia nerwu konieczna jest interwencja chirurgiczna celem odtworzenia anatomicznej łączności między kikutami przerwanego nerwu. Stosowaną obecnie metodą z wyboru jest zespolenie operacyjne nerwu koniec do końca.

Zespolenie nerwu pod napięciem znacząco pogarsza wynik regeneracji, dlatego w urazach przebiegających z ubytkiem nerwu konieczne jest jego uzupełnienie [9,14]. Autoprzeszczepy nerwów są obecnie najbardziej powszechną procedurą operacyjną stosowaną przy naprawie ubytku nerwów. Mostowanie defektu nerwu za pomocą autogenicznego nerwu dawcy ma szereg stron ujemnych, takich jak dodatkowe miejsce operacyjne, pobranie zdrowego nerwu, którego rezultatem są zaburzenia czucia, ryzyko powstania bolesnego nerwiaka [9,14,15,16,17].

Dlatego dąży się do lepszego poznania procesów sterujących regeneracją nerwów oraz znalezienia materiałów alternatywnych dla przeszczepów autogennych.

mechanical properties of peripheral nerve are important for protection of nerve fascicles and the integrity of their physiological functions. Connective tissue of nerves has an important function in maintaining specific environment of the endoneural space by acting as a diffusion barrier against several macromolecular substances. Changes in its diffusion properties or structural damage caused by stretching may lead to chronic or even permanent impairment of nerve function [12].

Treatment procedures

In the cases of nerve transection surgical intervention for anatomical nerve stumps coaptation is needed. Actually, a method of the first choice is end to end coaptation with few stitches binding epineurium.

Tension after nerve coaptation greatly deteriorates regeneration effect, therefore nerve injuries with nerve tissue loss require tissue defect supplementation. [9,14]. Nerve autografting is the most common surgical procedure currently used for repair of nerve injuries with nerve tissue loss defects. Bridging the defect with an autologous donor nerve is associated with several disadvantages, including an extra incision for harvesting of a healthy sensory nerve ultimately resulting in a sensory dysfunctions, risk of painful neurinoma formation [9,14,15,16,17].

For these reasons processes regulating nerve regeneration and alternative to the autologus nerve grafts artificial materials are still being investigated.

Requirements for artificial nerve guides implants

Ideal implant for nerve substitute should have the following characteristics:
1. biocompatibility;
2. bioresorbability;
3. potential for stimulating nerve regeneration;
4. material with an ability for l incorporation of nerve growth factors;
5. should have an appropriate mechanical properties described by Young's module;
6. easy for intraoperative handling;
7. inexpensive [18,19].

Regeneration process in nerve tube implant

One of the main research directions in peripheral nerve regeneration are experiments with membranes creating isolated environment for regenerating nerve tissue. Classic model of nerve tissue loss regeneration relates to empty tube-shape implants. The tube implant connects nerve ends and creates between them isolated environment for free tissue reconstruction.

Regeneration process in empty tube implant occurs in several subsequenty stages. Within the first hours after implantation implant's lumen tills-in with acellular fluid originating from nerve stumps inserted in tube. It is rich in nerothrophic and nerve regeneration stimulating agents. In the next stage, fluid is exchanged with loose, acellular extracellular matrix formed mainly by fibrin. After 7 days the fibrin is longitudinally organized lengthwise long implant's axis creating bridge between the nerve stumps, with hourglass-shape with the narrowest part located closer to distal nerve stump. Nerve bridge diameter is much thinner than tube [20]. Longitudinal fiber organization is regularly disorganized by arch-like bending of fibers creating in transversal section the characteristic arches with bases directed to the implants center [21].

Wymagania stawiane przed sztucznymi implantami nerwowymi

Idealny implant, który może być użyty do uzupełnienia ubytków nerwów obwodowych powinien charakteryzować się następującymi własnościami:
1. biozgodność;
2. bioresorbowalność;
3. stymulacja regeneracji nerwu
4. zdolny do generowania grup funkcyjnych na swojej powierzchni, pozwalających na inkorporację czynników modyfikujących regenerację włókien nerwowych
5. o zbliżonych do nerwów obwodowych właściwościach mechanicznych określanych przez moduł Younga;
6. poręczność chirurgiczna;
7. tani; [18,19]

Procesy regeneracji zachodzące w implancie

Głównym nurtem badań prowadzonych w celu zastąpienia przeszczepów z nerwów obwodowych materiałem sztucznym są projekty związane z budową membran tworzących odizolowane środowisko dla regenerującej tkanki nerwu. Modelowym przykładem pozwalającym na poznanie sekwencji zdarzeń mających miejsce podczas regeneracji/rekonstrukcji przez organizm ubytku nerwu są badania z zastosowaniem pustych implantów w kształcie rurki. Łączy ona kikuty nerwu zapewniając pomiędzy nimi odizolowane środowisko, w którym możliwa jest swobodna odbudowa tkanki.

Procesy regeneracji nerwu zachodzące w pustym wszczepie na bazie rurki przebiegają w kilku następujących po sobie etapach. W ciągu kilku godzin po implantacji światło implantu wypełnia się płynem będącym przesączem z kikutów nerwu. Jest on bogaty w czynniki neurotroficzne i stymulujące regenerację nerwów. W następnym etapie płyn wewnątrz implantu wypełnienia się luźną, bezkomórkową macierzą pozakomórkową zbudowaną głównie z fibryny. Do 7 doby po zabiegu włóknik organizuje się linijnie wzdłuż osi długiej implantu tworząc wewnątrz rurki pomost łączący kikuty nerwu. Jego kształt przypomina rozciągniętą klepsydrę z przesuniętym najwęższym punktem w kierunku kikuta dystalnego. Średnica pomostu jest z reguły cieńsza od średnicy rurki. W obrębie macierzy widoczne są pojedyncze erytrocyty, których ilość spada ku środkowi implantu[20]. Układ linijny wzdłuż osi długiej rurki jest regularnie zaburzony przez łukowate ugięcie się włókien tworząc na przekroju poprzecznym charakterystyczne łuki podstawą skierowane do środka implantu [21]

Na tak przygotowane środowisko wrastają komórki, początkowo są to elementy pozanerwowe. Jako pierwsze, około 4-7 dnia, pojawiają się fibroblasto-podobne komórki wywodzące się z unerwia. Zwykle pokrywają one najpierw zewnętrzną ścianę regeneratu, a następnie wypełniające także światło rurki. Za nimi postępują komórki Schwanna w formie łańcuchów oraz kolejno naczynia. W czasie formowania się bezkomórkowej macierzy wewnątrz implantu dochodzi do wzbudzenia i namnażania się komórek Schwanna w kikutach nerwu, w większym stopniu w kikucie dystalnym niż proksymalnym. Począwszy od około 4-7 doby zaczynają one migrować w światło implantu, najpierw od strony kikuta dystalnego[20,21,22]. Układają się linijnie, wzdłuż osi określonej przez układ włókien fibryny. Proces odbudowy komórkowej zachodzi najszybciej wzdłuż ścian, a następnie postępuje koncentrycznie do środka implantu. Od strony proksymalnej w światło implantu wrastają aksony, które pojawiają się pod koniec pierwszego tygodnia[20]. Towarzyszą im komórki Schwanna z kikuta proksymalnego budujące osłonkę w miarę wydłużania się aksonu. Ko-

Matrix is then colonized by cells, initially by extra neural elements extraneural. Between 4 and 7 day, fibroblast-like cells originating from perineurium appear. These cells typically first cover internal wall of the implant, followed by colonization at lumen. Fibroblasts are followed by Schwann cells forming bunds of Bunger and successively blood vessels. During acellular matrix formation Schwann cells in nerve stumps arouse and start to proliferate, more effective in distal than in proximal stump. Since 4-7 day Schwann cells start to migrate into tube lumen, beginning from distal stump [20,21,22]. They arrange longitudinally along an axis created by fibrin fibers arrangement. The most effective cellular reconstruction proceeds along the tube walls and subsequently concentrically to the implant centre. Axons growth into the implant, from proximal side, begins from the end of first week [20]. It is accompanied by Schwann cells from proximal stump that are creating axons myelin sheet as it elongates. During axon regeneration Schwann cells in the front or behind of growth cone are found. However, it is known, that Schwann cells are capable to colonize implant independently of contact with axon [20,22,23]. Regeneration process greatly enhances from 9 day after tube implantation [21]. After connection of proximal and distal regeneration parts (for implants 10 mm long it takes about 16-17 day, while for 25 mm long 21 day) digit-like processes take place with transiently disorganizing local longitudinal orientation [15,21]. After 7 days axons penetrate distal part of implant and elongate using support provided by Schwann cells originating from distal stump. The distal stump is reached after 21-28 days [20,21,24]. Growth of axons in distal part of implant is now oriented by longitudinal Schwann cell orientation. Direct contact of distal Schwann cells with axon stops their proliferation. If distal and proximal aspects of regeneration process are not connected, Schwann cells from distal stump and axons from proximal stump, after short migration (about 4-5 mm), usually stop to migrate. Schwann cells create cup-like structures covering distal stump [10,15,21,25,26]. Myelinization process between 14 - 36 day and advances from proximal to distal stump [20,22]. Simultaneously extracellular matrix created by fibroblasts maturates providing mechanical support for growing tissue. Excessive connective tissue or even cicatrice formation takes place in areas related to foreign body such as silicon or fibers of non-absorbable treads. Connective tissue greatly disturbs orientation of fibrin filaments and hampers cells and axons migration [21]. In late phases of regeneration number of counted axons in distal stump is greater than in proximal one. It is explained by the fact that the growth cones produce few independently regenerating processes that extend into the distal stump. This process increases chances of successful regeneration for particular single axon [21,22]. During the second week blood vessels start to grow into the implant, both from proximal and both distal stump. Vessels follow the front of migrating cells and axons. By the end of third week the vessels from stumps meet in the central regeneration zone nourishing about 10 mm tissue section [20,21]. Elimination of blood flow from nerve stumps makes impossible nerve tissue regeneration [23,27].

Regenerated nerve fibers are thinner; both axons and myelin sheaths [10,15,20,21,22,25,26,28]. During tissue maturation number of axons decreases while diameter of myelin sheahs increases [22,29,30]. Some implants, like silicone, show tendency to stimulate parietal connective tissue creation. This tissue tightens and narrows the nerve space inducting degenerative processes in regenerated nerve tissue. Nerve fibers are damaged showing morphological tissue image comparable with multiple crush injury [22]. This process greatly differs from aging process of re-

mórki Schwanna w trakcie postępowania regeneracji aksonu są stwierdzane przed lub za stożkiem wzrostowym, przy czym wiadomo, że komórki Schwanna mają zdolność kolonizować powstający regenerat niezależnie od kontaktu z aksonami [20,22,23]. Proces regeneracji tkanki nerwu ulega wyraźnemu przyspieszeniu od 9 doby po zabiegu [21]. Po zetknięciu się czoła obu tych procesów (przy implancie długości 10 mm następuje to około 16-17 dnia, przy długości 25 mm około 21 dnia) dochodzi do ich palczastego nachodzenia się i przejściowego zaburzenia osiowej orientacji w miejscu przejścia [15,21]. Po około 7 dniach aksony przechodzą do dystalnej części regeneratu i wykorzystując podporę komórek Schwanna pochodzących z kikuta dystalnego, osiągając około 21-28 dnia kikut dystalny [20,21,24]. Ich wzrost następuje teraz według kierunku określonego przez układ tych komórek (przypomina to wrastanie w kanały Büngera). Powoduje to zatrzymania namnażania się komórek Schwanna pochodzących z kikuta dystalnego. Jeżeli nie dochodzi do połączenia się obu procesów komórki Schwanna w kikucie obwodowym, aksony w kikucie proksymalnym, po przejściu pewnego odcinka (około 4-5 mm) przestają migrować. Komórki Schwanna tworzą strukturę na kształt "czapeczki", która pokrywa kikut dystalny[10,15,21,25,26]. Początek mielinizacji postępujący od kikuta proksymalnego w kierunku dystalnym obserwuje się między 14-36 dniem [20,22]. Jednocześnie dojrzewa substancja pozakomórkowa budowana przez fibroblasty dając mechaniczną podporę powstającej tkance. Nadmierne powstawanie tkanki łącznej, a nawet bliznowacenie ma miejsce w okolicach pokrywających powierzchnie ciała obcego, np. jakim jest sylikon lub włókna użytych szwów niewchałanialnych. Tkanka łączna w istotny sposób zaburza w tych rejonach orientację włókien fibryny oraz utrudnia migrację komórek i aksonów [21]. W późniejszych fazach regeneracji w kikucie dystalnym stwierdza się zdecydowanie większą ilość aksonów niż jest obecna w kikucie proksymalnym. Jest to związane z wytwarzaniem przez stożki wzrostowe kilku niezależnie wzrastających włókien, które regenerują poprzez kikut dystalny. Zwiększa to szanse powodzenia regeneracji pojedynczego aksonu [21,22]. W okresie drugiego tygodnia zaczynają w implant wzrastać naczynia krwionośne, początkowo od proksymalnego kikuta, następnie od dystalnego. Postępują one za czołową strefą migracji komórek aksonów. Pod koniec trzeciego tygodnia naczynia spotykają się w środkowej strefie regeneratu unaczyniając 10 mm odcinek tkanki [20,21]. Odcięcie ukrwienia pochodzącego od kikutów nerwów praktycznie uniemożliwia regenerację [23,27].

Zregenerowane włókna nerwowe są cieńsze, zarówno aksony jak i osłonki mielinowe [10,15,20,21,22,25,26,28] Z czasem dochodzi do zmniejszania się ilości aksonów oraz pogrubiania się osłonek mielinowych [22,29,30]. Pewną specyfiką implantów sylikonowych jest tendencja do powstawania włóknienia przyściennego. Prowadzi to do zaciśnięcia nerwu i wzbudzenia procesów degeneracyjnych w powstałej tkance nerwu. Niszczą one włókna nerwowe dając obraz morfologiczny tkanki porównywalny z wielokrotnym urazem zmiażdżeniowym [22]. Znacząco różnią się on od procesów starzenia się zregenerowanego nerwu czy dojrzewania powstałych włókien nerwowych i resorpcji niepotrzebnych bocznych gałęzi pojedynczego aksonu [29,30].

Formowanie macierzy pozakomórkowej, a następnie tkanki regeneratu jest zależne od średnicy i długości zastosowanej rurki i ubytku [27].

generated nerve or from maturation of regenerated nerve fibers and resorption of collateral needles branches of single completely regenerated axon [29,30].

Extracellular matrix formation and subsequent tissue regeneration depend on diameter and length of implanted tube and nerve tissue defect [27].

Membranes and fibers with potential application for peripheral nerve regeneration

Polymers membranes

Both biostable as well as biodegradable polymers are used as the carrier materials for regeneration of peripheral nerve. Most popular stable polymer materials are epoxy resins, polytetrafluoroethylene, polyimide and first of all silicon rubber. These polymers are biocompatible, electrically insolating and stable. To improve biocompatibility of polymer- based implants their bulk and surface properties can be modified in wide range[18].

Classic example of artificial implant used in surgery for many years are silicone tubes. Investigations of this material provided several important informations about nerve regeneration process [31,32]. Silicone tubes provide an "extrinsic" closed space within of which a spontaneously formed fibrin matrix allows for ingrowth of axons and non-neuronal cells [33]. One of silicone implants drawback is mismatching mechanical properties to those of tissue. Moreover, silicone material strongly stimulates fibrous tissue formation, and by consuming tube space limits or even inhibits regeneration, migration of axons from proximal to distal stump [34].

Actually biodegradable materials are being examined, in order to eliminate necessity of second operation for nerve guide removal after nerve regeneration is completed [35].

Several biodegradable synthetic materials, in the form of simple hollow conduits, have been shown to support nerve regeneration. Biodegradable polymers used as membranes or channel to regeneration of peripheral nerve are poly-l-lactide acid (PLLA), poly-glycolic acid, copolymer poly-l-lactide-co-glycolic acid (PGLA), chitosan, collagen and poly-3-hydroxybutyrate (PHB).

RYS. 1. Rurka silikonowa.
FIG. 1. Silicone tube.

Polyesters, such as polylactic acid (PLA), polyglycolic acid (PGA), poly-lactide-e-caprolactone and PLGA have been used extensively due to their availability, processability and low inflammatory response [36]. A suitable material should be biocompatible, probably bioresorbable, beneficial to nerve regeneration and maturation, resistant to scar invasion, and clinically applicable. PLLA, and polyglycolid acid (PGA) offer several advantages including their biode-

Membrany i włókna mogące znaleźć zastosowanie jako implanty do uzupełniania ubytków w nerwach obwodowych.

Membrany polimerowe

Polimery, zarówno stabilne jak i biodegradowalne, są najbardziej obiecującymi materiałami do produkcji implantów dla regeneracji nerwów obwodowych. Najbardziej popularnymi polimerami niebiodegradowalnymi są żywice epoksydowe, politetrafluoroetylen, poliimidy, a przede wszystkim silikon. Wymienione polimery są biozgodne, trwałe, a pod względem elektrycznym są izolatorami. Większość właściwości polimerów może być w pewnym stopniu modyfikowana, także powierzchnia polimerów może ulegać modyfikacji w celu poprawienia jej biozgodności [18].

Klasycznym obecnie przykładem sztucznego implantu są rurki sylikonowe stosowane od wielu lat w chirurgii. Badania z ich użyciem dostarczyły wielu danych o procesach regeneracji zachodzących w nerwach obwodowych [31,32]. Rurki silikonowe stanowią zamknięte środowisko, wewnątrz którego następuje samoistne formowanie się macierzy fibryny. Pozwala ona na wzrost aksonów, naczyń włosowatych i migrację komórek podporowych [33]. Wadą implantów silikonowych jest niedopasowanie ich własności mechanicznych z własnościami mechanicznymi tkanek, z którymi implant jest połączony, a także fakt, że jest to materiał niebiodegradowalny. Ponadto materiał sylikonowy silnie stymuluje powstawanie tkanki włóknistej, która przerastając światło rurki ogranicza bądź wręcz uniemożliwia regeneracje, przerastanie włókien nerwowych z części proksymalnej do części dystalnej ubytku [34].

Obecnie dąży się do zastosowania degradowalnych materiałów, aby uniknąć potrzeby ponownej operacji w celu usunięcia "nerve guide", gdy całkowita regeneracja nerwu dobiegnie końca [35].

Wiele biodegradowalnych materiałów syntetycznych w formie prostych, wdrążonych wewnątrz kanałów jest wykorzystywanych jako podpory dla regeneracji nerwów. Polimery bioresorbowalne stosowane do regeneracji nerwów występujące w formie membran bądź kanałów to: polilaktyd (PLA), poliglikolid, kopolimer poli-l-laktydu z poliglikolidem (PGLA), chitozan, kolagen, poli-3-hydroksybutyren (PHB).

Poliestry takie jak polilaktyd (PLA), poliglikolid (PGA), poli-e-kaprolakton i kopolimer laktydu z glikolidem (PLGA) są stosowane w szerokim zakresie ponieważ są łatwo dostępne, proste w obróbce i wywołują niewielki odczyn zapalny [36]. Odpowiedni materiał powinien być biozgodny, ulegać bioresorpcji, podtrzymywać regenerację nerwów i ich kształtowanie, a dodatkowo być poręczny chirurgicznie. Polilaktyd (PLA), poliglikolid (PGA) wykazują sporo pozytywnych cech takich jak: biodegradowalność, biozgodność oraz porowatą strukturę odpowiednią dla tworzenia się naczyń krwionośnych [1,37]

Kwas glikolowy jest łatwo dostępnym, biozgodnym materiałem o dobrych właściwościach mechanicznych. Ulega biodegradacji nie wytwarzając toksycznych produktów. Implant zbudowany z rurki poliglikolidowej wypełnionej kolagenem został zastosowany z powodzeniem dla uzupełnienia 15 mm ubytku nerwu strzałkowego u psa [38]. Podobny implant składający się z rurki poliglikolidowej pokrytej kolagenem i wypełnionej włóknami kolagenowymi pokrytymi lamininą zastosowano dla uzupełnienia ubytku 80 mm nerwu strzałkowego również u psa.

Implant mtaki zawiera większość znanych czynników wspomagających regenerację nerwu (osłonę rurki, podporę macierzy komórkowej, sekwencje sygnałowe błony podstawnej dla komórek Schwanna - laminina). Zastosowanie takiego implantu pozwoliło uzyskać powrót siły mięśniowej

gradability, porous structure for vascularization and consistency in design requirements [1,37].

Polyglycolic acid is easy available, biocompatible material with good mechanical properties. It biodegrades without any toxic products. Implant in the form of tube made of polyglycolid tube filled with collagen sponge was used successfully for bridging 15 mm peroneal nerve gap in dog [38]. Similar implant, polyglycolid acid tube coated with collagen and filled with laminin coated collagen fibers, was used for bridging 80 mm gap in dog's peroneal nerve. Such implant contains most of known factors stimulating nerve tissue regeneration (tube wall protection, extracellular matrix support, Schwann cell base membrane signal sequences - laminin). This implant application allowed for dog's muscle strength restoration adequate for normal walk without weight support on that limb. During 12 months of observation number of axons counted in regenerated tissue decreased (degeneration of lateral processes of axon's that successfully ended regeneration creating synaptic connection), an increase of myelin sheaths diameter, increase of amplitude and decrease of signal latency in regenerated tissue [39].

PGA implants were used in researches on humans. 43 digital nerves were connected. Final effect measured in two point discrimination test was as follows: 43% results were very good (S4 score British Medical Research Council) and 43% good (S3+ score BMRC). Treatment outcome was statistically better comparing to classic methods. Difference was greater for short gaps (4 mm and less) than for long (8-30 mm) [40]. In another study good results were indicated also for long gaps with 3 cm length [24].

The most promising material for reconstruction of peripheral nerve was poly-3-hydroxybutyrate (PHB). PHB is a natural biological polymer, manufactured as bioresorbable sheets, which can be formed into tubes [41]. PHB is an energy storage product of bacterias, occurring within the cell cytoplasm as granules. It is available in the form of bioabsorbable sheets, which are non-antigenic, easy to handle and have good tensile strength. PHB undergoes hydrolytic degradation and is completely absorbed within 24-30 months [42].

Chitosan is one of the most popular polysaccharides found in nature [43]. Natural polysaccharide usually contributes to cellular adhesion and inhibition of scar formation. Chitosan membranes and fibers have excellent neurogial cell affinity. Such material may repair certain distant nerve injury, causing little or no immune reaction of the body [44]. Chitosan is very hydrophilic allowing for its expansion in contact with water. However, its porous forms are attempted to be used as the constructs at artificial extracellular matrix suitable for the growth of neural cells. The molecular structure of chitosan is similar to that of glycosaminoglican, which resides in the basal membrane and extracellular matrix. It make it reacts with extracellular adhesive molecular, such as laminin, fibronectin and collagen IV, which promote cells to adhere, migrate and differentiate [44,45].

Collagen belongs to the most often used materials for nerve guide preparation due to its biocompatibility and desirable tensile strength [46]. Collagen is the main protein of connective tissue in animals and the most abundant protein in mammals, making up about 1/4 of the total proteins. Over 3 year observation, with proved usefulness of collagen implants for peripheral nerve gaps bridging [47,48]. Studies of regeneration processes in silicone and collagen tubes revealed their similarity. Important factor is stimulation of regeneration in prefilled tubes. Tubes are filled with collagen type I, mixture of type I and IV or collagen bonded with chondroityn sulphate [26]. Collagen implant durability

u psa umożliwiający zwierzęciu normalny chód. W czasie 12 miesięcznej obserwacji stwierdzono zmniejszenie się liczby aksonów w regeneracie (degeneracja bocznych wypustek aksonów, które wytworzyły połączenia) powiększanie się średnicy osłonek mielinowych, spadek latencji przewodzenia sygnałów przez zregenerowany nerw [39].

Implanty na bazie PGA zostały zastosowane w badaniach na ludziach. W jednym z badań wykonano zespolenie 46 nerwów palcowych uzyskując w badaniu czucia dwupunktowego po 43 % wyników bardzo dobrych (S4 według Britisch Medical Research Council) i dobrych (S3+ według BMRC). Wynik leczenia był statystycznie lepszy w porównaniu do metod klasycznych. Różnica była bardziej widoczna dla bardzo krótkich ubytków (do 4 mm) niż dłuższych (8-30mm) [40]. Kolejne badania wykazały dobre wyniki leczenia dla ubytków o długości 3 cm [24].

Bardzo obiecującym materiałem dla regeneracji nerwów obwodowych jest poli-3-hydroksybutyren (PHB). PHB jest naturalnym polimerem, produkowanym jako bioresorbowalne warstwy, które mogą być następnie przetwarzane w postać rurek [41]. PHB w postaci granul występuje w sposób naturalny w cytoplazmie komórki bakterii jako substancja magazynująca energię. PHB jest dostępny jako bioresorbowalne warstwy, o niskiej antygenowości, jest poręczny i cechuje się dobrą wytrzymałością na rozciąganie, PHB ulega degradacji hydrolitycznej i jest całkowicie usuwany w ciągu 24-30 miesięcy [42].

Chitozan jest jednym z najczęściej występujących w naturze polisacharydów o ładunku dodatnim (chitozan jest w całości bądź częściowo otrzymywany przez deacetylację chityny) [43]. Naturalne polimery wykazują wysokie zdolności adhezji komórek oraz inhibicji powstawania blizny. Membrany oraz włókna chitozanowe wykazują doskonałe powinowactwo do komórek neurogleju, dzięki czemu materiał ten może być z powodzeniem wykorzystany do rekonstrukcji uszkodzonych nerwów. W niewielkim stopniu lub nawet wcale wywołuje reakcje immunologiczną organizmu [44]. Chitozan jest bardzo hydrofilny, co powoduje, że wchłania duże ilości wody, jest wysoko porowatym materiałem, przez co może być wykorzystany do konstrukcji sztucznej macierzy zewnątrzkomórkowej odpowiedniej dla wzrostu komórek nerwowych. Struktura molekularna chitozanu jest podobna do glikozaminoglikanów, które znajdują się w błonie podstawowej oraz w macierzy zewnątrzkomórkowej. Sprawia to, że chitozan w łatwy sposób oddziałuje z zewnątrzkomórkowymi cząstkami adhezyjnymi takimi jak laminina, fibronektyna oraz kolagen typu IV, które pobudzają komórki do adhezji, migracji oraz różnicowania się [44,45].

Kolagen jest jednym z najczęściej stosowanych materiałów do produkcji "nerve guide" z powodu jego biozgodności oraz pożądanej wytrzymałości na rozciąganie [46]. Kolagen jest głównym białkiem tkanki łącznej zwierząt oraz najczęstszym białkiem występującym u ssaków, stanowiącym około 1 wszystkich białek. Ponad 3 letnia obserwacja na naczelnych potwierdziła przydatność kolagenowych pomostów do uzupełniania ubytków nerwów obwodowych [47,48]. Kolejne badania wskazują na identyczność procesów regeneracyjnych na bazie kolagenu i rurek sylikonowych. Ważnym aspektem jest stymulacja regeneracji w przypadku wypełnienia rurek. Stosuje się macierze zarówno z czystego kolagenu typu pierwszego, jak i mieszanin typu I i IV oraz kolagenu połączonego z siarczanem chondroityny [26]. Dla podniesienia wytrzymałości implantu kolagenowego stosuje się obróbkę przy użyciu ultrafioletu, ogrzewania lub poddanie wpływowi aldehydu glutarowego. Kolagen poddany obróbce termicznej ulega wchłonięciu po 6 tygodniach, jest dobrze unaczyniony, powstająca na jego bazie tkanka nerwowa jest podzielona w pseudopęczki z dużą ilością gęstej tkanki bliznowatej. Materiał poddany obróbce is modified using UV, heat treatment or glutar aldehyd. Heat treated collagen is fully absorbed after 6 weeks, well vascularised, nerve tissue is divided in pseudofascicles with large quantity of dense cicatricle tissue. UV treated material is poorly vascularised, nerve tissue maturates and after 12 weeks is comparable to autograft (number of myelined axons, muscle evoked potentials) [49]. Glutaraldehyd creates strongly hydrophobic and cytotoxic surface that greatly inhibits regeneration process [49,50]. Except of physical features of implant such, as pore network, pore diameter, three-dimensional canals localization, implant preparation technique is also important, and may greatly change its regenerative properties [49].

Previous studies have shown that collagen tubes cannot be used to bridge nerve defects greater than 15mm, since a long collagen tube can break and its lumen could collapse due to movement. Sometimes a collagen tube with a length of 20mm and an inner diameter of 1mm was coated with polymer, for examples poly(l-lactide-co-glycolic acid) (PLGA) to enhance its structural integrity and elasticity. The polymer layer performs two roles: reinforces collagen membrane and prevents collapse due to movement. On the other, hand, it creates a highly porous structure, which is important determinants for nutrient transport into the conduit . The collagen layer also prevents surrounding tissue from invading the tubes [51,52,53].

The polymers conduits are very often filled with fibers materials like poly(l-lactide-co-glycolide) (PLGA) fibers, poly-l-lactide acid (PLLA), alginian filaments and hydrogels, collagen filaments, carbon filaments, bioglass fibers, chitosan fibers or material with properties of hydrogel [44,54].

Collagen fibers can be used as scaffolds for axonal elongation. Collagen is a major component of the extracellular matrix and is known to promote cellular proliferation and tissue healing. It has also been reported that the biological properties of collagen make it a superior choice for the use in conjunction with nerve tubes as a promoter of peripheral nerve regeneration [37,55]. Nerve scaffold made of the collagen filaments can be length from 20 to 30mm and 20µm in diameter [56].

Bioglass fibers are not only biocompatible and bioresorbable, what are the fundamental requirements of successful devices, but also amenable to bioengineering. Such fibers have the potential for the use in the most challenging clinical cases, where there are long inter-stump gaps to be bridged. Bioglass fibers can be used to deliver growth factors and/or adherent cells within the lumen of a nerve conduit. Bioglass fibers used as scaffolds for axonal regeneration consist of SiO_3, Na_2O, CaO and P_2O_5 and, their dimensions are 0,5cm long and 25µm diameter. Scientists from United Kingdom have applied bioresorbable bioglass fibers as a scaffolds for axonal regeneration. 0,5cm fragment at the sciatic nervesof adult rats was reconstructed. The axonal regrowth was qualitatively and quantitively indistinguishable from that seen using an autograft [57].

Alginian based hydrogels are well recognized materials both in experimental studies as well as in clinical applications [58]. It is natural polymer extracted from sea algae, composed by turn of mannose and glucuronic acid. Ca ions addition to water alginate solution cause ionic bonds creation between polymer chains. This process turns the solution into hydrogel, and its solidity can be controlled by concentration of Ca ions [59]. Lack of specific cell bonding sections makes alginate chains ideal ground for construction of extracellular matrices. In order to facilitate material cell colonization, alginate chains are modified with cell's binding signal sequences. The most common sequence is RGD [59,60,61]. Alginates can be easing sterilized or modified chemically in order to change their properties [59]. 10 mm

UV jest słabo unaczyniony, jednak wstająca weń tkanka nerwowa szybko dojrzewa osiągając po 12 tygodniach postać podobną do autoprzeszczepu [49]. Glutaraldehyd powoduje powstanie powierzchni o silnej hydrofobowości oraz cytotoksyczności, co znacznie upośledza procesy regeneracyjne wewnątrz takiego implantu [49, 50]. Oprócz właściwości fizycznych implantu takich jak sieć porów, ich średnica, ułożenia przestrzenne kanałów ważna jest technika przygotowania implantu, która może znacznie wpłynąć na jego właściwości [49].

Wcześniejsze badania wykazały, że rurki kolagenowe nie mogą być zastosowane do uzupełniania ubytku nerwu większego niż 15 mm, ponieważ mogą ulegać złamaniu, bądź zapadaniu w wyniku przemieszczeń. W celu poprawienia elastyczności i odporności struktury na zniszczenie, rurki kolagenowe są pokrywane polimerem takim jak kopolimer polilaktydu |z poliglikolidem. Powłoka polimerowa spełnia dwie funkcje: po pierwsze wzmacnia jej ścianę oraz zapobiega jej zapadaniu w trakcie ruchu, po drugie tworzy wysokoporowatą strukturę, która jest bardzo ważna dla transportu substancji odżywczych do wnętrza implantu. Powłoki polimerowe na powierzchni rurek kolagenowych zabezpieczają także przed wtargnięcie tkanki zewnętrznej do wnętrza rurki [51,52,53]. Złącza polimerowe bardzo często są wypełniane materiałami włóknistymi takimi jak włókna z kopolimeru poli-ld-laktydu z poliglikolidem (dl-PLGA), włókna z poli-l-laktydu (PLLA), włókna alginianowe, kolagenowe, węglowe, włókna z bioszkieł, włókna chitozanowe a także materiałem wypełniającym może być hydrożel [44, 54].

Włókna kolagenowe mogą być używane jako podłoża dla wzrastających włókien nerwowych. Dzięki odpowiednim własnościom biologicznym, włókna kolagenowe są używane jako elementy wypełniające polimerowe implanty nerwów, ułatwiające ich regeneracje [37,55]. Podłoża dla regeneracji nerwów wykonane z włókien kolagenowych mogą mieć długość od 20 do 30mm i średnicę 20 µm [56].

Włókna z bioszkieł są biozgodne i bioresorbowalne, a także mają możliwość potencjalnego zastosowanie w wielu stanowiących wyzwanie dziedzinach, na przykład do mostowania długich przerw między kikutami. Mogą być zastosowane jako elementy do transportowania czynników wzrostu oraz/lub jako podpora dla wzrostu komórek nerwowych. Włókna z bioszkieł stosowane jako podłoża dla regeneracji aksonów zawierają SiO_3, Na_2O, CaO i P_2O_5, przy wymiarach 0,5cm długości oraz 25µm średnicy. Naukowcy z Wielkiej Brytanii zastosowali włókna z bioszkieł jako podłoże dla regeneracji aksonów dla 0,5cm ubytku nerwu kulszowego dorosłego szczura - różnica pomiędzy parametrami odbudowanego aksonu, po zastosowaniu włókien z bioszkieł, a autoprzeszczepu była praktycznie niedostrzegalna [57].

Hydrożele skonstruowane na bazie alginianów są dobrze poznanymi materiałami stosowanymi zarówno w badaniach doświadczalnych jak i mającymi uznane zastosowanie w medycynie[58]. Jest to naturalny polimer izolowany z alg morskich, zbudowany z położonych na przemian jednostek kwasu manuronowego i guluronowego. Dodatek jonów Ca do roztworu wodnego alginianów powoduje powstawanie wiązań jonowych pomiędzy łańcuchami polimeru, co prowadzi do przechodzenia roztworu w postać hydrożelu. Stopień upostaciowienia może być regulowany stężeniem dodanych jonów Ca [59]. Ze względu na brak specyficznych miejsc łączenia z komórkami w łańcuchach polimeru alginiany są idealnym podłożem do konstrukcji sztucznych macierzy pozakomórkowych [59,60,61]. Alginiany poddają się prostym procesom sterylizacji, są łatwe w modyfikacji chemicznej celem zmiany właściwości [59]. Zastosowano gąbki alginianowe jako pomosty dla regeneralginate sponge implanted as a bridge for nerve regeneration is absorber in 4 weeks. During that time axons manage to pass the gap. Characteristic is fact, that ingrowth of tissue into the implant starts with axons followed by Schwann cells. Schwann cells produce fully valuable myelin sheath. Simultaneously with proximal regeneration into the implant Schwann cells migrate from distal stump and create tuberouts for approaching axonal growth cones. After connection of these processes axons start to ingrowth into distal part of regeneration and elongate using Schwann cell tubes. This process proceeds off-centre, firsts taking place in parietal, and secondly in central part of implant. This aspect of regeneration is dependent on gel degradation preceded from external part of implant, gradually creating looser, easer penetrable environment for regenerating tissue. It points to fact that, at lest for alginate, more important factor controlling implant colonization are degradation processes than that of pore diameter. Morphological analysis of the regenerated tissue revealed of regenerated axon. The amount of such axons the presence corresponded to the half of the number at uninjured part of nerve, and electrophysiological analysis proved existence at functional connections [30]. Axonal elongation and creation of functional connections with target organ is possible for unmodified 50 mm alginate implants [62].

Neurotrofic substances in artificial nerve implants

For improvement of neuroregeneration promoting properties polymers tubes prior implantation are filled with several neurotrophic factors, which can promote early peripheral nerve regeneration. The most commonly used neurite-promoting factors include collagen gel, laminin and fibronectin [63,64] and the most extensively studied neurotrophic factor, nerve growth factor (NGF) [65]. The effect of NGF grafted onto membranes indicates that the procedure used in immobilization of NGF onto polymers membrane may be beneficial for adhesion of Schwann cells on the membranes. The immobilization NGF on polymer membrane is following: polymer membranes were soaked in chemical solution, for examples in 1-ethyl-3-(3 dimethylaminopropyl) carbodiimide (EDAC) solution and then transferred to NGF solution. In this process NGF reacts with bonds existed on the surface of polymer membranes [66].

Extracellular matrix fibers like laminin, fibronectin and collagen play important role in every tissue regeneration process [32]. Laminin is mainly produced by Schwann cells and widely dispersed in the peripheral nervous system. Fibronectin can be found in plasma, fibrous tissue, and basement membrane. Fibroblasts and Schwann cells also produce significant amounts of fibronectin. Laminin, fibronectin and collagen are major constituent of all extracellular matrices. Prefilling of nerve tube implants with these fibers can greatly enhance nerve regeneration processes in implant.

In order to improve peripheral nerve regeneration polymers conduits are incorporating with allogenic Schwann cells (SCs). The SCs are harvested, cultured to obtain confluent monolayers and injected into the biopolymers conduits [1]. Schwann cells play a crucial role in regeneration of peripheral nerves due to their neurotrophic influence, mechanic support and providing protection with myelin sheet. Schwann cells produce and accumulate trophic factors for regenerating axons and thus are essential for axonal regeneration, particularly for long gaps [44,67,68]. Schwann cells produce basal lamina components, such as collagen IV, which provide the extracellular matrix for attachment of the regenerating axons [1,69,70,71]. Precolonization of the implant with these cells shortens the time of regeneration by elimination of the fibrin bridge and it's cellular colonization period. Allo,

racji ubytku nerwu o długości 10mm i zaobserwowano ich całkowite wchłonięcie w ciągu 4 tygodni przy jednoczesnej regeneracji aksonów. Charakterystyczny jest fakt, że wrastanie tkanki w implant zaczyna się od aksonów, za którymi podążają komórki Schwanna. Wytwarzają one w pełni wartościowe osłonki mielinowe. Jednocześnie od bieguna dystalnego w obręb implantu napełzają komórki Schwanna tworząc tory dla zbliżających się stożków regenerujących aksonów włókien nerwowych. Po zetknięciu się tych dwóch procesów dochodzi do przejścia aksonów z proksymalnego pola wzrostowego w dystalne i dalszy wzrost na bazie utworzonego przez komórki Schwanna podłoża. Procesy te zachodzą ekscentrycznie zajmując najpierw obrzeże implantu a następnie coraz bardziej centralne części. Jest to związane z procesami degradacji żelu, który postępował stopniowo od zewnątrz do wewnątrz, tworząc środowisko łatwiej penetrowane przez regenerującą tkankę. Wskazuje to, że przynajmniej w przypadku alginianów, ważniejszym czynnikiem kontrolujących kolonizację implantu przez tkankę są procesy jej degradacji niż wielkość porów. Badania morfologiczne wykazują obecność zregenerowanych aksonów w ilości odpowiadających połowie ilości obecnych po stronie zdrowej, a badania elektrofizjologiczne wykazują wytworzenie funkcjonalnych połączeń [30]. Według badań możliwe jest uzyskanie przechodzenia aksonów przez niewzbogacone implanty alginianowe o długości 50mm z wytworzeniem funkcjonalnych połączeń [62].

Możliwości wykorzystania substancji neurotroficznych w sztucznych implantach nerwowych

Dla zwiększenia właściwości neuroregeneracyjnych rurki polimerowe stosowane jest wzbogacanie ich przed implantacją różnorodnymi czynnikami neurotroficznymi, dla pobudzenia wczesnych faz regeneracji nerwów obwodowych. Najczęściej stosowanymi czynnikami neurotroficznymi są żel kolagenowy, laminina, fibronektyna [63,64], oraz najlepiej poznany czynnik stymulujący neuroregenerację - czynnik wzrostu nerwu (NGF - nerve growth factor) [65]. Immobilizacja czynnika NGF we wnętrzu membrany polimerowej może wspomagać adhezję komórek Schwanna. Proces immobilizacji NGF do wnętrza membrany odbywa się następująco: membrana polimerowa najpierw zanurzona zostaje w roztworze chemicznym np. 1-ethyl-3-(3 dimethylaminopropyl) carbodiimide (EDAC), a następnie przeniesiona do roztworu NGF. W wyniku tego procesu NGF reaguje z wiązaniami znajdującymi się na powierzchni membrany polimerowej [66].

W procesie regeneracji wszystkich tkanek istotny udział mają włókna macierzy pozakomórkowej: laminina, fibronektyna oraz kolagen [32]. Laminina jest głównie produkowana przez komórki Schwanna, występuje w dużej ilości w całym obwodowym układzie nerwowym. Fibronektyna jest obecna w plazmie, tkance włóknistej oraz błonie podstawnej. W znacznej ilości produkowana jest przez fibroblasty oraz komórki Schwanna. Wypełnienie tymi materiałami implantowanych tub pozwala na znaczną modyfikację i przyspieszenie procesów regeneracji zachodzących w implancie.

W celu przyspieszenia regeneracji nerwów obwodowych stosuje się wzbogacanie implantów komórkami Schwanna (SCs) pochodzenia allogenicznego. Komórki Schwanna są hodowane w celu uzyskania konfluentnej monowarsty, a następnie wstrzykiwane do wnętrza implantu polimerowego [1]. SC pełnią decydującą rolę w regeneracji nerwów z uwagi ich neurotropowe i neurotroficzne właściwości. Stanowią podporę mechaniczna dla regenerujących aksonów, wytwarzają oraz akumulują czynniki odżywcze dla regenerujących się aksonów, co jest szczególnie ważne przy dużych ubytkach nerwu [44,67,68]. Komórki Schwanna produkują także składowe blaszki podstawnej, takie jak kola-

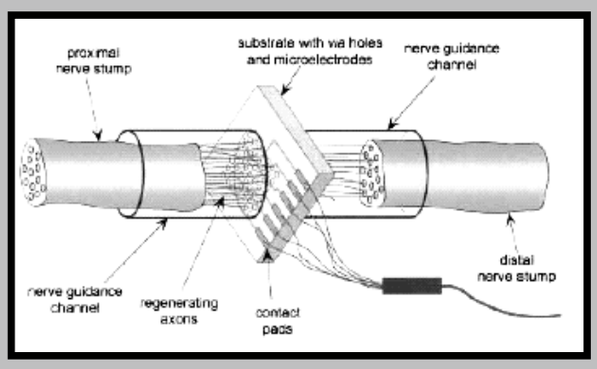

RYS. 2. Schemat elektrody dla regeneracji nerwów. [74].
FIG. 2. Electrode scheme for nerves regeneration.

kseno i autogenic cells are used, pre or not predegenerated. The best effects are found with autogenic, preinduced cells [72,73].

Microelectrodes for nerve regeneration

Interesting investigation areas pertain to composite implants used for stimulating nerve regeneration, passive extracellular matrix support and active electrical stimulation of nerve regeneration. These systems consist of microelectrodes placed on a sieve-shaped plate containing long, narrow holes, round in shape. The microelectrodes are situated close to the holes or constitute a part of the hole wall [74]. The electrode array of via holes is adapted into the expected path of the regenerating fibers in a fashion that the nerve fibers are allowed to regenerate through the perforations of the device. In order to assure the mechanical stability of all system, the electrodes are placed between polymer channel connecting proximal nerve stump with distal one.

The advantage of this approach is that the electrodes are in near contact with the nerve fibers, thas allowing for both accurate recording and efficient stimulation. The disadvantage of this method is that the nerve has to be cut in order to regenerate through the implanted device. The success of the whole operation can be assessed only several weeks after implantation, when the axons have been regenerated through the device. Sometimes, there is a possibility that nerve fibers may be damaged by the mechanical load imposed by the electrode or by the force within the via holes, especially over long term implantation [74,75].

Various techniques and materials have been used to fabricate the needed sieve electrodes. Some early electrodes were realized by embedding 25mm-diameter hollow gold cylinders into porous Teflon. Other was realized by mechanically drilling 100mm-diameter holes into epoxy modules and then embedding 77mm-diameter Teflon-coated silver wires into the holes [76]. The material very often used in the construction of regenerative electrodes is silicon. The silicon electrodes with dimensions and number of via holes compatible with the characteristics of peripheral nerves were used in axonal regeneration nerves of rat, and frog [19,21]. However, such silicon interfaces cause frequent signs of axonopathy, and constitute a physical barrier that limits the elongation of regenerating axons depending on the size of the via holes [75,76]. Recently the silicon electrodes are replaced by polyimide-based electrodes. Polyimide allows to make a higher number of holes than silicon dice of the same total area and to be micromachined in a variety of designs suitable for implantation in different nerve models.

gen typu IV czy laminina, które ułatwiają kontakt regenerujących włókien nerwowych z macierzą zewnątrzkomórkową [1,69,70,71]. Wzbogacenie implantu tymi komórkami skraca okres regeneracji o czas potrzebny na uformowanie pomostu fibrynowego i skolonizowanie go przez nadpełzające komórki Schwanna. Najkorzystniejsze wyniki daje zastosowanie autogennych wzbudzonych komórek Schwanna [72,73].

Mikroelektrody w regeneracji nerwów

Jednym z ciekawych podejść badawczo-eksperymentalnych są badania z użyciem kompozytowych implantów wykorzystujących stymulującę regeneracje włókien nerwowych właściwości biernego podparcia tkanki i czynnej stymulacji elektrycznej. Układy te zbudowane są z mikroelektrod umieszczonych na płytce w kształcie sita zawierającej długie, wąskie, okrągłe otwory. Mikroelektrody usytuowane są na brzegu otworów bądź są częścią ścianek otworów [74]. Elektrody umieszczane są w taki sposób w ubytku nerwu, aby regenerujące się włókna nerwowe mogły przechodzić przez znajdujące się w niej otwory.

W celu zapewnienia mechanicznej stabilności całego układu, elektrody usytuowane są pomiędzy polimerowymi kanałami łączącymi kikut proksymalnym nerwu z kikutem dystalnym.

Zaletą tego typu rozwiązania jest fakt, że urządzenie znajduje się w bliskiej odległości od włókien nerwowych, co pozwala na skuteczną ich stymulację. Powodzenie operacji może zostać ocenione w przeciągu kilku tygodni po implantacji, kiedy włókno nerwowe zdoła zregenerować poprzez urządzenie. Czasami włókna nerwowe mogą ulec uszkodzeniom w wyniku naprężeń mechanicznych pochodzących od elektrody bądź przez siły działające wewnątrz otworów powstałe w wyniku ich zarastania, zwłaszcza przy długim okresie implantacji [74,75].

Różnorodne techniki oraz materiały były stosowne przy konstruowaniu elektrod. Początkowo wykonywane były poprzez zatopienie złotych, pustych wewnątrz cylindrów o średnicy 25μm w porowatym teflonie. Innym sposobem jest mechaniczne wiercenie dziur o średnicy 100μm w elemencie epoksydowym, a następnie umieszczenie wewnątrz nich srebrnych drutów pokrytych teflonem [76]. Materiałem używanym najczęściej do konstrukcji elektrod do regeneracji nerwów jest krzem. Elektrody krzemowe o odpowiednich wymiarach i ilości otworów stosowane były do regeneracji aksonów nerwów u szczura oraz żaby [19,21].

Jednakże, krzem powoduje często objawy aksonopatii i stanowi fizyczną barierę ograniczającą wydłużanie regenerujących się aksonów [75,76]. Obecnie elektrody krzemowe zastępowane są elektrodami na bazie poliimidów. W przypadku poliimidów istnieje możliwość wytworzenia większej ilości otworów dla tej samej powierzchni całkowitej w porównaniu z płytką krzemową, a także istnieje możliwość stworzenie odpowiedniego modelu nerwu dopasowanego do miejsca implantacji. Elektrody na bazie poliimidu są biokompatybilne i stabilne zarówno w warunkach "in vivo" jak i podczas prób mechanicznych [79].

Nanomateriały w regeneracji nerwów

Obiecujące wyniki zastosowania nanorurek węglowych w badaniach na komórkach ośrodkowego układu nerwowego pozwalają na potencjalne ich zastosowanie w regeneracji obwodowego układu nerwowego. Odkryto, bardzo interesujące oddziaływanie pomiędzy neuronami, a materiałami w skali nano, w wyniku którego następuje osłabienie tworzenia się tkanki bliznowatej rdzenia kręgowego. Polyimide-based electrodes have been shown to be biocompatible and stable over several months of in vivo implantation and testing [79].

Nanomaterials for nerve regeneration

Good results of research using carbon nanostructures in central nervous system nerve cells cultures indicatestheir potential for the treatment peripheral nervous system. Promising interactions are found between neurons and nanoscale materials with potential minimalization of astrocytic spinal cord scar tissue formation. Carbon nanofibers are particularly attractive for the use in neural biomaterials not only due to these special properties, but also due to their high conductivity. Further investigation of carbon nanofiber materials is required to verify their properties as potential neural biomaterials [80,81,82].

Carbon nanotubes (CNT) are strong, flexible and conduct electrical current. Moreover, their biocompatibility and stabi8lity in living organism have already been proved [80]. They can be functionalized with different biomolecules like neuron growth factors and adhesion agents. These properties are useful in the formation of neuron hybrids. Such capabilities of carbon nanotubes make them potentially suitablel candidates to form scaffolds to guide neurite outgrowth. Zhang at al., demonstrated the capability of functionalized patterned vertical carbon nanotube arrays as support platforms for guiding neurite growth and forming synoptically communicative network. The study indicated that neurons "in vitro" conditions created communicative synaptic bridge between two nanotube patterns with a distance of separation of 20mm [83]. Telford et al., have cultured nerve cells from the brain's hippocampus region on substrates coated with network of carbon nanotubes, and found a large increase in neural signal transfer between cells. The data provided information on the supportive devices for bridging and integrating functional neuronal network "in vitro". [84].The results will impact on new tissue engineering strategies, where functional reconnection among neurons or the improvement in neural signal transfer is the main target. There is strong demand for deeper study on the properties of such materials and their physiological interactions with neurons in culture. This will provide the base for more exhaustive evaluation on animal models.

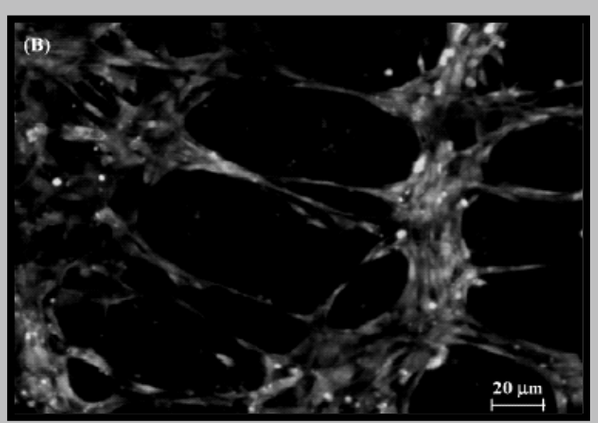

RYS. 3. Mikrofotografia przedstawiająca komunikujące się między sobą sieci synaptyczne na podłożu z nanorurek węglowych [83].
FIG. 3. Microphotograph of carbon nanotubes support for forming synoptically communicative network [83].

Nanowłókna węglowe są atrakcyjnym biomateriałem stosowanym jako implanty nerwów nie tylko z powodu szczególnych właściwości mechanicznych czy chemicznych, ale także z powodu ich wysokiej przewodności właściwej. Dalsze badania nad nanowłóknami węglowymi są konieczne, aby zweryfikować ich potencjalne zastosowanie jako biomateriałów dla regeneracji nerwów [80,81,82].

Nanorurki węglowe (CNT) są materiałem trwałym, giętkim, przewodzącym prąd elektryczny, biozgodnym oraz nie biodegradowalnym [80]. Mogą być sfunkcjonalizowane różnorodnymi biomolekułami takimi jak czynniki wzrostu neuronów. Takie własności nanorurek węglowych czynią z nich potencjalnego kandydata do konstrukcji podłoży dla kierowanego wzrostu aksonów. Zhang i współ. z uniwersytetu z Kaliforni zademonstrowali możliwości zastosowania modelu (układu) z pionowo ułożonych nanorurek węglowych jako podporę dla kierowanego wzrostu aksonów, a także dla tworzenia sieci połączeń synaptycznych. W badaniach "in vitro" zaobserwowano, że neurony tworzą mostki synaptyczne pomiędzy dwoma nanorurkowymi układami (wzorcami) oddalonymi od siebie o około 20µm [83].

Telford i współpracownicy opisują szereg doświadczeń z zastosowaniem komórek nerwowych pobranych z mózgu na specjalnym podłożu pokrytym ścieżkami z nanorurek węglowych. Stwierdzono znaczny przyrost wartości impulsów nerwowych wędrujących pomiędzy komórkami nerwowymi [84].

Uzyskane wyniki mogą zostać wykorzystane przy tworzeniu nowych strategii badań w inżynierii tkankowej mających na celu przywrócenie połączeń pomiędzy uszkodzonymi komórkami nerwowymi bądź polepszenie przekazywania sygnałów nerwowych. Niezbędne jest jednak poszerzenie aktualnej wiedzy na temat tego rodzaju materiałów oraz ich oddziaływania z komórkami nerwowymi w hodowlach "in vitro", przed zastosowaniem dla regeneracji układu nerwowego zwierząt i ludzi.

Zakończenie

Obecny stan wiedzy nad regeneracją obwodowego układu nerwowego pozwala na uzyskanie pozytywnych wyników regeneracji nerwu przy użyciu sztucznych implantów. Część wykorzystywanych materiałów dzięki wynikom regeneracji porównywalnym z przeszczepami z nerwów skórnych znajduje już zastosowanie w leczeniu ludzi. Mimo to konieczne są dalsze badania weryfikujące dotychczasowy stan wiedzy oraz pozwalające na poprawienie uzyskiwanych obecnie wyników leczenia.

Conclusion

Present state of knowledge on regeneration processes of peripheral nervous tissue allows for achieving good regeneration results with artificial implants. Some materials tested on animal models are now verified in the treatment of digital nerve injuries in humans. Consecutive investigations are however demanded for furtherr development of knowledge relevant to nervous tissue regeneration.

Piśmiennictwo Reference

[1] G.R.D. Evans,K. Brandt , S. Katz, P. Chauvin, L. Otto, M. Bogle, B. Wang, R.K. Meszlenyi, L. Lu, A.G. Mikos,Ch.W. Patrick Jr "Bioactive poly(l-lactic acid) conduits seeded with Schwann cells for peripheral nerve regeneration" Biomaterials 23 (2002) 841-848.

[2] Pielka S., Rutowski R., Bogdan K., Pytlasiński M., Wiącek R. "Uszkodzenia nerwów kończyny górnej u 1739 chorych w materiale Kliniki Chirurgii Urazowej i Chirurgii Ręki AM we Wrocławiu" III Międzynarodowy Kongres Polskiego Towarzystwa Chirurgii Ręki Białystok 2003.

[3] B.R. Rutowski, S. Pielka, J. Gosk, D. Szarek, W. Urbański "Ocena wyników operacji mikrochirurgicznych w uszkodzeniach nerwów kończyny górnej." Krzysztof; Adv Clin Exp Med 2005, 14, 6, 1199-1209.

[4] J. Braga-Silva "The Use of Silicone Tubing in the Late Repair of The Median and Ulnar Nerves in the Forearm" Journal of Hand Surgery (British and European Volume) 24B (1999) 6 703-706

[5] J. Haftek, H. Kasprzak, A. Radek, W. Jarmundowicz, J. Jóźwiak " Przeszczepy nerwowe w rekonstrukcji uszkodzonych pni nerwowych" Neurologia Neurochirurgia Polska, 1983, 17, 2, 253-258.

[6] Yuan Y., Zhang P., Yang Y., Wang X., Gu X. " The interaction of Schwann cells with chitosan membranes and fibers in vitro" Biomaterials 25 (2004) 4273-4278.

[7] Borschel G.H., Kia K.F., Kuzon W.M., Dennis R.G. "Mechanical Properties of Acellular Peripheral Nerve" Journal of Surgical Research 114 (2003) 133-139.

[8] Haftek J. "Stretch injury of peripheral nerves." J. Bon. J. Surg; 1970; 52-B, 2, 354.

[9] M. Mumenthaler, H. Schliack "Uszkodzenia nerwów obwodowych";; PZWL 1998; str 128; 142-143

[10] S. Hall "Nerve repair: a neurobilogist's view"; The Journal Of Hand Surgery; vol 26b; No2; april 2001; 129-136

[11] Ming-Shaung J., Chou-Ching K. L., Jia-Lin F., Rung-Jian Ch. "Transverse elasticity and blood perfusion of sciatic nerves under in situ circular compression" Journal of Biomechanics 39 (2006) 97-102.

[12] Kwan K.M., Woo S.L-Y. "Biomechanical properties of peripheral nerve".

[13] Sunderland S. "Nerves and nerve injures, ed.2. Edinburgh: Churchill - Livingstone, 1978.

[14] T. M. Myckatyn, S.E. Mackinnon "Surgical Techniques of Nerve Grafting (Standard/Vascularized/Allograft)"; OperTech Orthop 14:171-178; 2004

15] R. H. Gebelman; J.B. Lippincott "Operative nerve repair and reconstruction." Company, Philadelphia; 1991.

[16] M.F. Meek "Artificial Nerve Guides - assessment of nerve function", Proefschrift, 2000.

[17] E.O. Johnson, A.B. Zoubos, P.N. Soucacos "Regeneration and repair of peripheral nerves" Injury 36S (2005) 24-29.

[18] Heiduscha P., Thanos S. "Implantable bioelectronic interfaces for lost nerve functions" Progress in Neurobiology 55 (1998) 55-461.

[19] G. Verrecka, I. Chunb, Y. Lib, R. Katariab, Q. Zhangb, J. Rosenblattb, A. Decortea, K. Heymansa, J. Adriaensena, M. Bruininga, M. Van Remoorterea, H. Borghysa, T. Meerta, J. Peetersa, M. E. Brewster "Preparation and physicochemical characterization of biodegradable nerve guides containing the nerve growth agent sabeluzole" Biomaterials 26 (2005) 1307-1315.

[20] L. R. Williams, F.M. Longo, H.C. Powell, G. Lundborg, S. Varon,"Spatial-Temporal Progress of Peripheral Nerve Regeneration Within a Silicone Chamber: Parameters for a Bioassay." The Journal of Comparative Neurology, 218: 460-470 (1983).

[21] Ch.R. Noback, J. Husby, J.M. Girado, C. Andrew, L. Bassett, J.B. Campbell "Neural regeneration across long gaps in mammalian peripheral nerves: Early morphological findings.", Anat Rec 131 (1958) 633-647.
[22] J.M. L. Beau, M.H. Ellisman, H.C. Powell "Ultrastructural and morphometric analysis of long-term peripheral nerve regeneration through silicone tubes." , Journal of Neurocytology 17, 161-172 (1988).
[23] R.D. Madison, S.J. Archibald "Point Sources of Schwann Cells Result in Growth into a nerve Entubulation Repair Site in the Absence of Axons: Effects of Freeze-Thawing.", Experimental Neurology, 128, 266-275 (1994).
[24] M. Cuadros-Romero, A. Trueva "Nerve Regeneration Using Polyglicolic Acid As Alternative To Grafting". The Journal Of Hand Surgery Vol 28b Suplment 1.
[25] X. Navarro, E. Verdú, F.J. Rodriguez, D. Ceballo "Artificial nerve graft for the repair of peripheral nerve injuries." s; Neurol Sci (2001) 22: S7-S13.
[26] L.J. Chamberlain, I.V. Yannas, A. Arrizabalaga, H.-P. Hsu, T.V. Norregaard, M. Spector "Early peripheral nerve healing in collagen and silicone tube implants: Myofibroblasts and the cellular response.", Biomaterials 19(1999) 1393-1403.
[27] Q. Zhao, L.B. Dahlin, M. Kanje, G. Lundborg "Repair of the transected rat sciatic nerve: Matrix formation within implanted silicone tubes.", Restorative Neurology and Neuroscience, 5 (1993) 197-204.
[28] J.A. Bertelli, A.R. S. Dos Santos, Joao B. Calixto, J.C. Mira, M.F. Ghizoni "Long interpositional nerve graft consistently induces incomplete motor nad sensory recovery in the rat. An experimental model to test nerve repair.", Journal of neuroscience methods 134 (2004) 75-80.
[29] A.I. Gravvanis, A. Ladvas, A.E. Papalois, D.A. Tsoutsos, P.N. Pnayotou, D.C.-C. Chuang, I. Franceschini, M. Dubois-Dalcq, R. Matsas "Collagen tube lined with genetically modified Schwann cells with increased motility: A new promising bioartificial nerve graft"; Eur Surg (2005) 37/4: 204-212.
[30] T. Hashimoto, Y. Suzuki, M. Kitada, K. Kataoka, S. Wu, K. Suzuki, K. Endo, Y. Nishimura, C. Ide "Peripheral nerve regeneration through alginate gel: analysis of early outgrowth and late increase in diameter of regenerating axons."; Exp Brain Re (2002) 146: 256-368.
[31] I.V. Yannas, B.J. Hill "Seletion of biomaterials for peripheral nerve regeneration using data from the nerve chamber model"; Biomaterials 25(2004); 1593-1600.
[32]Yueh-Sheng Che, Ching-Liang Hsieh, Chin-Chuan Tsai, Ter-Hsin ChenWen-Chiang Cheng, Cheng-Li Hu, Chun-Hsu Yao "Peripheral nerve regeneration using silicone rubber chambers filled with collagen, laminin and fibronectin" Biomaterials 21 (2000) 1541-1547.
[33] G. Lundborg, L. Dahlin, D. Dohi, M. Kanje, N. Terada "A New Type of "Bioartificial" Nerve Graft for Bridging Extended Defects in Nerves" Journal of Hand Surgery (British and European Volume, 1997) 22B: 3:299-303.
[34] Chen-Jung C., Shan-Hui H. "The Effects Of Low-Intensity Ultrasound On Peripheral Nerve Regeneration In Poly(Dl-Lactic Acid-Co-Glycolic Acid) Conduits Seeded With Schwann Cells" Ultrasound In Med. & Biol. 8 (2004) 1078-1084.
[35] Y. Katayama, R. Montenegro, T. Freier, R. Midha, J.S. Belkas, M.S. Shoichet "Coil-reinforced hydrogel tubes promote nerve regeneration equivalent to that of nerve autografts" Biomaterials 27 (2006) 505-518.
[36] C. Sundbacka, T. Hadlockb, M. Cheneyb, J. Vacantia "Manufacture of porous polymer nerve conduits by a novel low-pressure injection molding process" Biomaterials 24 (2003) 819-830
[37] Nakamura T., Inada Y., Fukuda S., Yoshitani M., Nakada A., Itoi S., Kanemaru S., Endo K., Shimizu Y. "Experimental study on the regeneration of peripheral nerve gaps through a polyglycolic acid-collagen (PGA-collagen) tube" Brain Research 1027 (2004) 18-29.
[38] T. Nakamura, Y. Inada, S. Fukuda, M. Yoshitani, A. Nakada, S. Itoi, S. Kanemaru, K. Endo, Y. Shimizu "Experimental study on the regeneration of peripheral nerve gaps through a polyglycolic acid-collagen (PGA-collagen) tube, Brain Research 1027 (2004) 18-29.
[39] K. Matsumoto, K. Ohnishi, T. Kiyotani, T. Sekine, H. Ueda, T. Nakamura, Ka. Endo, Y. Shimizu "Peripheral nerve regeneration across an 80-mm gap bridged by a polyglycolic acid (PGA)-collagen tube filled with laminin-coated collagen fibers: a histological and electrophisiological evaluation of regenerated nerves."; Brain Reserch 868 (2000) 315-328.
[40] R.A. Weber, W.C. Breidenbach, R.E. Brown, M.E. Jabaley, D.P. Mass "A Randomized Prospective Study of Polyglycolic Acid Conduits for Digital Nerve Reconstruction in Humans.", Plast. Reconstr. Surg. 106: 1036, 2000).
[41] R. C. Young, M. Wiberg, G. Terenghi "Poly-3-hydroxybutyrate (PHB): a resorbable conduit for long-gap repair in peripheral nerves" British Journal of Plastic Surgery 55 (2002) 235-240.
[42] A. Hazari, M. Wiberg, G. Johansson-Rudén, C. Green, G. Terenghi "A resorbable nerve conduit as an alternative to nerve autograft in nerve gap repair" British Journal of Plastic Surgery 52 (1999) 653-657.
[43] Kurita K. "Chemistry and application of chitin and chitosan as fiber and film formers" Polym. Degrad. Stabil. 70 (1998) 7-12.
[44] Yuan Y., Zhang P., Yang Y., Wang X., Gu X. " The interaction of Schwann cells with chitosan membranes and fibers in vitro" Biomaterials 25 (2004) 4273-4278.
[45] Suzuki T., Mizushima Y."Characterization of silica-chitosan complex adhesiveness of L-929 cells cultured on the biomembrane" J. Ferment Bioeng. 1997;84(2):128.
[46] M. R.Ahmed, S. Vairamuthu, Md. Shafiuzama, S. H. Bashad, R. Jayakumar "Microwave irradiated collagen tubes as a better matrix for peripheral nerve regeneration" Brain Research 1046 (2005) 55 - 67.
[47] Ch. Krarup, S.J. Archibald, R.D. Madison."Factors That Influence Peripheral nerve Regeneration: An Elektrophysiological Study of the Monkey Median Nerve." Ann. Neurol 2002; 51: 69-81
[48] S.J. Archibald, J. Shefner, C. Krarup, R.D. Madison "Monkey Median Nerve Repair by Nerve Graft or Collagen Nerve Guide Tube.", The Journal of Neuroscience, may 1995, 15(5):4109-4123
[49] S. Itoh, K. Takakuda, S. Kawabata, Y. Aso, K. Kasai, H. Itoh, K. Shinomiya, "Evaluation of cross-linking procedures of collagen tubes used in peripheral nerve repair" Biomaterials 23(2002) 4475-4481
[50] S. Yoshii, M. Oka, M. Shima, A. Tanigochi, M. Akagi "30 mm regeneration of rat sciatic nerve along collagen filaments."; Brian Reserch 949 (2002) 202-208
[51] D.Y. Lee, B.H. Choi, Jh Park, Sj Zhu, By Kim, Jy. Huh, Sh. Lee, Jh. Jung, Sh. Kim "Nerve Regeneration With The Use Of A Poly(L-Lactide-Co-Glycolic Acid)-Coated Collagen Tube Filled With Collagen Gel" Journal Of Cranio-Maxillofacial Surgery (2006) 34, 50-56.
[52] Kiyotani T., Teramachi M., Takimoto Y., Nakamura T., Shimizu Y., Endo K. "Nerve regeneration across a 25-mm gap bridged by a polyglicolic acid-collagen tubes: a histological and electrophysiological evaluation of regenerated nerves" Brain Research 740 (1996) 66-74.
[53] Archibald S.J., Krarup C., Shefner J., Li S., Madison R.D. "A collagen-based nerve guide conduit for peripheral nerve repair: An electrophysiological study of nerve regeneration in rodents and nonhuman primates", J. Comp. Neurol. 306 (1991) 685-696.
[54] N. B., Chauhan, H.M. Figlewicz, T.Khan "Carbon filaments direct the growth of postlesional plastic axons after spinal cord injury" PII: S0736-5748(1999)00003-9.
[55] G. Keilhoff, F. Stang, G. Wolf, H. Fansa, Bio-compatibility of type I/III collagen matrix for peripheral nerve reconstruction, Biomaterials 24 (2003) 2779- 2787.
[56] S. Yoshii , M. Oka , M. Shima , A. Taniguchi , M. Akagi "30 mm regeneration of rat sciatic nerve along collagen filaments" Brain Research 949 (2002) 202-208
[57] Bunting S., L. Di Silvio, Deb S., Hall S. "Bioresorbable glass fibres facilitate peripheral nerve regeneration" Jurnal of Hand Surgery 3(2005)242-247.
[58] B. Balakrishnana, M. Mohantyb, P.R. Umashankarc, A. Jayakrishnana "Evaluation of an in situ forming hydrogel wound dressing based on oxidized alginate and gelatin.", Biomaterials 26 (2005) 6335-6342.
[59] J.A. Rowley, G. Madlambayan, D.J. Mooney "Alginate hydrogels as synthetic extracellular matrix materials."; Biomaterials 20 (1999) 45-53.

[60] M. Martins-Green"The dynamics of cell-ecm interactions, with implications for tissue engineering" Department of Biology, University of California, Riverside, Ca 92521.
[61] E. Ruoslahti "RGD and other recognition sequences for integrins", Annu. Rev. Cell Dev. Biol. 1996, 12: 697-715.
[62] Y. Suzukia, M. Taniharab, K. Ohnishic, K. Suzukia, K. Endod, Y. Nishimuraa "Cat peripheral nerve regeneration across 50 mm gap repaired with a novel nerve guide composed of freeze-dried alginate gel"; Neuroscience Letters 259 (1999) 75-78.
[63] Labrador RO, Buti R, Navarro X "Influence of collagen and laminin gels concentration on nerve regeneration after resection and tube repair" Exp Neurol 149: 243-252, 1998.
[64] I. H. Whitworth, R. A. Brown, C. J. Dore, P. Anand, C. J. Green, G. Terenghi "Nerve Growth Factor Enhances Nerve Regeneration Through Fibronectin Grafts" Journal of Hand Surgery (British and European Volume, 1996) 2lB." 4:514-522.
[65] Hollowell JP, Villadiego A, Rich KM. "Sciatic nerve regeneration across gaps within silicone chambers: long-term e!ects of NGF and consideration of axonal branching" Exp Neurol 1990;110: 45-51.
[66] Pei-Ru Chena, Ming-Hong Chena, Jui-Sheng Sunc, Mei-Hsiu Chend, Chien-Chen Tsaie, Feng-Huei Linf "Biocompatibility of NGF-grafted GTG membranes for peripheral nerve repair using cultured Schwann cells" Biomaterials 25 (2004) 5667-5673.
[67] Hurtado A., Moon L.D.F., Maquet V., Blits B., Jerome R., Oudega M. "Poly (D,L-lactic acid) macroporous guidance scaffolds seeded with Schwann cells genetically modified to secrete a bi-functional neurotrophin implanted in the completely transected adult rat thoracic spinal cord" Biomaterials 27(2006)430-442.
[68] Ide C. "Peripheral nerve regeneration" Neurosci Res 1996;25: 101-21.
[69] Gulati AK, Rai DR, Ali AM. Influence of cultured Schwann cells on regeneration through acellular basal lamina grafts. Brain Res 1995;705:118-24.
[70] E. O. Johnson, A. B. Zoubos, P. N. Soucacos "Regeneration and repair of peripheral nerves" Injury 36S (2005) S24-S29.
[71] Campbell YZ, Anderson PN, Martini R, Schachner M, Lieberman AR. Molecular basis of interactions between regenerating adult rat thalamic axons and Schwann cells in peripheral nerve grafts I. Neural cell adhesion molecules. J Comput Neurol 1995; 361:193-209.
[72] C. Ide, K. Tohyama, K. Tajima, K. Endoch. K. Sano, M. Tamura, A. Mizoguchi, M. Kitada, T. Morihara, M. Shirasu "Long Acellular Nerve Transplants for Allogeneic Grafting and the Effects of basic Fibroblast Growth Factor on the Growth of Regenerating Axona in Dogs: A Preliminary Report."; Experimental Neurology 154, 99-112 (1998).
[73] A.K. Gulati, D.R. Rai, A. M. Ali "The influence of cultured Schwann cells an regeneration through acellular basal lamina grafts."; Brain Research 705 (1995) 118-124.
[74] Heiduschka P., Thanos S. "Implantable bioelectronic interfaces for loset nerve function" Progress in Neurobiology 55 (1998) 433-461.
[75] Lago N.,Ceballos D.,Rodriguez F.J. Stieglitz T., Navarro "Long term assessment of axonal regeneration through polyimide regenerative electrodes to interface the peripheral nerve" Biomaterials 26 (2005) 2021-2031.
[76] Akin T., Najafi K., Smoke R.H., Bradley R.M. " A micromachined silicon sieve electrode for nerve regeneration applications" Transactions of Biomedical Engineering 41 (1994)
[77] Navarro X, Calvet S, But!i M, G!omez N, Cabruja E, Garrido P, Villa R, Valderrama E. Peripheral nerve regeneration through microelectrode arrays based on silicon technology. Restor Neurol Neurosci 1996;9:151-60.
[78] Zhao Q, Drott J, Laurell T, Wallman L, Lindstr.om K, Bjursten LM, Lundborg G, Montelius L, Danielsen N. "Rat sciatic nerve regeneration through a micromachined silicon chip" Biomaterials 18 (1997) 75-80.
[79] Navarro X, Calvet S, Rodr!iguez FJ, Stieglitz T, Blau C, But!i M, Valderrama E, Meyer JU. "Stimulation and recording from regenerated peripheral nerves through polyimide sieve electrodes" J Peripher Nerv System 2 (1998) 91-101.
[80] X. Zhang, S. Prasad, S. Niyogi, A. Morgan, M. Ozkan, C. S. Ozkan "Guided neurite growth on patterned carbon nanotubes" Sensors and Actuators B 106 (2005) 843-850
[81] M. Tatagiba, C. Brosamle, M.E. Schwab, Regeneration of injured axons in the adult mammalian central nervous system, Neurosurgery 40 (3) (1997) 541.
[82] J.L. McKenzie, M.C. Waid, R. Shi, T.J. Webster " Decreased functions of astrocytes on carbon nanofiber materials" Biomaterials 25 (2004) 1309-1317
[83] Roche Stephan "Carbon nanotubes: exceptional mechanical and electronic properties",nn. Chim. Sci. Mat, 2000, 25, pp.529-532.
[84] Telford M. "Carbon nanotubes boost neural signaling" Research News 2005.

PROJEKTOWANIE WŁASNOŚCI RESORBOWALNYCH, METALICZNYCH IMPLANTÓW KOSTNYCH – ZASTOSOWANIE W WARUNKACH *IN VIVO*

Friedrich-Wilhelm Bach*, Rafael Kucharski*, Dirk Bormann*,Dieter Besdo, Silke Besdo**, Christian Hackenbroich***, Fritz Thorey****, Andrea-Meyer-Lindenberg*****

* Institute of Materials Science, Schönebecker Allee 2, 30823 Garbsen, Germany
** Institut für Kontinuumsmechanik, Appelstraße 11, 30167 Hannover, Germany
***Department of Orthopaedic Surgery, Hanover Medical School, Hanover, Germany
****Clinic for Small Animals, University of Veterinary Medicine Hanover, Foundation, Germany
E-mail: bach@iw.uni-hannover.de

Streszczenie

Celem pracy było określenie stopnia zrostu zwierzęcej kości udowej w warunkach in vivo. Badania przeprowadzono poprzez wykorzystanie metody badania stopnia sztywności w warunkach wzrostu wartości siły w czteropunktowym ugięciu. Do badania zakwalifikowano grupe zwierzat doswiadczalnych rasy królik nowozelandzki (New Zeland Rabit). W pierwszej fazie badań jak wszczepy zastosowano materiały kontrolne z PLA. Wyniki badań określają zarys możliwości zastosowania w chirurgii kostnej materiałów na ubytki kostne wykonanych z resorbowalnych struktur na bazie stopów magnezu. W pracy przedstawiono ponadto metodykę wytwarzania oraz kontrole jakości procesu wytwarzania struktur magnezowych z porami otwartymi z zastosowaniem na implanty w chirugii kostnej. Tak określone materiały implantacyjne zostaną przebadane w drugiej fazie badań w warunkach in vivo metoda określenia stanu sztywnosci w czteropunktowym ugięciu. Badania umożliwią pełne określenie wpływu implantów na czas i warunki osteosyntezy.

***Słowa kluczowe**: gąbki magnezowe, metodyka wytwarzania, kontrola jakości, badania w warunkach in vivo, badania własności mechanicznych.*

[Inżynieria Biomateriałów, 56-57,(2006),54-58]

Wstęp

Zastosowanie nowych implantów kostnych wytworzonych na bazie stopów magnezu stwarza nowe możliwości dla leczenia ubytków kostnych. Stopy magnezu poprzez możliwość kontrolowanej resorpcji w warunkach pracy w płynach fizjologicznych w najbliższej przyszłości znajdą zastosowanie kliniczne jako materiał na implanty czasowe [1,2]. Implanty te po spełnieniu swojej funkcji stabilizacyjno-leczniczej zostają w sposób naturalny usunięte (resorpcja) z organizmu [3,4]. Powyższa właściwość stwarza oprócz zalet zdrowotnych dla pacjenta także oszczędności finansowe związane z ominięciem zabiegu reimpaltacji[5]. Na bazie materiału resorbowalnego, jakim są stopy magnezu wytworzono strukturę z porami otwartymi z zewnętrzną warstwą litą wzorując się na spongiozie i kortikalis kości natu-

DESIGN OF RESORPTION PROPERTIES OF THE METAL BONE IMPLANTS – APPLICATION *IN VIVO*

Friedrich-Wilhelm Bach*, Rafael Kucharski*, Dirk Bormann*,Dieter Besdo, Silke Besdo**, Christian Hackenbroich***, Fritz Thorey****, Andrea-Meyer-Lindenberg*****

* Institute of Materials Science, Schönebecker Allee 2, 30823 Garbsen, Germany
** Institut für Kontinuumsmechanik, Appelstraße 11, 30167 Hannover, Germany
***Department of Orthopaedic Surgery, Hanover Medical School, Hanover, Germany
****Clinic for Small Animals, University of Veterinary Medicine Hanover, Foundation, Germany
E-mail: bach@iw.uni-hannover.de

Abstract

The purpose of the dissertation was to optimize the casting method of producing the magnesium alloy implants for the purpose of filling bone defects. Characteristics of the resulting material structure were tested using computer micro-tomography. Also the mechanical properties were tested. The results obtained had a direct impact on the design of the size of pores and thickness of internal walls of the spongy metallic materials. The dissertation also presents the methodology and results of the testing adhesion of the animal femoral bone in vivo. The evaluation of the bone reconstruction was performed using the method of four-point bending. The tests were carried out on the New Zealand Rabbit experimental animals. First stage of the tests concerned measuring of the stiffness in vivo, in which the PLA control materials were used. The research results obtained in vivo set out the possibilities of designing resorbing structures with open pores derived on the basis of magnesium alloys for the purpose of the application in the bone surgery as filling materials for bone defects.

***Key words:** magnesium sponges, manufacturing method, quality control, in vivo research, mechanical properties examination*

[Inżynieria Biomateriałów, 56-57,(2006),54-58]

Introduction

Applying new osseous implants based on magnesium alloys brings new possibilities in bone losses treatment. Due to possibility of controlled resorption in physiologic fluids, in the nearest future magnesium alloys will be applied as a material for temporary implants [1,2]. These implants after having fulfilled their stabilising and curing purpose, are naturally removed (resorbed) from the organism[3,4]. This feature, apart from wholesome advantages for the patient, also brings financial savings, due to avoiding the reimplantation intervention[5]. Based on resorbing magnesium alloy, a structure with open pores and solid outer layer was created. This structure is patterned upon spongiosis and kortikalis of the natural bone. To examine the influence of the implanted material on the bone healing process, osteotomy interventions were carried out on shank bones of

ralnej. Aby zbadać wpływ zaimplantowanego materiału na proces leczenia kości przeprowadzono u doświadczalnych osobników królika zabieg osteotomii kości podudzia (Tibiae) z udziałem implantu oraz bez udziału implantu.

Pomiar sztywności wykonywano w czasie całego procesu leczenia w warunkach in vivo określając wartości sił w czteropunktowym ugięciu.

Materiał i metody

Metaliczne struktury z porami otwartymi wykonano metodą odlewniczą stosując wypełniacz ceramiczny. Jako wypełniacz zastosowano cząstki NaCl o wielkości 250 i 500µm. Jako materiału infiltrującego zastosowano stopy magnezu. Połączenia materiałów dokonano metoda odlewnicza infiltrując cząstki soli ciekłym metalem [6,7,8].

Otrzymany kompozyt: cząstki ceramiczne w osnowie stopu magnezu, przygotowano do nieniszczących badań kontroli jakości stopnia infiltracji. W tym celu wykonano cylindryczne próby o wysokości 10mm i średnicy 8mm w seriach z odlewów z pięciu stopów magnezu. Otrzymane w ten sposób cylindry przebadano metodą radiologiczną w urządzeniu µCT firmy Scanco Medical. W celu dokładniejszej kontroli jakości wybranych cylindrów zastosowano metodę mikroskopii skaningowej Mikroskopem Firmy Jeol przed i po chemicznym wypłukaniu fazy ceramicznej.

Ocenę wytrzymałości mechanicznej porowatych struktur przeprowadzono stosując metodę ściskania z jednostajną prędkością zgniotu (aparatura f-my Zwick) (RYS.3).

U wybranych przedstawicieli zwierząt doświadczalnych wykonano zabieg osteotomii prawej kości piszczelowej. Zabieg osteotomii został przeprowadzony przy wspomaga-

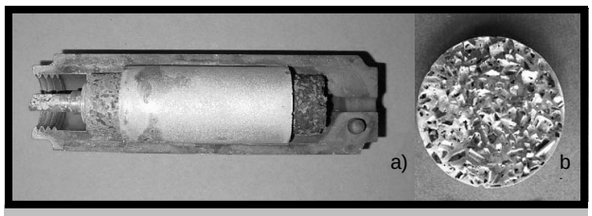

RYS. 2. a) Obraz kompozytu metal-ceramika w formie odlewniczej.
b) Obraz struktury z porami otwartymi.
FIG. 2. a) Metal-ceramic composite in casting mould.
b) Open pore structure.

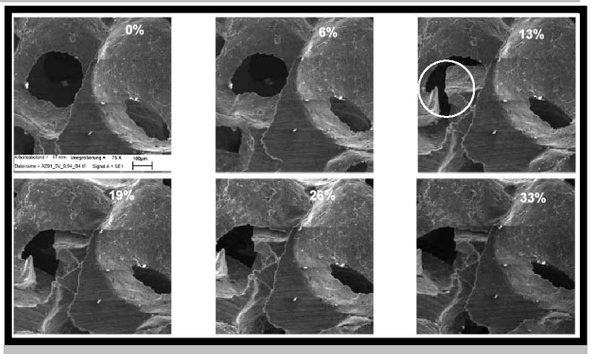

RYS. 3. Gąbka wykonana ze stopu magnezu w poszczególnych fazach badania odporności na ściskanie.artymi.
FIG. 3. Sponge made of magnesium alloy in several phases of compressive strength

experimental rabbit individuals with and without application of the implant. The rigidity measurements were taken during the whole process of healing in in vivo condidions. In the measurements force values were determined for four-point deflection.

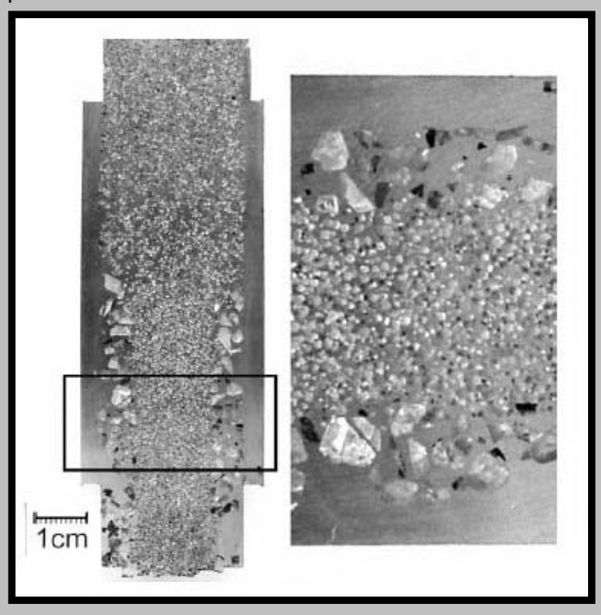

RYS. 1.
FIG. 1.

Material and methods

Metallic structures with open pores were created using founding methods with ceramic filling. The filling were the NaCl particles of 250µm and 500µm size. The infiltrating material was the magnesium alloy. The materials merging was made with founding methods, infiltrating salt particles with the liquid metal [6,7,8].

The obtained composite: ceramic particles In metallic matrix has been prepared for nondestructive quality control and the degree of infiltration. For this purpose, cylindric samples od 10 mm height and 8 mm diameter were manufactured in series of casting of five magnesium alloys. The obtained cylinders have been examined using radiologic methods in the Sanco Medical µCT device. For more precise control of selected cylinders, a scanning microscope method was applied with use of the JEOL microscope before and after chemical washing the ceramic phase out.

The mechanic strength of porous structures assessment has been taken using the method of compression with steady speed of deformation

On selected experimental animal individuals an osteotomy intervention on right tibia bone was carried out. The intervention was uniplanetary aided with internal stabilizers.

For measurements, the stabilizers hale been dismantled. This allowed measuring the fracture during the entire process of healing with no influence of external agent (external stabilizer)

The aim of the research was to compare the influence of bone implants based on magnesium alloys and PLA implants on bone fracture healing. Until now, the research was carried out on a group of experimental animals without implants in osteotomy region and a group of animals with PLA polyactide control bars. The group of animals with magnesium bar implants will be examined in the further stage of research. First examinations were carried out 4 weeks after the implantation. During 6-7 weeks, twice a week force meas-

niu unipalnetarnym ze stabilizatorem zewnętrznym.

W czasie przeprowadzenia pomiaru zdemontowano stabilizator. Umożliwiało to wykonanie pomiaru fraktury w czasie całego procesu leczenia bez wpływu czynnika dodatkowego (stabilizator zewnętrzny).

Celem badania było porównanie wpływu wszczepianych implantów kostnych wytworzonych na bazie stopów magnezu i implantów z PLA na leczenie fraktury kości.

Do chwili obecnej badaniom poddano grupę doświadczalnych zwierząt bez implantu w przedziale osteotomii oraz grupę zwierząt z wszczepami prętów kontrolnych wykonanych z polilaktydu PLA. Grupa zwierząt z wszczepami z prętów magnezowych zostanie przebadana w dalszym etapie doświadczeń. Pierwsze badania przeprowadzono po 4 tygodniach od momentu zabiegu implantacyjnego. Przez okres 6-7 tygodni dwa razy w tygodniu wykonywano badania pomiaru siły w czteropunktowej próbie ugięcia.

Zwierzęta pod narkozą, leżały w pozycji brzusznej na zaadoptowanym do tego badania stole operacyjnym i poddane zostały zabiegowi osteotomii. Prawa kończyna dolna została podtrzymana od stawu kolanowego do stawu biodrowego (RYS. 6).

Pomiar sił przeprowadzano dostosowując odpowiednie obciążenie przez przyrząd przenoszący nacisk do prętów mocujących stabilizator zewnętrzny, położonych najbliżej miejsca osteotomii. Stanowisko pomiarowe umożliwiało zmianę zadanego obciążenia w przedziale co 25g. Na początku doświadczenia maksymalne obciążenie wynosiło 100g. W ciągu dalszego procesu leczenia wielkość obciążenia wzrosła do 500g.

Wyniki pomiaru naprężeń i wartości ugięcia zostały zarejestrowane dla każdej z grup badanych zwierząt.

Wyniki

W procesie odlewniczym (RYS.7) otrzymano struktury magnezowe o gradientowym rozłożeniu pór otwartych.

Kontrolę jakości otrzymanych struktur metalicznych na bazie pięciu wybranych stopów magnezu przeprowadzono stosując dwie metody. W metodzie pierwszej do oceny wytworzonych struktur z porami otwartymi użyto metody określenia naprężenia w stosunku do odkształcenia Pierwsza metoda badań kontroli jakości otrzymanego wyrobu polegała na scharakteryzowaniu struktur gąbczastych poprzez wykreślenie zależności krzywej wartości odkształcenia w stosunku do wartości naprężenia metodą pomiaru wytrzymałości na ściskanie (RYS.8).

W każdej z przeprowadzonych prób określono w przedziale odkształcenia 10-20% charakterystyczną wartość plato dla materiałów porowatych niezależną od użytego

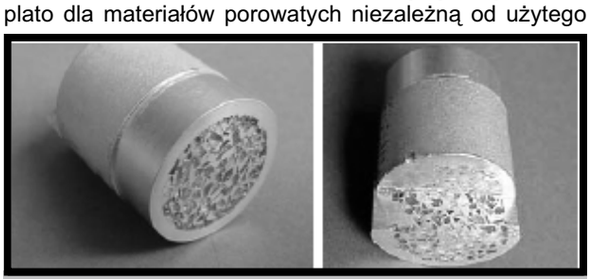

RYS. 7. Struktura z porami otwartymi przed usunięciem wypełnienia ceramicznego z zewnętrzną warstwą litą wykonaną na wzór kości naturalnej.
FIG. 7. Structure with open pores before removing the ceramic filling with solid outer layer, patterned upon a natural bone.

RYS. 4.
FIG. 4.

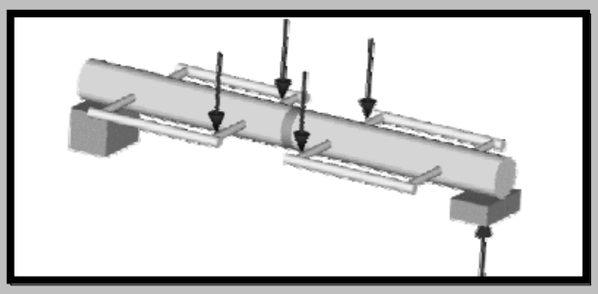

RYS. 5. Schemat warunków przeprowadzenia badań w czteropunktowym ugięciu.
FIG. 5. Scheme for conditions of four-point deflection research.

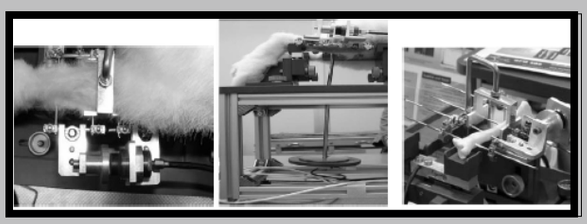

RYS. 6.
FIG. 6.

urements in four-point deflection were made.

The anesthetized animals lying in ventral position on a specially adapted operating table were subjected to osteotomy intervention. The right hindlimb was held from a knee joint to a hip joint (FIG. 6).

Force measurement was carried out after adjusting the appropriate load by the device transmitting the load to the bars fixing the external stabilizer closest to the osteotomy region.

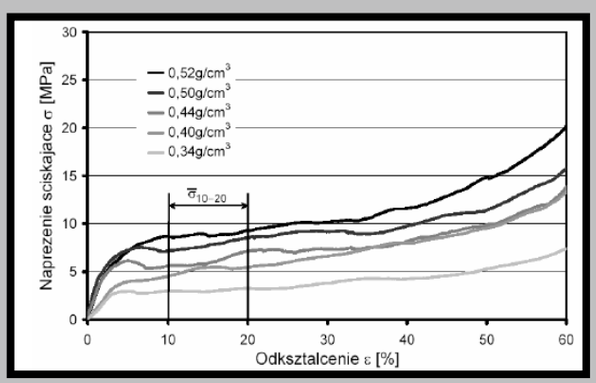

RYS. 8.
FIG. 8.

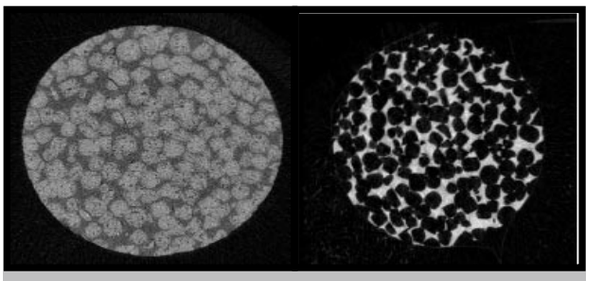

RYS. 9.
FIG. 9.

RYS. 10.
FIG. 10.

materiału.

Do badań użyto stopów wg ASTM czystego magnezu oraz jego stopów: AM 20, AE 42, AM50, AM60.

Jako drugą metodę kontroli jakości, z uwagi na zalety badań nieniszczących jak i czas wykonania samego badania, wybrano metodę mikrotomografii komputerowej.

Badaniu poddano odlew stopu magnezu z wypełniaczem ceramicznym oraz odlew po usunięciu chemicznie wypełniacza (RYS. 9 i 10).

Badanie mikro-CT pozwala na dokładne określenie zawartości wypełniacza ceramicznego w gąbce magnezowej. Brak badań jakościowych na tym etapie procesu wytwarzania może wykazać bezużyteczność produktu w czasie dalszych badań czasu resorpcji. Wypełnienie ceramiczne NaCl w roztworze wodnym prowadzi do lokalnych ognisk korozyjnych dyskwalifikujących omawiany materiał jako wypełnienie ubytków kostnych.

Z badań stanu sztywności (RYS.12) wynika, iż w czasie leczenia osteotomii wartość sztywności kości wzrasta. Widoczny jest również związek pomiędzy wartością siły a ugięciem, dla niewielkich obciążeń o przebiegu liniowym.

Obliczenia wartości sił ugięcia uzyskanych w dotychczasowych badaniach jako funkcje wyznaczające skuteczność leczenia złamania wykazują rozrzut wyników

Wykreślając linię trendu według polynomu trzeciego stopnia widoczna jest następująca prawidłowość: wartość sztywności wzrasta by później ulec stabilizacji a następnie znowu wzrastać.

Dyskusja

Sposobem odlewniczym otrzymywano struktury porowate na bazie stopów magnezu. Optymalizacja procesu od-

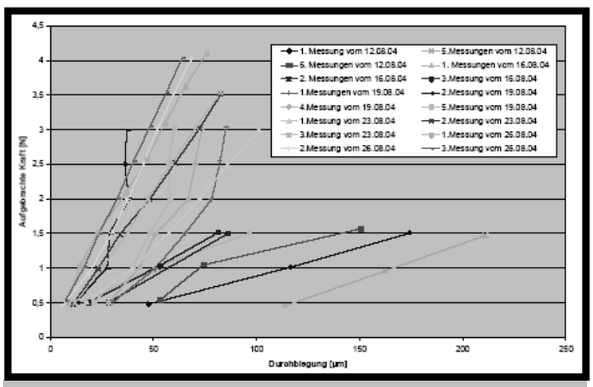

RYS. 11. Wykres wartości siły w stosunku do wartości osiągniętego ugięcia u królika numer 316364 w okresie leczenia uszkodzenia kostnego.
FIG. 11. Force in relation to deflection. Rabbit No 316364 during healing the bone damage.

The measurement station allowed changing the load every 50 grams. In the beginning of the experiment, the maximal load was 100 grams. During the healing process the value of load raised up to 500 grams. Tension measurement results and deflection values were recorded for each of the examined animals group.

Results

In the casting process (RYS. 7) magnesium structures of gradient distribution of open pores were obtained.

The quality control of the metallic structures based on five magnesium alloys was carried out with the use of two methods. In the first case, for assessment of the structures with open pores a method of determining tension in relation to distortion was used (FIG. 8).

In every test, within 10-20% distortion a characteristic value of plateau for porous materials, independent on the material used was determined. The following ASTM alloys were used: AM 20, AE 42, AM50, AM60 and pure magnesium.

Due to advantages of non-destructive examinations, as well as the short time of the very examination, a computer assisted microtomography method has been chosen. The method was applied for examining the state of the magnesium alloy with the ceramic filling and after removing the filling. The CAmT examination allows precise determining content of the ceramic filling in the magnesium sponge. Lack of qualitive examinations in this stage of manufacturing may cause the product to be useless during resorption time research. Ceramic NaCl filling in water solution causes formation of local corrosion centres, which disqualify the material as a filling of bone losses.

The research on rigidity state (RYS. 11) reveals that during the osteotomy healing the value of bone rigidity increases. Also a relation between the force value and deflection for low linear loads is visible.

The calculations of deflection forces obtained in the up to the present research as functions determining effectiveness of healing of the fracture reveal results to be scattered. After plotting the third degree polynomial trend line, the following rule is wisible: The rigidity increases, then stabilizes and finally increases again.

Discussion

Using foundry methods, magnesium alloy porous structures were obtained. Optimizing the foundry process as-

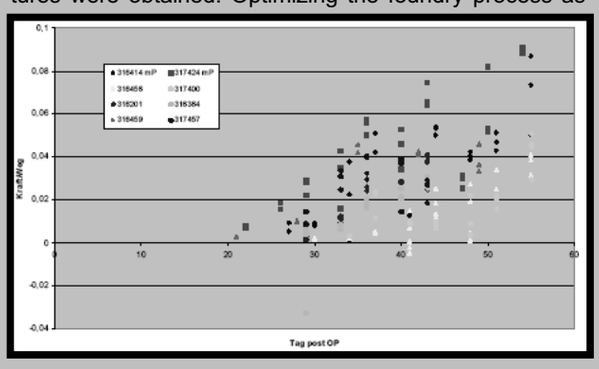

RYS. 12. Obliczenia wartości sił ugięcia uzyskanych w dotychczasowych badaniach jako funkcje wyznaczające skuteczność leczenia złamania.
FIG. 12. Calculations of the forces of deflection obtained on the up to present research as functions determining effectiveness of healing the fracture.

lewniczego zapewnia powtarzalność i wysoką jakość uzyskanych gąbek magnezowych. Celem charakteryzacji otrzymanych gąbek magnezowych materiał poddano badaniom mechanicznym w próbie wytrzymałości na ściskanie. Próba częściowo symuluje warunki późniejszej pracy gąbek magnezowych jako implanty na wypełnienia ubytków kostnych w organizmie. Kontrola jakości wykonania implantów dzięki technice µCT pozwalają na optymalizację procesu wykonania gąbek magnezowych.

Badania sztywności kości metodą czteropunktowego ugięcia wskazują na wzrost wartości sztywności u wszystkich przebadanych zwierząt. Rozrzut wyników może być efektem różnic anatomicznych u poszczególnych osobników. Ponadto zaobserwowano, że przy blisko połowie przebadanych zwierząt z wszczepionymi prętami wykonanymi z PLA wzrost wartości sztywności ugięcia następował szybciej niż u zwierząt kontrolnych bez prętów z PLA. Powyższe wyniki wskazują na korzystny wpływ biodegradowalnych implantów na proces zrastania się kości. Pozwala to sądzić, że zastosowanie porowatych struktur metalicznych na bazie stopów magnezu jako implantów czasowych będzie wpływać na znaczny wzrost wartości sztywności kości a tym samym na przyspieszenie przebiegu leczenia.

Podziękowania

Autorzy dziękują za pomoc i wsparcie Niemieckiej Wspólnocie Naukowej.

Piśmiennictwo

[1] Hayes, W.C.; Bouxsein, M.L.: Biomechanics of Cortical and Trabecular Bone:Implications for Assessment of Fracture Risk. In: Basic Orthopaedic Biomechanics, Editors: Mow,V.C.; Hayes, W.C. Lippincott-Raven Publishers, Philadelphia, 1997
[2] Nie2004 Unterlagen zur Vorlesung "Biokompatible Werkstoffe", PD Dr.-Ing. M. Niemeyer, 2004
[3] Kam+2000 Magnesium Taschenbuch, Aluminium-Verlag Düsseldorf, 2000

sures repeatability and high quality of the obtained magnesium sponges. To characterize the obtained sponges, the material has been subjected to mechanical compression strength tests. The test in some way simulates conditions of future sponge performance in the organism. Quality control of the implant allows, thanks to Cant, optimizing the manufacturing process for the magnesium sponges.

The examination of rigidity with the use of four-point deflection marks the increase of rigidity in all cases of the examined animals. The scatter of the results may be the effect of anatomic differences of every individual. Moreover, it has been observed, that for almost half of the animals with the PLA bars implanted the rigidity increase was faster than for the control animals without the PLA bars. The results presented above show positive influence of biodegrading implants on the process of bone healing. This allows assuming, that applying porous metallic structures based on magnesium alloys as temporary implants will influence the significant increase of bone rigidity and thus hasting the healing process.

Acknowledgements

The authors wish to tank for hel pand suport to the German Scientific Collectivity.

References

[4] Gro2003 Offenporige Metallstrukturen nach dem Platzhalterverfahren.
[5] Bach Fr.-W., Bormann D., Kucharski R., Wilk P.: Production and Properties of Foamed Magnesium; Cellular Metals and Polymers, Eds.: R. F. Singer, C. Körner, V. Altstädt, H. Münstedt, Trans Tech Publications, Zuerich 2005, S. 77-80.
[7] Bach Fr.-W., Bormann D., Kucharski R. November Colloquium 2005.
[8] Bach F, Bormann D., Kucharski R., Jendras M., Windhagen M., Hackenbroich Ch., Krause A., Meyer-Lindenberg A. "Resorbowalne, metaliczne implanty kostne".

MAGNEZOWE STRUKTURY HYBRYDOWE W ZASTOSOWANIU NA LECZENIE UBYTKÓW KOSTNYCH

Friedrich-Wilhelm Bach, Rafael Kucharski, Dirk Bormann

Institute of Materials Science,
Schönebecker Allee 2, 30823 Garbsen, Germany
E-mail: bach@iw.uni-hannover.de

Streszczenie

W pracy wykazano możliwość wytwarzania hybrydowych struktur składających się z litego materiału oraz otaczających jego powierzchnie ugrupowań z materiału porowatego z porami otwartymi wytworzonych na bazie stopów magnezu. Otrzymane w ten sposób struktury wytworzono metoda odlewnicza infiltrując wypełnienie ceramiczne. Przedstawiono ko-

MAGNESIUM COMPOUND STRUCTURES FOR THE TREATMENT OF BONE DEFECTS

Friedrich-Wilhelm Bach, Rafael Kucharski, Dirk Bormann

Institute of Materials Science,
Schönebecker Allee 2, 30823 Garbsen, Germany
E-mail: bach@iw.uni-hannover.de

Abstract

The dissertation demonstrates possibilities of producing one-phase compound structures on the basis of magnesium alloys composed of solid material, partially or wholly wrapped in the porous external layer.

Compound moulders were produced using the casting method with the application of ceramic filler (NaCl) infiltration. Characteristics of the compounds obtained

lejne fazy wytworzenia struktur hybrydowych oraz ich charakterystykę wykorzystując badania mikrostruktury w elektronowej mikroskopii skaningowej (SEM - skaning elektrony microscopy) oraz nienieszczace badania modelowe w skali 3D uzyskane dzięki zastosowaniu mikrotomografii komputerowej.

Cel wytworzonej struktury hybrydowej został określony zarówno jako wzmocnienie mechaniczne wykonane przez kształtkę z litego materiału jak również przedłużenie czasu resorpcji kształtki w porównaniu do wytwarzanych obecnie magnezowych materiałów resorbowalnych o strukturze gąbczastej.

Zastosowanie tak wykonanych struktur hybrydowych określono jako nowe tworzywa w leczeniu ubytków kostnych zarówno w kościach długich jak i płaskich.

Słowa kluczowe: *gąbki magnezowe, hybrydowe struktury porowate, metodyka wytwarzania, kontrola jakości.*

[Inżynieria Biomateriałów, 56-57,(2006),58-61]

Wstęp

Zastosowanie nowych implantow kostnych wytworzonych na bazie stopow magnezu stwarza nowe mozliwosci dla leczenia ubytkow kostnych [1, 2].

Dzięki właściwością temporalnym ujawniającym się podczas pracy w warunkach "in vivo" stopy magnezu posiadają potencjał kwalifikujący je na materiały na wypełnienia ubytków kostnych. Jednakże poprzez nie zoptymalizowany czas resorpcji [3], [4] nie mogą do tej pory znaleźć zastosowania w warunkach klinicznych. Jedną z dróg poprawiających tę niedogodność jest metoda wytwarzania struktur hybrydowych. Struktury hybrydowe oparte na tym samym materiale wsadowym - stopie magnezu jako materiale jednofazowym powinny charakteryzować się dobrymi właściwościami mechanicznymi. Istota jednofazowej struktury hybrydowej polega na połączeniu wiązaniem metalicznym materiału litego z materiałem otwarto porowatym. Dzięki temu połączeniu otrzymujemy materiał z właściwościami otwarto porowatymi pozwalającymi na przepływ płynów fizjologicznych i fiksację z naturalną kością, materiał lity natomiast daje większe możliwości w stworzeniu szkieletu do przenoszeń obciążeń ułatwiając tym samym i wspomagając rozwój naturalnego metabolizmu układu kostnego[5], [6]. Stwarza to nowe możliwości dla zastosowania stopów magnezu mogących jako temporalne implanty zostać użyte na większe systemy wypełnień ubytków kostnych będące nie dostępne do tej pory dla gąbek tylko o strukturze otwarto porowatej. Właściwości magnezu przedstawiono w TABELI 1.

Materiał i metody

Metaliczne struktury hybrydowe z porami otwartymi wykonano metodą odlewniczą z zastosowaniem wypełniacza ceramicznego. Jako wypełniacza użyto cząstek NaCl o wielkosci 250 i 500 um. Jako materialu inflitrujacego z uwagi na właściwości odlewnicze dla prekursora zastosowano stop magnezu AZ91, składający się z ok. 9% Al. i ok. 1% Zn. Połączenia materiałów dokonano metodą odlewniczą infiltrując cząstki soli wraz z elementami z tego samego stopu oraz bez ciekłym metalem AZ91.

Z otrzymanego kompozytu: cząstki ceramiczne w osnowie stopu magnezu, usunięto w procesie chemicznego płukania [7] wypełniacz ceramiczny otrzymując jednofazową strukturę hybrydową z magnezu.

Otrzymane w ten sposob materiały przebadano meto-

were tested using the scanning electron microscopy SEM (analysis of microstructure) and non-destructing 3D model analysis performed using computer micro-tomography.

The purpose of the compound structure was to enhance properties through using of the solid material and extending the resorption period of the moulder, compared to the spongy resorbing magnesium materials currently produced.

Thus obtained compound structures can be used as a new material in the treatment of the bone defects both in the long and flat bones.

Key Words: *magnesium sponges, porous hybrid structures, manufacturing methods, quality control.*

[Engineering of Biomaterials, 56-57,(2006),58-61]

Introduction

Application of new bone implants based on magnesium alloys brings new possibilities in bone losses treatment [1], [2]. Thanks to temporal properties, revealing during operation in vivo magnesium alloys can be qualified as a bone loss filling material. Yet, due to not optimised resorption time, they cannot be applied in clinical conditions. One of the methods, improving this inconvenience is manufacturing hybrid structures. These, based on the same core - on magnesium alloy as a monophase material should be characterized by fair mechanical properties. The idea of monophase hybrid structure leans upon linking the solid material with the open pore one with a metallic bond. Thanks to this connection, an open pore properties are obtained. These allow physiologic fluids flow as well as fixing with natural bone. The solid material, in turn, brings greater possibilities of building the skeleton for load bearing, enhancing the development of natural metabolism of the osseous system. [5], [6]. This brings new possibilities for applying the magnesium alloys, which, as temporary implants may be used in vast systems of bone fillings, not available for sponges of only porous structure so far. Magnesium properties have been presented in TABLE 1.

Material and methods

Metallic hybrid structures with open pores were made with use of foundry methods with application of ceramic filling. As a ceramic filling NaCl particles of 250µm and 500µm size were used. As an infiltrating material, due to its casting properties an AZ91 magnesium alloy has been used as a precursor. This alloy consists of 9% Al and about 1% Zn. Materials were fixed with casting methods by infiltration of salt particles with and without the elements of the same alloy with liquid AZ91 metal.

From the composite: ceramic particles in magnesium

Materiał Material	Masa molekularna Molecular mass [g/mol]	E-Modul E-Modulus [GPa]	Wytrzymałość na rozciąganie Strength [MPa]
Poly-L-lactid	50000	1,2	28
	100000	2,7	50
Kortikalis	-	10-30	110-160 (ściskanie)
Magnesium	24	44	150
Steel 316L	56	200	400

TABELA 1.
TABLE 1.

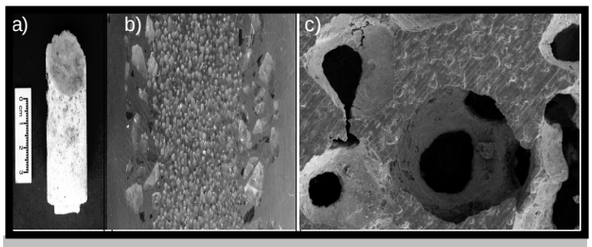

RYS.1. a) Ceramiczne wypełnienie formy przed infiltracją ciekłym stopem magnezu NaCl, b) Zgład: materiał kompozytowy osnowa magnezowa wypełniona ceramicznym wypełniaczem z NaCl, c) SEM: Materiał otwarto porowaty po całkowitym usunięciu ceramicznego wypełniacza.
FIG.1. a) NaCl ceramic mould filling before liquid magnesium alloy infiltration, b) Microsection: composite material. magnesium groundmass with NaCl ceramic filling, c) Scanning microscope. Open pore material after complete removal of the ceramic filling.

dą radiologiczną w urządzeniu uCT firmy Scanco Medical. (RYS.1c).

W celu dokładniejszej kontroli wybrane cylindry przebadano metoda mikroskopii skaningowej Mikroskopem Firmy Jeol przed i po chemicznym wyplukaniu fazy ceramicznej.

Celem otrzymania jednorodnego materiału a tym samym połączenia metalicznego pomiędzy strukturą otwarto porowatą a materiałem litym wykonano formy solne wypełnione wypełniaczem ceramiczny i ukształtowane aby zgromadzić materiał lity schemat numer

W dalszym etapie badań użyto różnego rodzaju kształtek odpowiedni z preparowanych celem usunięcia warstwy tlenku magnezu i przygotowanych w podgrzanej formie wypełnionej ceramicznym wypełniaczem.

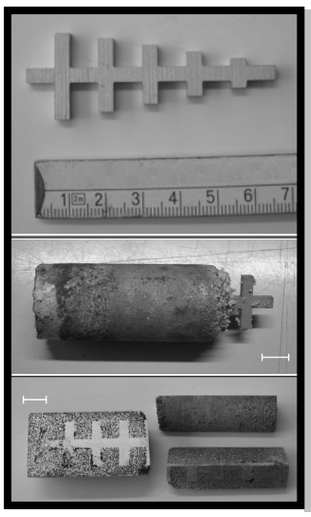

RYS. 4. Hybrydowy materiał kompozytowy przed usunięciem wypełniacza ceramicznego.
FIG. 4. Hybrid composite material before ceramic filling removal.

Wyniki

W procesie odlewniczym, jak ukazuje RYS.5 wykazano, iż możliwe jest otrzymanie tą metodą jednofazowej struktury hybrydowej. Można otrzymać struktury o gradientowym rozłożeniu porów otwartych. Konieczne są dalsze badania w optymalizacji powyższej metody celem dostosowania na konkretne aplikacje.

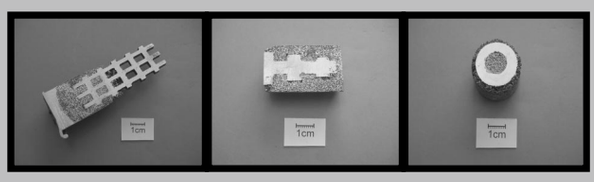

RYS. 2. Kształtki ze stopu AZ91 zatopione w tworzywie otwarto porowatym ze stopu AZ 91.
FIG. 2. AZ91 shapes founded in open pore AZ91.

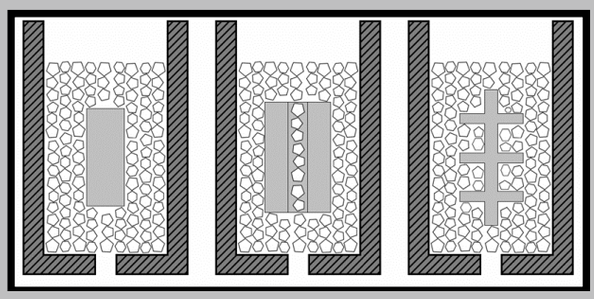

RYS. 3. Usytuowanie kształtek w formie z wypełniaczem ceramicznym.
FIG. 3. Shape location in the mould with ceramic filling.

alloy groundmass the ceramic filling has been removed in chemical rinsing [7]. This way, a monophase magnesium structure has been obtained. The obtained structures have been examined with radiological methods in a uCT Scanco Medical device (FIG.1c)

For more accurate control, selected cylinders were examined with the scanning Jeol microscope. The examination took place before and after the chemical rinsing.

In order to obtain a homogenous material, and thus linking the solid metal with open pore structure, salt moulds filled with ceramic filling were made. These were specially shaped in order to gather the solid material (FIG.3).

In the further stage of research, different shapes were prepared in a heated mould with ceramic filling, in order to remove the magnesium oxide layer

Results

As it is shown in FIG. 5, the casting process revealed that it is possible to obtain a monophase hybrid structure with this method. It is also possible to obtain structures of gradient distribution of the open pores. In order to adjust the method described above for particular applications,further research is necessary to be carried out.

The quality of the magnesium alloy casting with ceramic filling has been examined with the use of Computer Aided Micro-Tomography (CAμT). As it is shown in FIG. 5 (with filling) and 8 (without filling), the CAμT allows precise determination of the ceramic filling content in the magnesium sponge Lack of qualitive examinations in this stage of manufacturing may cause the product to be useless during resorption time research. Ceramic NaCl filling in water solution causes formation of local corrosion centres, which disqualify the material as a filling of bone losses.

Discussion

The quality of the hybrid material has been derived from the state of the solid material - open pore structure connection. it seems that the greatest problem is proper sealing of the mould and properly chosen point of vacuum infiltration

W metodzie drugiej dokonywano badań metodą mikrotomografii komputerowej stanu odlewu stopu magnezu z wypełniaczem ceramicznym, oraz po jego usunieciu chemicznie ze stopu. Jak wykazują RYS.5 odpowiednio z wypełnieniem i bez, charakterystyka w mikro-CT pozwala na dokladne określenie zawartości wypełniacza ceramicznego w gąbce magnezowej. Brak badań jakościowych na tym etapie procesu wytwarzania może okazać bezużyteczność produktu w czasie badań czasu resorbcji. Wypełnienie ceramiczne NaCl w roztworze H_2O prowadzi do lokalnych ognisk korozyjnych dyskwalifikujacych omawiany materiał jako wypelnienie ubytkow kostnych.

Dyskusja

Jakość wytworzonego materiału hybrydowego określono na podstawie stanu połączenia materiału litego ze strukturą otwarto porowatą. Wydaje się, iż największy problem wiąże się w procesie jednoczesnego wytworzenia materiału hybrydowego z odpowiednim uszczelnieniem formy i odpowiednio dobranym miejscem infiltracji podciśnieniem formy. W procesie odlewniczego zalewania kształtek magnezowych tym samym stopem w formie wypełnionej ceramicznym wypełniaczem trudności przysparza odpowiednie pozbycie się warstwy powierzchniowej tlenku magnezu na kształtkach mimo odpowiedniego przygotowania poprzez mechaniczne ściągniecie warstwy tlenku.

Rozwiązaniem kwestii pierwszej wydaje się wykonanie odpowiednio szczelnej formy, co ukazują dalsze badania i ich wyniki. Natomiast w kwestii pokrywania tlenkiem wydaje się, iż wykonanie odlewu w atmosferze gazu ochronnego, przygotowanie kształtek magnezowych i utrzymywanie ich w odpowiedniej do procesu odlewniczego temperaturze, blokującej możliwości lokowania się tlenków magnezu poprzez stapianie warstwy powierzchniowej jest odpowiednim rozwiązaniem, co ukazuje niniejsza praca.

Podziękowania

Autorzy dziękują za pomoc i wsparcie Niemieckiej Wspónocie Naukowej.

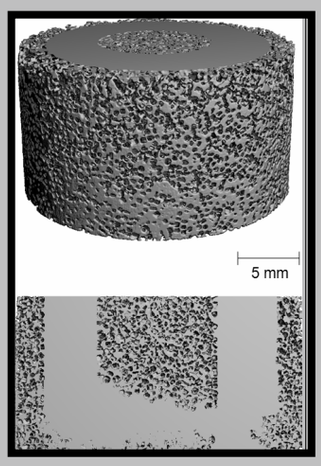

RYS. 5. Badania kontroli jakościowej w micro-CT firmy Scanco medical.
FIG. 5. Quality control in the Scanco Medical CAμT.

of the mould in the process of simultaneous manufacturing of the hybrid material.

In the mould pouring process for the magnesium shapes with the same alloy in the mould with ceramic filling, it is a certain difficulty to dispose of the surface layer of magnesium oxide from the surface of the shapes, despite proper preparation by mechanical removal of the oxide layer

The first problem may be solved by manufacturing enough hermetic mould, which is revealed by further research. The problem of oxide layers, in turn, seems to be solved by manufacturing the cast in the protective gas atmosphere, preparing the magnesium shapes and maintaining them in appropriate for the casting process temperature, preventing the oxides from locating on the surface by melting the surface layer.

Acknowledgements

The authors wish to tank for help and support to the German Scientific Collectivity.

Piśmiennictwo

[1] Switzer EN.: Resorbierbares metallisches Osteosynthesematerial - Untersuchungen zum Resoptionsverhalten im Meerschweinchenmodell, Vet.Met.Diss., Hannover, 2005.
[2] Schritt in die Zukunft - Medizintechnik gefordert durch das BMBF Bundesministerium fur Bildung und Forschung., Bonnj 2001.
[3] Chłopek J., Bach Fr.-W., Kucharski R., Bormann D.: „Nowe implanty dla chirurgii kostnej z resorbowalnych metali i polimerów", Proceed. of ITEM, Bytów, 2006.

References

[4] Bach Fr.-W., Kucharski R., Bormann D.: Proceed. ofXXII Conference of Orthopaedics of Polish Armee, Bydgoszcz, 2005.
[5] Bach Fr.-W, Bormann D., Kucharski R., Wilk P.: Production nad Propereties of Foamed Magnesium; Cellular Metals and Polymers, Eds. R.F.Springer, C.Korner, V.Altstadt, H.Munstedt, Prans.Tech.Publ., Zurich 2005, pp.77-80.
[6] Bach Fr.-W., Bormann D., Kucharski R.: November Colloquium 2005.

STUDIA PODYPLOMOWE 2006/2007

Nazwa studium podyplomowego:

Biomateriały – Materiały dla Medycyny

Organizator studium podyplomowego:

Akademia Górniczo-Hutnicza
Wydział Inżynierii Materiałowej i Ceramiki
Katedra Biomateriałów

Adres, telefon, fax, e-mail organizatora:

30 -059 Kraków, Al. Mickiewicza 30
tel. 12 617 34 41, 12, 617 47 38
email; epamula@agh.edu.pl mblazew@uci.agh.edu.pl stodolak@agh.edu.pl

Charakterystyka studium:

Zajęcia obejmujące wykłady i seminaria, dotyczyć będą kluczowych zagadnień z dziedziny inżynierii biomateriałów. Program studiów obejmować będzie charakterystykę tworzyw wykorzystywanych w medycynie: metali i ich stopów, polimerów, ceramiki oraz węgla syntetycznego i kompozytów. Omówione zostaną przykłady zastosowań tworzyw syntetycznych w różnych dziedzinach medycyny a mianowicie ortopedii, chirurgii kostnej, laryngologii, kardiologii, okulistyce i stomatologii i innych. Przedstawione zostaną metody projektowania i wytwarzania materiałów spełniających wymagania stawiane przez medycynę. Słuchaczom studium zaprezentowane zostaną metody fizykochemiczne stosowane zarówno do charakterystyki materiału jak i przebiegu jego degradacji (w sztucznym i naturalnym środowisku biologicznym) oraz metody biologiczne do analizy zjawisk zachodzących na powierzchni tworzyw implantacyjnych w kontakcie z żywą komórką i tkanką. Na zajęciach prezentowane będą (w oparciu o konkretne przykłady) metody: FTIR, SEM, AFM, mikroskopia optyczna oraz badania mechaniczne z uwzględnieniem badań parametrów mechanicznych naturalnych tkanek oraz metody analizy fizycznych parametrów powierzchni (energia powierzchniowa, twardość, chropowatość). Wykłady dotyczyć będą badania biozgodności w warunkach *in vitro* i *in vivo*, omówienia normy ISO 10993 (Biologiczna ocena wyrobów medycznych) oraz regulacji prawnych i aspektów etycznych związanych z badaniami na zwierzętach. Dodatkowo omówione zostaną sposoby organizacji, nadzoru i monitorowania badań klinicznych.Słuchacze studium zapoznani zostaną z najnowszymi osiągnięciami inżynierii tkankowej, metodami wytwarzania podłoży tkankowych i konstrukcją bioreaktorów.

Kierownik: Dr inż . Elżbieta Pamuła	*Czas trwania:* Jeden semestr (letni 2006/2007)
Zasady naboru: Zgłoszenie pisemne z deklaracją opłaty za studium.	
Termin zgłoszeń: 02.02. 2007	
Opłaty: 1.800 PLN	
Informacje dodatkowe: Zajęcia – 8 zjazdów 18 godzinnych Przewidywana ilość godzin -144. przewidywana data rozpoczęcia 24.02. 2007.	

Wskazówki dla autorów

Prace do opublikowania w czasopiśmie "Inżynieria Biomateriałów" będą przyjmowane wyłącznie z tłumaczeniem na język angielski.

Prosimy je nadsyłać na dyskietkach wyłącznie w formacie Word 6.x (lub wyższy) wraz z jednym egzemplarzem kontrolnego wydruku i kompletem rysunków i zdjęć.

Możliwe jest również dołączanie ilustracji w różnych formatach grafiki typu .eps, .jpg, .tif, .cdr, .cpt, .gif.

Rozmiar artykułu:

- przeglądowego i pracy oryginalnej - do 10 stron standardowego maszynopisu,
- komunikatu - do 5 stron,
- noty technicznej - do 3 stron

Obowiązuje układ jednostek SI.

Rysunki, tabele i równania powinny być kolejno ponumerowane.

Struktura artykułu:

- streszczenie (do 200 słów),
- słowa kluczowe (3-10 słów),
- wprowadzenie,
- materiał i metodyka,
- wyniki,
- dyskusja,
- wnioski,
- piśmiennictwo (wg systemu Harvard).

Odnośniki literaturowe w tekście należy podawać jako kolejne liczby arabskie w nawiasach kwadratowych.

Pismiennictwo (zawierające nazwiska autorów i skróty ich imion, tytuł artykułu, tytuł czasopisma, tom, rok w na wiasach okrągłych i strony) powinno być zamieszczone na końcu artykułu. Skrótów tytułów czasopism należy unikać bądź podawać zgodnie z Chemical Abstract. Cytując książki należy podawać numery odpowiednich rozdziałów.

Nie przewiduje się wypłacania honorariów autorskich.

Prace należy nadyłać na adres:

Redakcja “Inżynieria Biomateriałów”
Akademia Górniczo - Hutnicza
Katedra Biomateriałów
30-059 Kraków, al. Mickiewicza 30/A-3
fax. (48-12) 617-33-71
tel. (48-12) 617-22-39
e-mail: apowroz@uci.agh.edu.pl

Warunki prenumeraty

Wydawnictwo Polskie Stowarzyszenie Biomateriałów w Krakowie przyjmuje zamówienia na prenumeratę, która może obejmować dowolny okres, w którym wydawane są kolejne zeszyty. Zamawiający otrzyma zaprenumerowane zeszyty począwszy od daty dokonania wpłaty. Zamówienia wstecz będą realizowane w miarę posiadanych zapasów.

Realizacja zamówienia

Warunkiem realizacji zamówienia jest otrzymanie z banku potwierdzenia dokonania wpłaty przez prenumeratora.

Konto

Polskie Stowarzyszenie Biomateriałów
30-059 Kraków, al.Mickiewicza 30/A-3
Bank Śląski S.A. O/Kraków,
nr rachunku 63 1050 1445 1000 0012 0085 6001

Należy podać swój adres, tytuł czasopisma, okres prenumeraty i liczbę zamawianych egzemplarzy.

Opłata

Cena numeru 56-57- 40PLN

Instructions to authors

Contributions in English language version should be submitted to:

Editorial Office
"Engineering of Biomaterials"
AGH University of Science and Technology
Department of Biomaterials,
Al. Mickiewicza 30/A-3, 30-059 Kraków, Poland
fax. (48-12) 617-33-71, tel. (48-12) 617-22-39
e-mail: apowroz@uci.agh.edu.pl

Texts should be delivered on a 3.5-inch diskette, accompanied by a printout (with a double spacing) including drawings, photographs, tables etc. Recommended is IBM-compatible MS format, e.g. Word 6.x (or higher). Illustrations can be enclosed on diskettes in the formats: .eps, .jpg, .tif, .cdr, .cpt, .gif.

Advised paper length is:

- review papers and accounts of original unpublished research - up to 10 pages (standard manuscript pages);
- short communications - up to 5 pages;
- technical notes - up to 3 pages.

SI units should be used in the text.

Figures, Tables and Equations should be numbered in corresponding consecutive series of the Arabic numbers.

Layout of the paper should be the following:

- Abstract (up to 200 words)
- Key words (3-10 words)
- Introduction
- Materials and Methods
- Results
- Discussion
- Conclusions
- References

References should be made in the text by using consecutive Arabic numbers in brackets. Full references (including author's surname and abbreviated names, title of the paper, title of the journal, volume, year in parenthesis and pages) should be given in a list at the end of the paper. Abbreviations of journal titles should be avoided or used in accordance with those listed in Chemical Abstracts. Whenever a book is cited, the number of the relevant chapter should be given.

The journal makes no page charges.

Subscription terms

Subscription orders should be addressed to the Polish Society for Biomaterials in Kraków.

The ordered issues will be delivered consecutively starting from the date of payment, acknowledged by the bank.

Earlier issues will be supplied if available.

Subscription rates:

Cost of number 56-57 - 40.00 PLN

Payment should be made to:

Polish Society for Biomaterials,
Al. Mickiewicza 30/A-3,
30-059 Kraków, Poland
Bank Śląski S.A. O/Kraków,
account no. 63 1050 1445 1000 0012 0085 6001

It is requested to quote the subscriber's name, title of the journal, desired subscription period and number of the ordered copies.